A supramolecular chemistry approach for potentiating live attenuated whole-organism vaccines

Duszenko, N.

A supramolecular chemistry approach for potentiating live attenuated whole-organism vaccines

Nikolas Duszenko

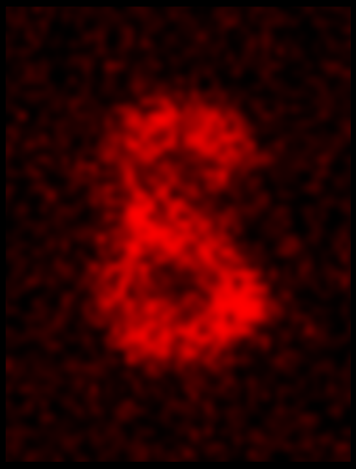

ISBN:	xxx
Cover design:	Designed by Nikolas Duszenko
Layout:	Nikolas Duszenko, with generous support of Eline Brombacher
Printing:	xxx

The work described in this thesis was performed at the department of Parasitology at the Leiden University Medical Center, Leiden, The Netherlands. The work was supported by the LUMC (grant awarded to Profs. Meta Roestenberg and Fijs van Leeuwen).

A supramolecular chemistry approach for potentiating live attenuated whole-organism vaccines

Proefschrift

ter verkrijging van
de graad van doctor aan de Universiteit Leiden,
op gezag van rector magnificus prof.dr.ir. H. Bijl,
volgens besluit van het college voor promoties
te verdedigen op donderdag 16 mei 2024
klokke 13.45 uur

door

Nikolas Duszenko
geboren te Hamburg
in 1991

Promotors:	Prof. Meta Roestenberg Prof. Fijs W.B. van Leeuwen
Leden promotiecommissie:	Prof. Leo Visser Dr. Tessa Buckle Dr. Aldrik H. Velders (Wageningen University) Dr. Matthew M. McCall (Nigmegen University)

Table of contents

1

Introduction & Dissertation Outline

Introduction

Malaria has been a uniquely destructive infectious disease in humanity's history. Once widespread throughout the world (Cox, 2002), the disease is now mostly confined to tropical regions, where it continues to be a major source of mortality and morbidity: in 2020 alone an estimated 627,000 deaths were attributed to malaria (WHO World Malaria Report 2021). Some success has been had in driving down mortality/morbidity via interventions targeting the Anopheles mosquito responsible for malaria transmission (Bhatt et al., 2015), but a plateauing of annual deaths in recent years suggests that further reductions of malaria's burden will require use of an effective vaccine.

Initial efforts at developing a subunit-based vaccine against the circumsporozoite protein (CSP) found abundantly on the malaria sporozoite (SPZ) surface, known as RTS,S, did not yield high levels of protection in a large Phase 3 trial, with only 30% protection after 18 months (Rts et al., 2012). The more recent focus of malaria vaccine design has turned to whole SPZ-based vaccines that better activate the immune system. Studies in malaria-naïve individuals have shown that complete protection from malaria challenge can be achieved by immunization with such vaccines (Mordmuller et al., 2017; Roestenberg et al., 2009; Seder et al., 2013). However, field trials in endemic areas have yielded considerably lower levels of protection (Oneko et al., 2021; Sissoko et al., 2017). These findings indicate the need for further improving the immunogenicity of SPZ-based malaria vaccines.

In this dissertation, a strategy for improving SPZ-based malaria vaccine immunogenicity is presented in which the SPZ cell surface is chemically augmented with immunogenic adjuvants. The conceptual basis of this strategy is derived from advances in the field of supramolecular chemistry that have shown the power of harnessing multivalent supramolecular interactions to drive very strong interactions between manifold chemical moieties and biological entities – such as a cell's enveloping lipid bilayer (Roy et al., 2020). Building on such findings, this dissertation describes application of the principle to anchor onto both bacterial and malaria SPZ cells a supramolecular scaffold enabling chemical augmentation of their cell surfaces. These chemical scaffolds are subsequently engineered with immunogenic adjuvants whose presence on the (SPZ) cell surface induces a more vigorous immune response compared to unadulterated cells.

Dissertation Outline

This dissertation presents the development and immunological assessment of a strategy for chemically augmenting SPZ immunogenicity.

I. Chemical augmentation technology

In **Chapter 2**, the concept – namely, using supramolecular chemistry to functionalize microbial cell surfaces via an in situ pre-targeting host-guest strategy – was investigated in several bacterial model systems. Next to establishing this novel technique for pathogen surface functionalization, its effect on (normal) macrophage behavior, a key immune cell early in immune responses, was investigated. In **Chapter 3**, the chemical functionalization strategy was evaluated in vivo in a pre-targeting paradigm. Using a bacterial infection model, it was shown that polymers, when intravenously administered, could home in on infected tissue containing pre-targeted bacteria and there remain stably associated.

II. Vaccine development

Chapter 4 expanded on the concept by using the same chemical strategy to introduce an adjuvant onto the cell surface of (poorly immunogenic) bacteria. The key question here addressed was: does an adjuvant complexed in this manner induce a more pro-inflammatory response to bacteria? This was indeed so, as macrophages responded to adjuvanted bacteria with significantly increased production of the pro-inflammatory cytokine IL-6. These findings supported translation of the concept to increase SPZ-based malaria vaccines' immunogenicity. In **Chapter 5**, minor changes in functionalization strategy allowed translation of the concept to malaria SPZ, which yielded markedly improved immune responses in an in vitro macrophage model. A more extensive immunological characterization in an in vivo mouse model of malaria followed, the results of which suggested that chemically augmented SPZ did indeed possess a better immunogenicity than wild-type SPZ.

In **Chapter 6**, a summary of the findings and future outlooks, particularly in the context of advancing malaria vaccines, is outlined, including preliminary data postulating a refinement of the presented adjuvanting strategy.

References

Bhatt, S., Weiss, D.J., Cameron, E., Bisanzio, D., Mappin, B., Dalrymple, U., Battle, K., Moyes, C.L., Henry, A., Eckhoff, P.A.*, et al.* (2015). The effect of malaria control on Plasmodium falciparum in Africa between 2000 and 2015. Nature *526*, 207-211.

Cox, F.E. (2002). History of human parasitology. Clin Microbiol Rev *15*, 595-612.

Mordmuller, B., Surat, G., Lagler, H., Chakravarty, S., Ishizuka, A.S., Lalremruata, A., Gmeiner, M., Campo, J.J., Esen, M., Ruben, A.J.*, et al.* (2017). Sterile protection against human malaria by chemoattenuated PfSPZ vaccine. Nature *542*, 445-449.

Oneko, M., Steinhardt, L.C., Yego, R., Wiegand, R.E., Swanson, P.A., Kc, N., Akach, D., Sang, T., Gutman, J.R., Nzuu, E.L.*, et al.* (2021). Safety, immunogenicity and efficacy of PfSPZ Vaccine against malaria in infants in western Kenya: a double-blind, randomized, placebo-controlled phase 2 trial. Nat Med *27*, 1636-1645.

Roestenberg, M., McCall, M., Hopman, J., Wiersma, J., Luty, A.J., van Gemert, G.J., van de Vegte-Bolmer, M., van Schaijk, B., Teelen, K., Arens, T.*, et al.* (2009). Protection against a malaria challenge by sporozoite inoculation. N Engl J Med *361*, 468-477.

Roy, S., Cha, J.N., and Goodwin, A.P. (2020). Nongenetic Bioconjugation Strategies for Modifying Cell Membranes and Membrane Proteins: A Review. Bioconjug Chem *31*, 2465-2475.

Rts, S.C.T.P., Agnandji, S.T., Lell, B., Fernandes, J.F., Abossolo, B.P., Methogo, B.G., Kabwende, A.L., Adegnika, A.A., Mordmuller, B., Issifou, S.*, et al.* (2012). A phase 3 trial of RTS,S/AS01 malaria vaccine in African infants. N Engl J Med *367*, 2284-2295.

Seder, R.A., Chang, L.J., Enama, M.E., Zephir, K.L., Sarwar, U.N., Gordon, I.J., Holman, L.A., James, E.R., Billingsley, P.F., Gunasekera, A.*, et al.* (2013). Protection against malaria by intravenous immunization with a nonreplicating sporozoite vaccine. Science *341*, 1359-1365.

Sissoko, M.S., Healy, S.A., Katile, A., Omaswa, F., Zaidi, I., Gabriel, E.E., Kamate, B., Samake, Y., Guindo, M.A., Dolo, A.*, et al.* (2017). Safety and efficacy of PfSPZ Vaccine against Plasmodium falciparum via direct venous inoculation in healthy malaria-exposed adults in Mali: a randomised, double-blind phase 1 trial. Lancet Infect Dis *17*, 498-509.

2

A supramolecular platform technology for bacterial cell surface modification

Nikolas Duszenko, Danny M. van Willigen, Mick M. Welling, Clarize M. de Korne, Roos van Schuijlenburg, Beatrice M.F. Winkel, Fijs W.B. van Leeuwen and Meta Roestenberg

Adapted from:

ACS Infect Dis. 2020 Jul 10;6(7): 1734-1744.
PMID: 32364374
DOI: 10.1021/acsinfecdis.9b00523.

Abstract

In an era of antimicrobial resistance, a better understanding of the interaction between bacteria and the sentinel immune system is needed to discover new therapeutic targets for combating bacterial infectious disease. Sentinel immune cells such as macrophages phagocytose intact bacteria and thereby initiate ensuing immune responses. Bacterial surface composition is a key element which determines macrophage signaling. To study the role of bacterial cell surface composition in immune recognition, we developed a platform technology for altering bacterial surfaces in a controlled manner with versatile chemical scaffolds. We show that these scaffolds are efficiently loaded onto both Gram-positive and -negative bacteria, and that their presence does not impair the capacity of monocyte-derived macrophages to phagocytose bacteria and subsequently signal to other components of the immune system. We believe this technology thus presents a useful tool to study the role of bacterial cell surface composition in disease etiology and potentially for novel interventions utilizing intact bacteria for vaccination.

Introduction

The rise of drug-resistant bacteria has led to the reemergence of bacterial infectious diseases once thought vanquished with the discovery of antibiotics (Willyard, 2017). Novel vaccines and drugs are needed to combat this growing threat. A better understanding of the interactions between bacteria and the immune system can facilitate the identification of new targets for interventions.

Interactions between bacteria and the immune system are initiated by cells of the innate immune system, such as macrophages (MΦs). These cells are responsible for orchestrating the ensuing immune response (Wynn et al., 2013). MΦs are able to recognize bacteria by their size and unique bacterial cell wall components (Kumar et al., 2011; Mogensen, 2009). These features prompt the MΦ to internalize the bacteria by phagocytosis and degrade them. Doing so liberates the bacterial cell wall components, which dose-dependently trigger intracellular signaling cascades that modulate MΦ effector functions (Wolf and Underhill, 2018). The bacterial cell wall composition is thus thought to be responsible for the large heterogeneity in bacteria-host interactions, ranging from the vigorous systemic inflammatory response syndromes seen with Gram-negative bacteria such *Escherichia coli* to the comparatively weak responses to many Gram-positive bacteria like *Staphylococcus aureus* (Annane et al., 2005; Goldmann and Medina, 2018).

A single bacterial cell surface component of Gram-negative bacteria, lipopolysaccharide (LPS), is responsible for the previously mentioned systemic inflammatory response syndromes. LPS potency in priming immune responses has been utilized in vaccine development, where chemically modified LPS variants have been successfully used to create potent new vaccines for hepatitis B and human papillomavirus (Kong et al., 2008; Paavonen et al., 2009). Bacteria like the Gram-positive *S. aureus* lack highly immunogenic components such as LPS, resulting in dampened immune responses which allow *S. aureus* to establish chronic infections that the immune system is unable to clear (Bekeredjian-Ding et al., 2017; Naber, 2009). Other pathogenic bacteria have instead evolved modifications of immunogenic components that render them inert. There are for example a number of Gram-negative bacterial species, like *Salmonella enterica* and *Helicobacter pylori*, whose unusual LPS structure does not elicit a proper immune response (Maldonado et al., 2016). Much like *S. aureus*, these bacteria can establish chronic infections. Further unraveling which bacterial cell wall components are responsible for directing MΦ responses is thus an important step in advancing our understanding of interactions between bacteria and the immune system.

To study the role of bacterial cell wall components in early immune responses, we envisioned a tool which would allow us to alter the bacterial cell wall in a

controlled manner without disturbing the bacteria's structural integrity. Reproducible chemical modification of (bacterial) cell surfaces is in itself a challenging endeavor, but doing so in the context of introducing immunomodulatory compounds presents unique challenges (Bi et al., 2018; Gautam et al., 2013; Mongis et al., 2017). As immune responses are influenced by immunomodulator quantity, it is essential to clearly define loading rates. One way of doing this is by using a generic chemical platform that standardizes the loading rate regardless of the compound being introduced. Recently, we have developed pre-targeting methods which enable precise quantification of loading rate. By harnessing supramolecular chemistry we reproducibly loaded macro-aggregated albumin (MAA) microparticles and eukaryotic cells with scaffolds that remained stable under chemically challenging *in vitro* and *in vivo* conditions (Rood et al., 2017; Spa et al., 2018; Welling et al., 2019). The multivalent host-guest interactions between β-cyclodextrin (CD) and adamantane (Ad) underpinning these scaffolds have already found widespread use for controllably introducing various chemical and biological functionalities onto inorganic svurface (Gonzalez-Campo et al., 2010; Neirynck et al., 2013; Rodell et al., 2015). We thus reasoned that these scaffolds might similarly be used as a generic chemical platform for controllably introducing (immunomodulatory) components onto bacterial cells while preserving viability and original biological composition.

The aim of this study was to investigate the use of supramolecular scaffolds as a generic chemical platform to modify bacterial cell surface composition. To this end, we first assessed the loading of our supramolecular scaffolds onto both Gram-positive (*Staphylococcus aureus*) and Gram-negative (*Escherichia coli*) bacteria, using MAA microspheres as a validated control. We then assayed the effects of these scaffolds on MΦ responses.

Results

In this study we used three different entities to investigate the loading of a chemical scaffold **Cy3$_{1.5}$CD$_{100}$PIBMA$_{389}$** onto bacterial cell surfaces and the resultant effects on MΦ recognition and response as gauged by three major immunological parameters – phagocytosis, surface marker expression and cytokine production – using a monocyte-derived MΦ (MoMΦ) assay (Figure 1).

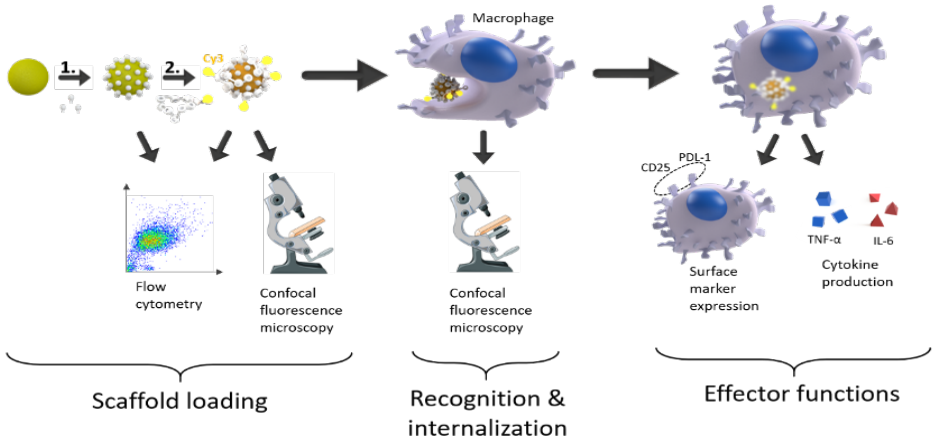

Figure 1: Experimental setup of the described study. Schematic illustrating the process by which the scaffold **Cy3$_{1.5}$CD$_{100}$PIBMA$_{389}$** was loaded onto three different entities and its concomitant effects on immune responses were assessed. The surface of each entity was first functionalized with adamantane (**1.**), followed by **Cy3$_{1.5}$CD$_{100}$PIBMA$_{389}$** loading (**2.**). The presence of loaded scaffold was then confirmed by flow cytometry and confocal fluorescence microscopy. Thereafter, the ability of MoMΦ to recognize and internalize **Cy3$_{1.5}$CD$_{100}$PIBMA$_{389}$**-loaded entities was analyzed by confocal fluorescence microscopy. Finally, MoMΦ effector functions in response to **Cy3$_{1.5}$CD$_{100}$PIBMA$_{389}$**-loaded entities – as gauged by surface marker expression and cytokine

Cy3$_{1.5}$CD$_{100}$PIBMA$_{389}$ is a versatile scaffold that is efficiently loaded onto both Gram-positive and -negative bacteria

Our experimental setup was first validated using 10-20 μm MAA microspheres. To assess whether functionalizing MAA by conjugating Ad to the primary amines of lysine residues via amide linkages was a promising strategy, we used an analogous reagent to couple Cy5 to MAA via amide linkages. Flow cytometric analysis of the resulting Cy5 signal showed this to be an efficient process (Figure 2ai, 2aii). We next confirmed the loading of **Cy3$_{1.5}$CD$_{100}$PIBMA$_{389}$** onto Ad-functionalized MAA by confocal fluorescence microscopy (Figure 3a). Flow cyto-

metric analysis showed **Cy3$_{1.5}$CD$_{100}$PIBMA$_{389}$** loading (Figure 4ai) to be highly efficient, resulting in 98.5±0.25% MAA particles loaded with **Cy3$_{1.5}$CD$_{100}$PIBMA$_{389}$**, and demonstrated that Ad functionalization facilitated **Cy3$_{1.5}$CD$_{100}$PIBMA$_{389}$** loading more than 2-fold (3,556±224 vs 1,606±668, $p < 0.01$, Figure 4aii).

We subsequently moved onto transferring our technology to *Staphylococcus aureus*, a Gram-positive bacterium, and *Escherichia coli*, a Gram-negative bacterium. Doing so involved an alternative Ad functionalization, where Ad was first conjugated to a cationic peptide (UBI$_{29-41}$) known to insert itself into bacterial cell membranes that served as a vector for then introducing Ad onto the bacterial cell surface (Welling et al., 2004). We assessed the feasibility of this approach using a Cy5-labeled UBI$_{29-41}$, and via flow cytometry observed UBI$_{29-41}$ to the efficiently incorporated into both *S. aureus* (Fig 2bi, 2bii) and *E. coli* (Figure 2ci, 2cii). Following this validation we confirmed loading of **Cy3$_{1.5}$CD$_{100}$PIBMA$_{389}$** via confocal fluorescence microscopy onto both Ad-functionalized *S. aureus* (Figure 3b) and *E. coli* (Figure 3c), as evinced by clear Cy3 surface signals that contrasted with Hoechst counterstaining of the cells' cytoplasm (Figure 3d, 3e). Subsequent flow cytometry analysis showed **Cy3$_{1.5}$CD$_{100}$PIBMA$_{389}$** loading rates of 99.5±0.1% for *S. aureus* (Figure 4bi) and 96.4±1.4% for *E. coli* (Figure 4ci). There was a discrepancy between our bacterial platforms regarding the importance of Ad functionalization for facilitating **Cy3$_{1.5}$CD$_{100}$PIBMA$_{389}$** loading: Ad$_2$-UBI$_{29-41}$ surface functionalization enhanced **Cy3$_{1.5}$CD$_{100}$PIBMA$_{389}$** loading to Gram-positive *S. aureus* more than 3-fold (51,786±1,999 vs 17,464±1,273, $p < 0.01$, Figure 4bii), whereas the increase was less than 2-fold for Gram-negative *E. coli* (64,519±10,083 vs 46,456±7,290, $p = 0.07$, Figure 4cii).

Previously, supramolecular host-guest chemistry on cell surfaces has been shown to not adversely affect cell viability (Rood et al., 2017). We similarly did not note any adverse effects of **Cy3$_{1.5}$CD$_{100}$PIBMA$_{389}$** loading on viability for *S. aureus* as gauged by colony counts (12.8±2.9 vs 12±3.3, $p = 0.66$, Figure 5a). However, *E. coli* viability did appear hampered by scaffold loading (4.5±1.5 vs 13.2±7.7, $p = 0.022$, Figure 5b).

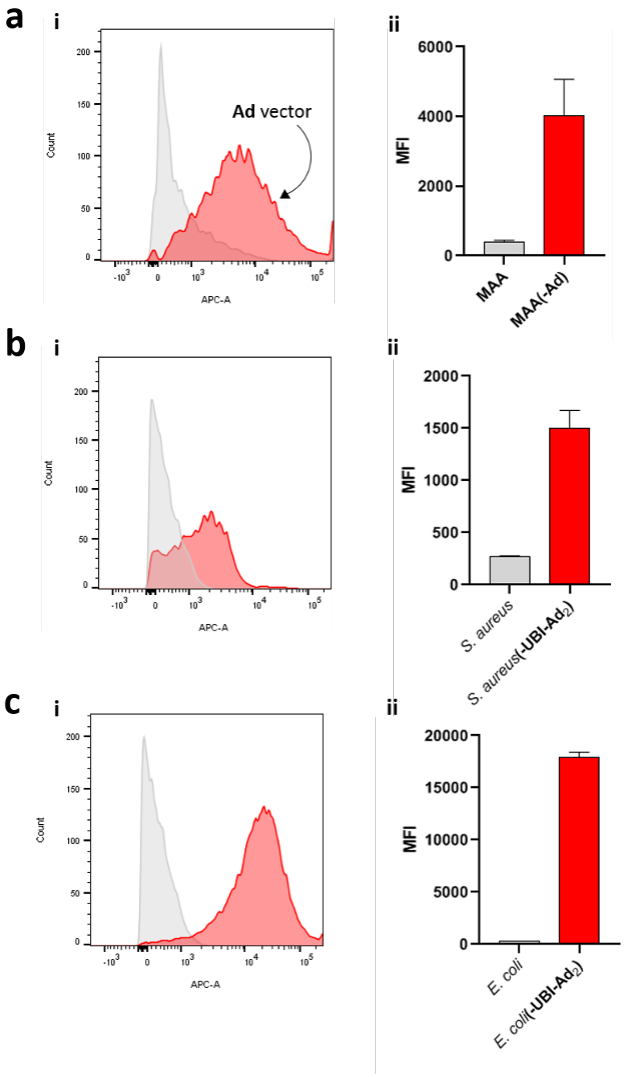

Figure 2: Ad functionalization efficiency for MAA (a), *S. aureus* (b) and *E. coli* (c). Potential Ad functionalization efficiency was assessed with the use of Cy5-labeled vectors (amide bond for MAA, UBI_{29-41} for bacteria) onto MAA/bacterial surfaces. After functionalization Cy5 signals were measured on a flow cytometer **(i)**. Median fluorescent intensities (MFI) of these Cy5 signals for functionalized MAA or bacteria (red) versus unlabeled controls (grey) are given in **(ii)** as means ± standard deviation for a representative experiment of n = 3. Ad = adamantane; MAA = macro-aggregated albumin.

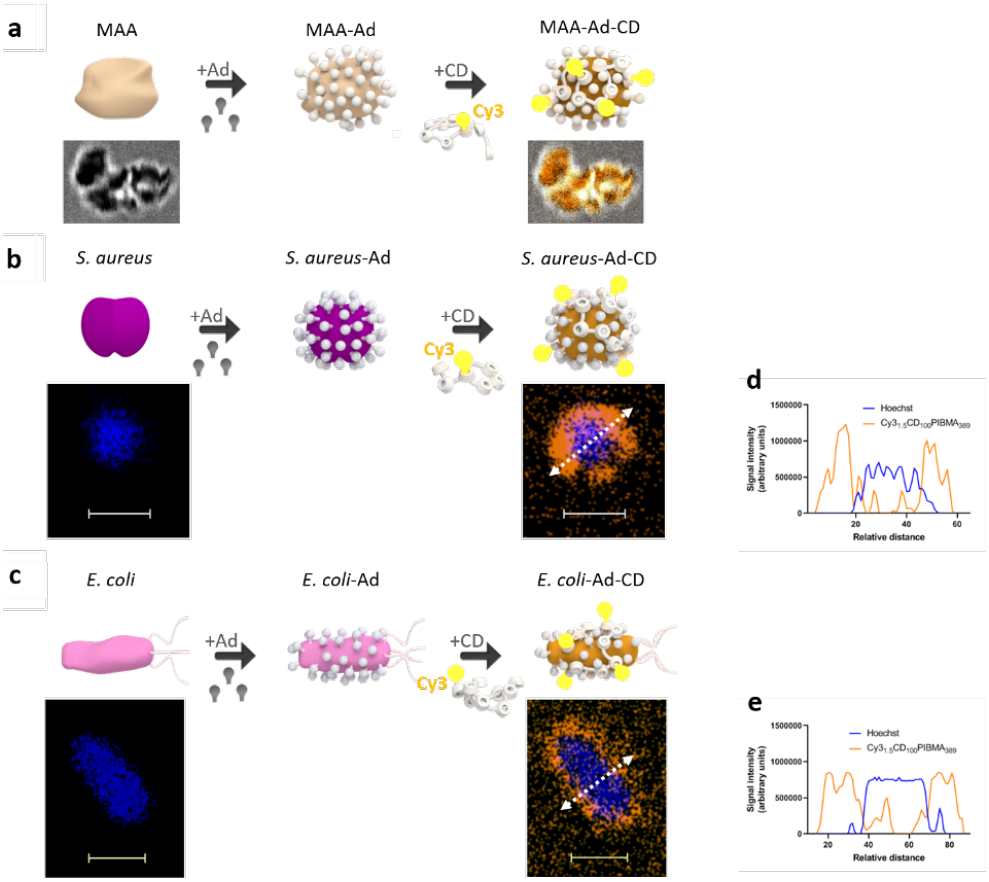

Figure 3: $Cy3_{1.5}CD_{100}PIBMA_{389}$ loading onto a microbial model (a) and two different bacteria (b)(c). Confocal fluorescence microscopy demonstrating the presence of **$Cy3_{1.5}CD_{100}PIBMA_{389}$** loaded onto MAA **(a)**; *S. aureus*, a typical Gram-positive bacterium **(b)**; and *E. coli*, a typical Gram-negative bacterium **(c)**. To assess the location of **$Cy3_{1.5}CD_{100}PIBMA_{389}$** on bacteria, the fluorescent signal intensities of Cy3 and Hoechst in a cross section of the bacteria were analyzed and plotted for *S. aureus* **(d)** and *E. coli* **(e)**. Scale bar = 1 µm. Ad = adamantane; CD = **$Cy3_{1.5}CD_{100}PIBMA_{389}$**; MAA = macro-aggregated albumin.

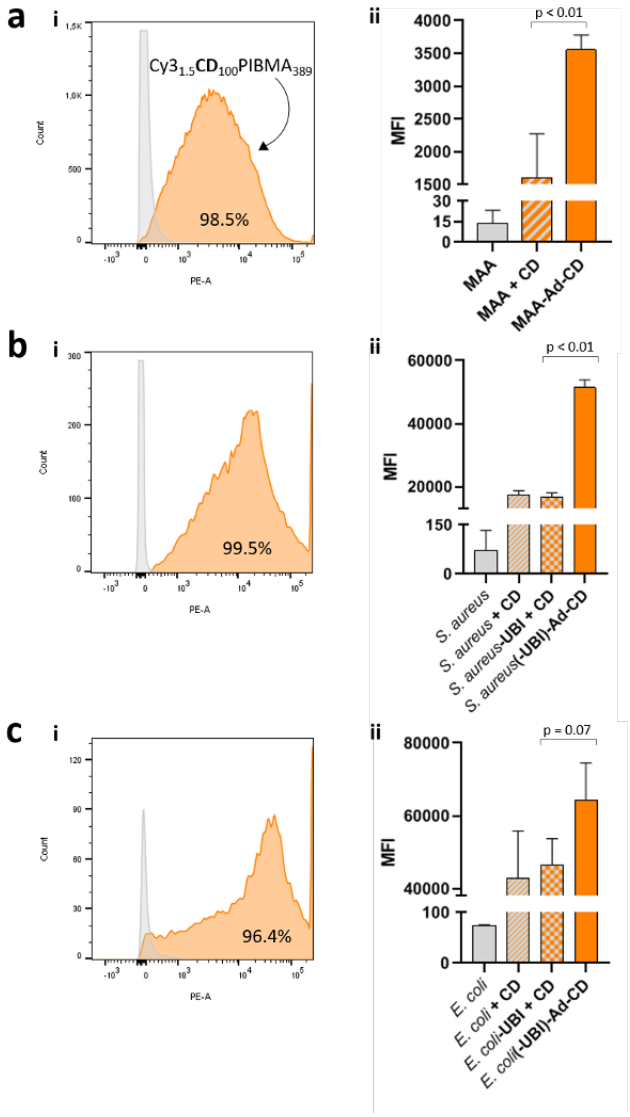

Figure 4: Cy3$_{1.5}$CD$_{100}$PIBMA$_{389}$ loading efficiency for MAA (a), *S. aureus* (b) and *E. coli* (c). Loading was assessed by measuring Cy3 signal intensities **(i)** on a flow cytometer. Median fluorescent intensities (MFI) of these Cy3 signals for loading in the presence of Ad (orange), loading without Ad but with UBI present (grey/orange checkers), loading without Ad and UBI (grey/orange stripes) and unloaded controls (grey) are given in **(ii)** as means ± standard deviation for a representative experiment of n = 3. CD = **Cy3$_{1.5}$CD$_{100}$PIBMA$_{389}$**; MAA = macro-aggregated albumin.

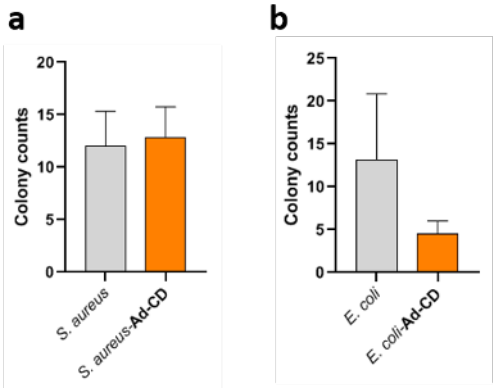

Figure 5: Effect of $Cy3_{1.5}CD_{100}PIBMA_{389}$ loading on viability of *S. aureus* (a) and *E. coli* (b). After **$Cy3_{1.5}CD_{100}PIBMA_{389}$** loading of bacteria ten-fold serial dilutions were prepared and plated in 10 µL aliquots onto BHI agar plates. These plates were incubated overnight, whereafter colonies at the appropriate dilution were counted. Counts are shown as the mean ± standard deviation of loaded (orange) versus unloaded (grey) bacteria in a representative experiment of n = 6. Ad = adamantane; CD = **$Cy3_{1.5}CD_{100}PIBMA_{389}$**.

$Cy3_{1.5}CD_{100}PIBMA_{389}$ loading does not interfere with the core functionalities of monocyte-derived macrophages

To assess whether **$Cy3_{1.5}CD_{100}PIBMA_{389}$** loading adversely affects the functioning of (sentinel) immune cells, we first examined via confocal microscopy the response of monocyte-derived macrophages (MoMΦ) to our **$Cy3_{1.5}CD_{100}PIBMA_{389}$**-loaded MAA/bacteria. **$Cy3_{1.5}CD_{100}PIBMA_{389}$**-loaded MAA particles were readily phagocytosed within 10 minutes, an illustration of which can be seen in Figure 6a. Quantitated phagocytosis of **$Cy3_{1.5}CD_{100}PIBMA_{389}$**-loaded MAA vs control particles showed the two phagocytosed in comparable quantities (37.5±13.6% vs 30.1±9.9%, p = 0.491). Similarly, we found that **$Cy3_{1.5}CD_{100}PIBMA_{389}$**-loaded *S. aureus* (Figure 6b) and *E. coli* (Figure 6c) were phagocytosed within 10 minutes, quantitation of which again showed comparable uptake between loaded and control *S. aureus* (11.1±2.4 vs 14.3±2.7 A.U., p = 0.194) and *E. coli* (7.1±1.6 vs 9.6±3.2 A.U., p = 0.284).

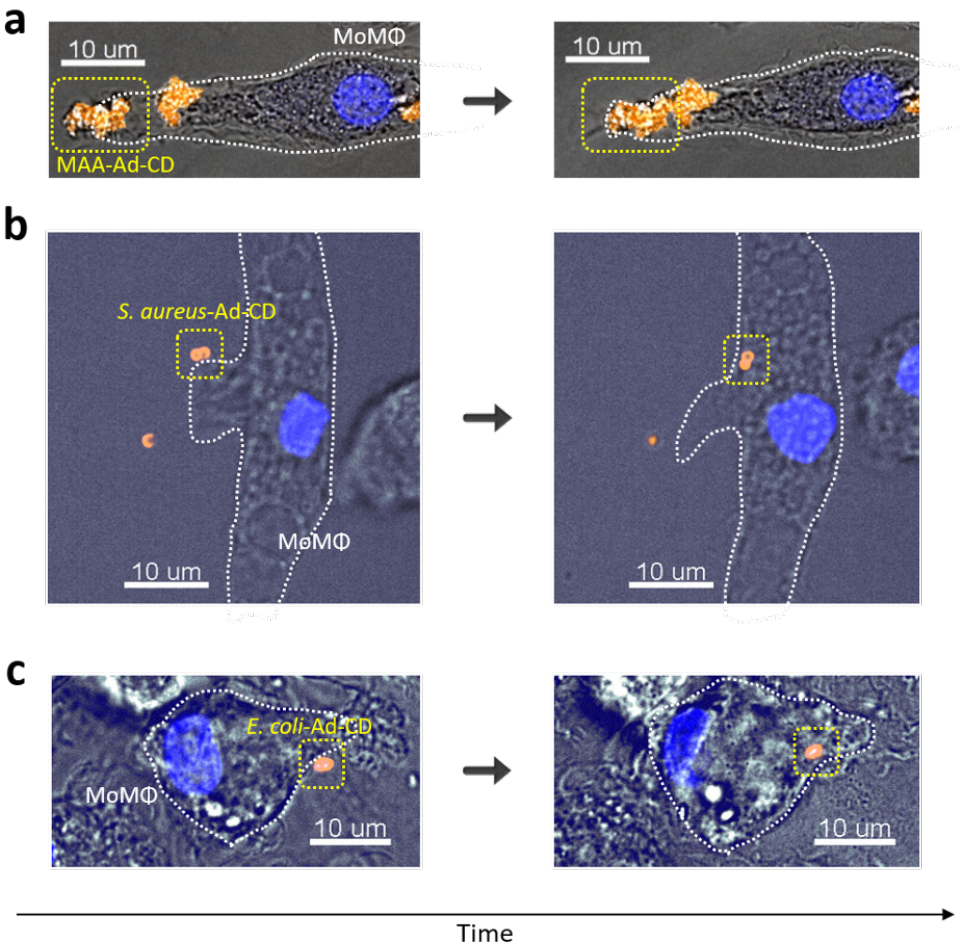

Figure 6: Phagocytic response of MoMΦ to $Cy3_{1.5}CD_{100}PIBMA_{389}$-loaded MAA (a), *S. aureus* (b) and *E. coli* (c). Snapshots demonstrating phagocytic uptake by MoMΦ over a course of about 10 minutes. Ad = adamantane; CD = **$Cy3_{1.5}CD_{100}PIBMA_{389}$**; MAA = macro-aggregated albumin; MoMΦ = monocyte-derived macrophage.

We next assayed the effects of loaded **$Cy3_{1.5}CD_{100}PIBMA_{389}$** on the typical effector functions of MoMΦ: surface marker expression and cytokine production. When stimulated with **$Cy3_{1.5}CD_{100}PIBMA_{389}$**-loaded MAA particles, MoMΦ displayed similar dose-dependent responses in surface marker expression of

CD25 and PDL-1 as seen in response to control MAA particles. At high particle concentrations (1:1 ratio with MoMΦ) both CD25 (2.20±0.55 vs 1.25±0.22 fold-change, Figure 7ai) and PDL-1 (3.02±0.35 vs 1.90±0.19 fold-change, Figure 7aii) expression were elevated in response to **$Cy3_{1.5}CD_{100}PIBMA_{389}$**-loaded MAA particles. Cytokine production also showed increases in TNF-α (281.1±197.8 vs 87.8±48.4 pg/mL, Figure 8ai) and IL-6 (1,402±269.3 vs 616.7±135.6 pg/mL, Figure 8aii) in response to **$Cy3_{1.5}CD_{100}PIBMA_{389}$**-loaded MAA particles at a 1:1 ratio with MoMΦ. However, both increases in surface marker expression and cytokine production were not comparable to responses in positive controls (LPS and IFN-γ stimulated MoMΦ), suggesting that their relevance might be limited. Analogous results were obtained when MoMΦ were stimulated with soluble **$Cy3_{1.5}CD_{100}PIBMA_{389}$** alone (data not shown).

Similar responses were seen in MoMΦ exposed to **$Cy3_{1.5}CD_{100}PIBMA_{389}$**-loaded versus control *S. aureus*. Dose-dependent increases in surface marker expression were again elevated in response to **$Cy3_{1.5}CD_{100}PIBMA_{389}$**-loaded *S. aureus*, especially at high concentrations (4:1 ratio of bacteria to MoMΦ), as seen with increases for CD25 (2.27±0.56 vs 1.4±0.29 fold-change, Figure 7bi) and PDL-1 (2.58±0.49 vs 1.46±0.28 fold-change, Figure 7bii) expression. Cytokine production showed a similar dose-dependent pattern, which at a 4:1 ratio of bacteria to MoMΦ resulted in increases in TNF-α (518.67±394.8 vs 216.7±81.1 pg/mL, Figure 8bi) and IL-6 (28.1±23.9 vs 4.1±4.9 ng/mL, Figure 8bii). Notably, cytokine production was also influenced by Ad functionalization itself: TNF-α production in response to Ad-functionalized *S. aureus* was nearly as high at a 4:1 ratio as that seen in response to **$Cy3_{1.5}CD_{100}PIBMA_{389}$**-loaded *S. aureus* (319.6±197.6 vs 518.67±394.8 pg/mL, Figure 8bi), and IL-6 production was comparable (29.1±19.5 vs 28.1±23.9 ng/mL, Figure 8bii). At lower (1:1 ratio) bacterial concentrations, TNF-α production was actually somewhat higher in response to Ad-functionalized *S. aureus* versus **$Cy3_{1.5}CD_{100}PIBMA_{389}$**-loaded *S. aureus* (447.2±511.9 vs 276.0±326.3 pg/mL, Figure 8bi). As with MAA, these increases were of minor magnitudes compared to increases seen in LPS and IFN-γ stimulated positive controls.

Responses to **$Cy3_{1.5}CD_{100}PIBMA_{389}$**-loaded *E. coli* mostly paralleled the dose-dependent responses seen with MAA and *S. aureus*. Dose-dependent increases elevated over control *E. coli* were observed for both CD25 and PDL-1 expression. These increases were however relatively small compared to the already robust responses to control bacteria (as is typical of *E. coli*), as seen at high bacterial concentrations (4:1 ratio of bacteria to MoMΦ) for both CD25 (8.02±1.51 vs 6.84±0.79 fold-change, Figure 7ci) and PDL-1 (5.97±1.06 vs 4.69±0.81 fold-change, Figure 7cii). Cytokine production with respect to TNF-α was unaffected by loaded **$Cy3_{1.5}CD_{100}PIBMA_{389}$** even at high bacterial concentrations of 4:1 (2,043±942 vs 2,898±919 pg/mL, Figure 8ci). IL-6 production was also com-

parable between **Cy3$_{1.5}$CD$_{100}$PIBMA$_{389}$**-loaded and control *E. coli* at high bacterial concentrations (4:1); however, at lower bacterial concentrations (1:1 ratio) loaded **Cy3$_{1.5}$CD$_{100}$PIBMA$_{389}$** and Ad functionalization appeared to depress IL-6 production (7.6±6.1 vs 22.5±16.5 ng/mL, Figure 8cii).

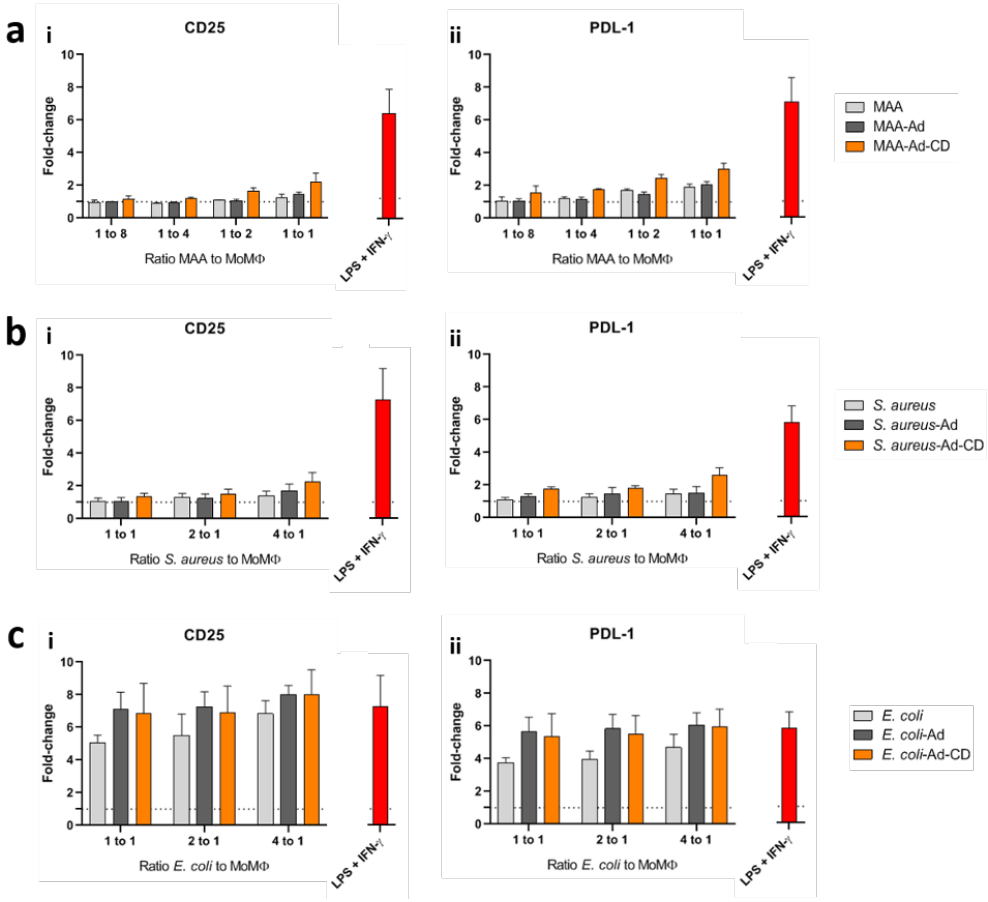

Figure 7: Surface marker responses of MoMΦ to Cy3$_{1.5}$CD$_{100}$PIBMA$_{389}$-loaded MAA (a), *S. aureus* (b) or *E. coli* (c). Expression levels of CD25 **(i)** and PDL-1 **(ii)** given as fold-change of median fluorescent intensity versus baseline expression in unstimulated MoMΦ by flow cytometry. Control MAA/bacteria are given in light grey, Ad-functionalized controls in dark grey, and loaded MAA/bacteria in orange; positive controls stimulated with LPS and IFN-γ are shown in red. Data are represented as means ± standard deviation for representative experiments of n = 3. MAA = macro-aggregated albumin; MoMΦ = monocyte-derived macrophages; Ad = adamantane.

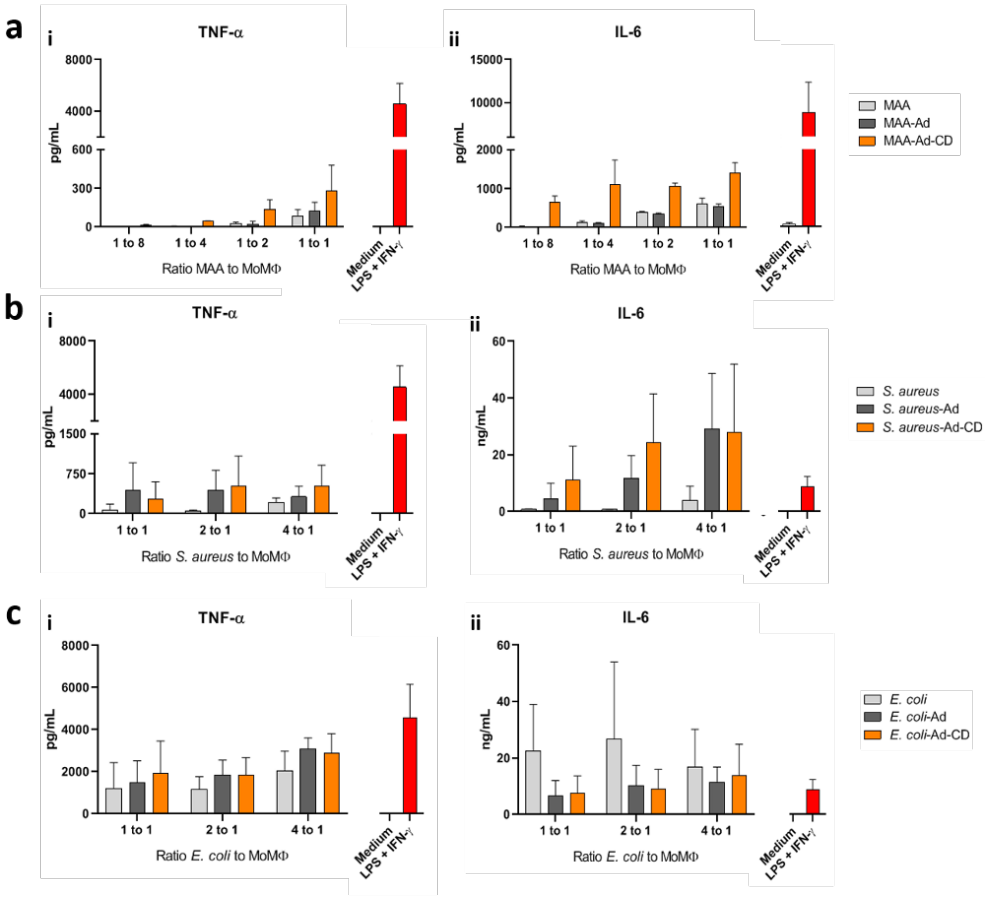

Figure 8: Cytokine responses of MoMΦ to $Cy3_{1.5}CD_{100}PIBMA_{389}$-loaded MAA (a), *S. aureus* (b) or *E. coli* (c). Concentrations of the cytokines TNF-α **(i)** and IL-6 **(ii)** in MoMΦ culture supernatants 24 hours after stimulation, as measured via ELISA. Control MAA/bacteria are given in light grey, Ad-functionalized controls in dark grey, and loaded MAA/bacteria in orange. MoMΦ stimulated with medium (beige) or LPS and IFN-γ (red) served as negative and positive controls, respectively. Data shown are means ± standard deviation for representative experiments of n = 3. MAA = macro-aggregated albumin; MoMΦ = monocyte-derived macrophages; Ad = adamantane.

Discussion

The present study shows that supramolecular host-guest chemistry can be effectively harnessed to load both Gram-positive and-negative bacterial surfaces with a versatile chemical scaffold. The scaffold **$Cy3_{1.5}CD_{100}PIBMA_{389}$** loaded

onto bacteria did not impair immune recognition of these bacteria by MoMΦs, as gauged by phagocytic capacity, surface marker expression and cytokine production. This technology may thus be an attractive platform for future investigations requiring precise introduction of immunomodulatory components onto bacterial pathogens.

Existing strategies for modifying bacterial surfaces have generally relied on covalently binding moieties of interest to either cell surface amines/thiols or unnatural chemical ligands, such as aldehydes, introduced metabolically (Bi et al., 2018; Dumont et al., 2012; Taherkhani et al., 2014). Our modification method demonstrates that non-covalent chemistry harnessing supramolecular interactions between CD and Ad is equally able to modify bacterial surfaces, and unlike covalent binding does not generally perturb normal functioning of e.g. cell surface proteins (Bi et al., 2018). Introduction of Ad functionalization on the surface of MAA and bacteria significantly promoted the loading of **$Cy3_{1.5}CD_{100}PIBMA_{389}$**, particularly for the Gram-positive *S. aureus*, probably because these bacteria lack the highly heterogenous constituents of Gram-negative surfaces containing certain hydrophobic structures able to mimic Ad's supramolecular interactions with CD (Hooda and Moraes, 2018; Rood et al., 2017; Thanassi et al., 2012; Whitfield and Trent, 2014).

We found that our cell surface modification method preserved the capacity of MoMΦs to engage and recognize **$Cy3_{1.5}CD_{100}PIBMA_{389}$**-loaded MAA and bacteria. Phagocytosis of **$Cy3_{1.5}CD_{100}PIBMA_{389}$**-loaded MAA and bacteria was not inhibited by the presence of CD carbohydrates, an important finding for possible future application of the technology to introduce immunomodulatory components onto bacteria. MoMΦs that phagocytosed **$Cy3_{1.5}CD_{100}PIBMA_{389}$**-loaded MAA and bacteria retained their ability to respond normally to these entities as gauged by surface marker expression and cytokine production. This was most evident in analyzing responses to *E. coli*: robust CD25 and PDL-1 expression and TNF-α production were seen for both control and **$Cy3_{1.5}CD_{100}PIBMA_{389}$**-loaded *E. coli*. Altogether, these findings suggest our **$Cy3_{1.5}CD_{100}PIBMA_{389}$** chemical scaffolds are well-suited for introducing modifications onto bacterial surfaces and can be used to investigate interactions between bacteria and the immune system.

An unexpected finding to emerge from this study was that our **$Cy3_{1.5}CD_{100}PIBMA_{389}$** scaffolds are in themselves somewhat immunogenic. We generally observed dose-dependently increased pro-inflammatory responses to **$Cy3_{1.5}CD_{100}PIBMA_{389}$**-loaded MAA, *S. aureus* and *E. coli*. Remarkably, these increases were most evident with MAA. However, the increases were also notable in bacteria, especially *S. aureus*, with respect to cytokine production. Such disparities between surface markers and cytokines are reflective of the complexity of assess-

ing immune processes using simplified *in vitro* models and indicate the need to ultimately fully evaluate immune responses in more representative *in vivo* models. The immunogenicity of **Cy3**$_{1.5}$**CD**$_{100}$**PIBMA**$_{389}$ is likely mediated by its CD carbohydrates, as studies have identified various immunogenic carbohydrate structures in plants, bacteria and parasites (Matsuo et al., 2014; Pazur and Forsberg, 1980; Weiss et al., 1986). This is a natural consequence of the important role that carbohydrate diversity plays in recognition of self and non-self structures (Amon et al., 2014; Moremen et al., 2012). In addition, Ad$_2$-UBI$_{29-41}$ alone also seemed to have a mildly proinflammatory potential as suggested by the cytokine profiles, possibly mediated by the hydrocarbon components (Brinchmann et al., 2018; Michael et al., 2013; Osgood et al., 2017). While these unexpected immunogenic properties were interesting to note, they were very modest compared to positive controls and as such are unlikely to significantly impact implementation of the presented technology.

Theoretically, the presented technology could be utilized as a tool for adjuvanting (bacterial) whole-organism vaccines. Although whole-organism vaccines generally have less attractive safety profiles, they may be considered for diseases where subunit vaccines provide insufficient protection. The presented technology provides a means of further boosting immune responses to intact bacterial vaccines by physically conjugating immunogenic adjuvants. For instance, introducing LPS-like immunogens onto whole-organism vaccines could, analogously to subunit vaccinology, enhance the immunogenicity of any bacterium.

In conclusion, we have here shown that supramolecular host-guest chemistry between CD and Ad can be utilized to efficiently load versatile chemical scaffolds onto both Gram-positive and negative bacteria, and that these scaffolds are well-tolerated by a canonical immune cell. We thus believe this method provides a useful tool for future investigations seeking to alter the immunogenic properties of (bacterial) pathogens for the purposes of either dissecting the complex host-pathogen interactions involved in infectious disease etiology or developing novel interventions against infectious diseases.

References

Amon, R., Reuven, E.M., Leviatan Ben-Arye, S., and Padler-Karavani, V. (2014). Glycans in immune recognition and response. Carbohydr Res *389*, 115-122.

Annane, D., Bellissant, E., and Cavaillon, J.M. (2005). Septic shock. Lancet *365*, 63-78.

Bekeredjian-Ding, I., Stein, C., and Uebele, J. (2017). The Innate Immune Response Against Staphylococcus aureus. Curr Top Microbiol Immunol *409*, 385-418.

Bi, X., Yin, J., Chen Guanbang, A., and Liu, C.F. (2018). Chemical and Enzymatic Strategies for Bacterial and Mammalian Cell Surface Engineering. Chemistry *24*, 8042-8050.

Brinchmann, B.C., Skuland, T., Rambol, M.H., Szoke, K., Brinchmann, J.E., Gutleb, A.C., Moschini, E., Kubatova, A., Kukowski, K., Le Ferrec, E.*, et al.* (2018). Lipophilic components of diesel exhaust particles induce pro-inflammatory responses in human endothelial cells through AhR dependent pathway(s). Part Fibre Toxicol *15*, 21.

Dumont, A., Malleron, A., Awwad, M., Dukan, S., and Vauzeilles, B. (2012). Click-mediated labeling of bacterial membranes through metabolic modification of the lipopolysaccharide inner core. Angew Chem Int Ed Engl *51*, 3143-3146.

Faria, M., Bjornmalm, M., Thurecht, K.J., Kent, S.J., Parton, R.G., Kavallaris, M., Johnston, A.P.R., Gooding, J.J., Corrie, S.R., Boyd, B.J.*, et al.* (2018). Minimum information reporting in bio-nano experimental literature. Nat Nanotechnol *13*, 777-785.

Gautam, S., Gniadek, T.J., Kim, T., and Spiegel, D.A. (2013). Exterior design: strategies for redecorating the bacterial surface with small molecules. Trends Biotechnol *31*, 258-267.

Goldmann, O., and Medina, E. (2018). Staphylococcus aureus strategies to evade the host acquired immune response. Int J Med Microbiol *308*, 625-630.

Gonzalez-Campo, A., Hsu, S.H., Puig, L., Huskens, J., Reinhoudt, D.N., and Velders, A.H. (2010). Orthogonal covalent and noncovalent functionalization of cyclodextrin-alkyne patterned surfaces. J Am Chem Soc *132*, 11434-11436.

Hooda, Y., and Moraes, T.F. (2018). Translocation of lipoproteins to the surface of gram negative bacteria. Curr Opin Struct Biol *51*, 73-79.

Kong, N.C., Beran, J., Kee, S.A., Miguel, J.L., Sanchez, C., Bayas, J.M., Vilella, A., Calbo-Torrecillas, F., Lopez de Novales, E., Srinivasa, K.*, et al.* (2008). A new adjuvant improves the immune response to hepatitis B vaccine in hemodialysis patients. Kidney Int *73*, 856-862.

Kumar, H., Kawai, T., and Akira, S. (2011). Pathogen recognition by the innate immune system. Int Rev Immunol *30*, 16-34.

Maldonado, R.F., Sa-Correia, I., and Valvano, M.A. (2016). Lipopolysaccharide modification in Gram-negative bacteria during chronic infection. FEMS Microbiol Rev *40*, 480-493.

Matsuo, K., Kagaya, U., Itchoda, N., Tabayashi, N., and Matsumura, T. (2014). Deletion of plant-specific sugar residues in plant N-glycans by repression of GDP-D-mannose 4,6-dehydratase and beta-1,2-xylosyltransferase genes. J Biosci Bioeng *118*, 448-454.

Michael, S., Montag, M., and Dott, W. (2013). Pro-inflammatory effects and oxidative stress in lung macrophages and epithelial cells induced by ambient particulate matter. Environ Pollut *183*, 19-29.

Mogensen, T.H. (2009). Pathogen recognition and inflammatory signaling in innate immune defenses. Clin Microbiol Rev *22*, 240-273, Table of Contents.

Mongis, A., Piller, F., and Piller, V. (2017). Coupling of Immunostimulants to Live Cells through Metabolic Glycoengineering and Bioorthogonal Click Chemistry. Bioconjug Chem *28*, 1151-1165.

Moremen, K.W., Tiemeyer, M., and Nairn, A.V. (2012). Vertebrate protein glycosylation: diversity, synthesis and function. Nat Rev Mol Cell Biol *13*, 448-462.

Naber, C.K. (2009). Staphylococcus aureus bacteremia: epidemiology, pathophysiology, and management strategies. Clin Infect Dis *48 Suppl 4*, S231-237.

Neirynck, P., Brinkmann, J., An, Q., van der Schaft, D.W., Milroy, L.G., Jonkheijm, P., and Brunsveld, L. (2013). Supramolecular control of cell adhesion via ferrocene-cucurbit[7]uril host-guest binding on gold surfaces. Chem Commun (Camb) *49*, 3679-3681.

Osgood, R.S., Upham, B.L., Bushel, P.R., Velmurugan, K., Xiong, K.N., and Bauer, A.K. (2017). Secondhand Smoke-Prevalent Polycyclic Aromatic Hydrocarbon Binary Mixture-Induced Specific Mitogenic and Pro-inflammatory Cell Signaling Events in Lung Epithelial Cells. Toxicol Sci *157*, 156-171.

Paavonen, J., Naud, P., Salmeron, J., Wheeler, C.M., Chow, S.N., Apter, D., Kitchener, H., Castellsague, X., Teixeira, J.C., Skinner, S.R.*, et al.* (2009). Efficacy of human papillomavirus (HPV)-16/18 AS04-adjuvanted vaccine against cervical infection and precancer caused by oncogenic HPV types (PATRICIA): final analysis of a double-blind, randomised study in young women. Lancet *374*, 301-314.

Pazur, J.H., and Forsberg, L.S. (1980). The sugar sequence of a streptococcal, immunogenic tetraheteroglycan: a revision. Carbohydr Res *83*, 406-408.

Rodell, C.B., Mealy, J.E., and Burdick, J.A. (2015). Supramolecular Guest-Host Interactions for the Preparation of Biomedical Materials. Bioconjug Chem *26*, 2279-2289.

Rood, M.T., Spa, S.J., Welling, M.M., Ten Hove, J.B., van Willigen, D.M., Buckle, T., Velders, A.H., and van Leeuwen, F.W. (2017). Obtaining control of cell surface functionalizations via Pre-targeting and Supramolecular host guest interactions. Sci Rep *7*, 39908.

Spa, S.J., Welling, M.M., van Oosterom, M.N., Rietbergen, D.D.D., Burgmans, M.C., Verboom, W., Huskens, J., Buckle, T., and van Leeuwen, F.W.B. (2018). A Supramolecular Approach for Liver Radioembolization. Theranostics *8*, 2377-2386.

Taherkhani, S., Mohammadi, M., Daoud, J., Martel, S., and Tabrizian, M. (2014). Covalent binding of nanoliposomes to the surface of magnetotactic bacteria for the synthesis of self-propelled therapeutic agents. ACS Nano *8*, 5049-5060.

Thanassi, D.G., Bliska, J.B., and Christie, P.J. (2012). Surface organelles assem-

bled by secretion systems of Gram-negative bacteria: diversity in structure and function. FEMS Microbiol Rev *36*, 1046-1082.

Weiss, J.B., Magnani, J.L., and Strand, M. (1986). Identification of Schistosoma mansoni glycolipids that share immunogenic carbohydrate epitopes with glycoproteins. J Immunol *136*, 4275-4282.

Welling, M.M., Spa, S.J., van Willigen, D.M., Rietbergen, D.D.D., Roestenberg, M., Buckle, T., and van Leeuwen, F.W.B. (2019). In vivo stability of supramolecular host-guest complexes monitored by dual-isotope multiplexing in a pre-targeting model of experimental liver radioembolization. J Control Release *293*, 126-134.

Welling, M.M., Visentin, R., Feitsma, H.I., Lupetti, A., Pauwels, E.K., and Nibbering, P.H. (2004). Infection detection in mice using 99mTc-labeled HYNIC and N2S2 chelate conjugated to the antimicrobial peptide UBI 29-41. Nucl Med Biol *31*, 503-509.

Whitfield, C., and Trent, M.S. (2014). Biosynthesis and export of bacterial lipopolysaccharides. Annu Rev Biochem *83*, 99-128.

Willyard, C. (2017). The drug-resistant bacteria that pose the greatest health threats. Nature *543*, 15.

Wolf, A.J., and Underhill, D.M. (2018). Peptidoglycan recognition by the innate immune system. Nat Rev Immunol *18*, 243-254.

Wynn, T.A., Chawla, A., and Pollard, J.W. (2013). Macrophage biology in development, homeostasis and disease. Nature *496*, 445-455.

Methods

Preparation of $Cy3_{1.5}CD_{100}PIBMA_{389}$-bound protein aggregates and bacteria

The material characteristics of **$Cy3_{1.5}CD_{100}PIBMA_{389}$** in the context of these experiments as per recommended guidelines (Faria et al., 2018) are as follows. **$Cy3_{1.5}CD_{100}PIBMA_{389}$** synthesis was accomplished by grafting the nucleophiles β-CD-NH_2 and Cy3-NH_2 onto the anhydrides of poly(isobutylene-*alt*-maleic-anhydride) in a solution of dry DMSO together with DIPEA, followed by hydrolyzing the non-reacted anhydrides to carboxylates. Thereafter, ethanolamine was conjugated to the free carboxylates via an amide linkage backbone in order to sequester the carboxylates' negative charges, and the product purified by dialysis. The exact conditions used can be found as previously described (Rood et al., 2017). ^{1}H-NMR and NMR Diffusion Ordered Spectroscopy (DOSY) determined the product to contain about 100 β-CD units and 1.5 Cy3 units. The product, in linear form, was estimated to be about 240 nm long and 4 nm wide, with a weight of approximately 190 kDa.

To first bind **$Cy3_{1.5}CD_{100}PIBMA_{389}$** to macro-aggregated albumin (MAA), a protein aggregate representing a simplified bacterium, 100 µL MAA (2 mg/mL) (TechneScan LyoMAA, London, UK) was sonicated (to break up larger aggregates), added to 100 µL of a 1 µM solution of Ad-TFP (tri(2-furyl)phosphine) in PBS supplemented with 2 mg/mL bovine serum albumin (BSA) and incubated for 30 minutes at 37 °C with shaking. The reaction mixture was centrifuged at 1,600 RCF for 3 minutes, supernatant removed and the pellet resuspended in 1 mL PBS with BSA; washing was repeated twice. Subsequently, the pellet was resuspended in 100 µL of a 1 µM solution of **$Cy3_{1.5}CD_{100}PIBMA_{389}$** in PBS and incubated for 60 minutes at 37 °C with shaking. Subsequently, this mixture was similarly washed three times by centrifuging at 1,600 RCF for 3 minutes, removing supernatant and resuspending the pellet in 1 mL PBS with BSA. After resuspending the product in 100 µL PBS with BSA, the concentration in units of particles/mL was determined using a Bürker counting chamber. This value was used to prepare eventual dilutions in RPMI (Life Sciences™ GIBCO®, Thermo Fischer Scientific, Waltham, MA, USA) + 10% fetal bovine serum (FBS) (Capricorn Scientific, Ebsdorfergrund, Germany) for analysis by confocal microscopy and flow cytometry.

To initially bind **$Cy3_{1.5}CD_{100}PIBMA_{389}$** to bacteria using Ad functionalization introduced via cell surface lysine residues, 10^7 bacteria (*Staphylococcus aureus* and *Escherichia coli*) were added to 100 µL of a 1 µM solution of Ad-TFP in PBS (also containing 10 µM Hoechst 33342 (Sigma-Aldrich (St. Louis, MO, USA)) and incubated for 30 minutes at 37 °C with shaking. The reaction mixture was then

centrifuged at 10,000 RCF for 5 minutes, supernatant was removed, and the pellet resuspended in 1 mL PBS; washing was repeated twice. After washing, the pellet was resuspended in 100 μL of a 1 μM solution of **$Cy3_{1.5}CD_{100}PIBMA_{389}$** in PBS and incubated for 60 minutes at 37 °C with shaking. The mixture was then washed thrice with PBS as described above. After washing, the pellet was resuspended in 100 μL PBS and analyzed by confocal microscopy.

To alternatively bind **$Cy3_{1.5}CD_{100}PIBMA_{389}$** to bacteria using Ad functionalization introduced via a membrane-adhering ubiquicidin peptide (UBI_{29-41}), 10^7 bacteria were added to 100 μL of a 8 μM solution of UBI-Ad_2 in 25 mM ammonium acetate buffer pH 5 (also containing 10 μM Hoechst 33342) and incubated for 30 minutes at 37 °C with shaking. The mixture was then centrifuged at 10,000 RCF for 5 minutes, supernatant was removed, and the pellet resuspended in PBS; washing was repeated twice. Subsequently, the pellet was resuspended in 100 μL of a 1 μM solution of **$Cy3_{1.5}CD_{100}PIBMA_{389}$** in PBS and incubated for 30 minutes at 37 °C with shaking. The mixture was then washed 3 times in PBS, and finally resuspended in 100 μL RPMI + 10% FBS to create a stock solution used to prepare dilutions in RPMI + 10% FBS for analysis by confocal microscopy and flow cytometry.

Analysis of $Cy3_{1.5}CD_{100}PIBMA_{389}$-bound protein aggregates and bacteria

$Cy3_{1.5}CD_{100}PIBMA_{389}$ bound to MAA or bacteria was first qualitatively detected by confocal microscopy performed on a Leica Sp8 WLL confocal microscope using LAS X software. Prior to microscopy, 10 μL inoculums containing ~10^6 units MAA or bacteria were added to glass bottom microwell dishes (MatTek Corporation, Ashland, MA, USA), overlaid with 1% agarose pads (to eliminate Brownian motion interfering with digital image acquisition), and finally overlaid with a coverslip.

Quantitation of Ad functionalization and **$Cy3_{1.5}CD_{100}PIBMA_{389}$** binding efficiency was performed by flow cytometry on BD (Franklin Lakes, NJ, USA) LSRFortessa ™ X-20 or FACSCanto II instruments using FACSDiva ™ software using the abovementioned procedures and reagents or analogues thereof. Bacteria were isolated from debris by gating on their Hoechst signal.

To assess the viability of **$Cy3_{1.5}CD_{100}PIBMA_{389}$**-bound bacteria, $6.4x10^6$ CFU/mL bacteria underwent the abovementioned procedure. These bacteria were then serially diluted 10-fold and 10 μL inoculums from each dilution pipetted onto BHI agar plates. These plates were cultured overnight at 37 °C, after which colonies on plates were counted.

Analysis of phagocytic responses

MoMΦ were prepared as follows. Peripheral blood from volunteers was diluted 1:1 with room temperature HBSS (Life Sciences™ GIBCO®) containing 100 U/mL penicillin and 100 μg/mL streptomycin. Ficoll (Apotheek AZL, Lokeren, The Netherlands) was added underneath diluted blood and samples were spun at 400 RCF for 25 minutes with slow deceleration. Peripheral blood mononuclear cells (PBMCs) above the Ficoll phase were carefully isolated with a Pasteur pipette and diluted 1:1 with HBSS + 1% fetal bovine serum (FBS). PBMCs were spun at 200 RCF for 20 minutes. Supernatant was removed, and the pellet resuspended in HBSS + 1% FBS. PBMCs were again spun at 200 RCF for 20 minutes. Supernatant was removed, and the pellet resuspended in MACS buffer (PBS + 0.5% BSA + 2 mM EDTA). After PBMCs were counted, PBMCs were centrifuged at 300 RCF at 4 °C for 10 minutes. Supernatant was removed, and cells were resuspended in 95 μL/10^7 cells MACS buffer. To this suspension 5 μL/10^7 cells Miltenyi Biotec MACS CD14 MicroBeads (Cologne, Germany) were added. PBMCs were then incubated for 15 minutes at 4 °C. After incubation, cells were washed with MACS buffer and centrifuged at 300 RCF at 4°C for 10 minutes. Supernatant was removed, cells were resuspended in 1 mL MACS buffer, and the suspension was run through a Miltenyi Biotec MACS LS column attached to a magnetic separator. The column was washed thrice with MACS buffer. After removing the column from the magnetic separator, the column was flushed with RPMI (Life Sciences™ GIBCO®) containing 100 U/mL penicillin and 100 μg/mL streptomycin. Monocytes were centrifuged at 300 RCF at 4 °C for 10 minutes. After removing supernatant, monocytes were resuspended in RPMI + 10% FBS and counted.

To differentiate monocytes into macrophages, monocytes were plated at a density of 400.000 cells/mL in RPMI + 10% FBS supplemented with 20 ng/mL macrophage colony-stimulating factor and incubated at 37 °C. After 2-3 days, medium was refreshed. After 6 days, macrophages were resuspended by scraping with a pipette tip and counted, whereafter they were ready for downstream applications.

Confocal microscopy was performed on a Leica Sp8 WLL confocal microscope using LAS X software. One day prior to microscopy, $5*10^4$ MoMΦ were incubated on glass bottom microwell dishes (MatTek Corporation) in a 200 μL drop of RPMI + 10% FBS for 2 hours at 37 °C. Once MoMΦ had adhered, an additional 1.8 mL RPMI + 10% FBS was added, and MoMΦ were incubated at 37 °C overnight. Immediately prior to microscopy the next day, RPMI + 10% FBS was removed from the confocal dish, a 10 μL inoculum added to the MoMΦ, and a coverslip overlaid on the cells. MoMΦ behavior was then analyzed in a 37 °C environment.

Analysis of immune responses

All experiments were performed in triplicate. MoMΦ post-harvesting were plated at a density of 10^5 cells/100 µL in 96-well plates (Thermo Fischer Scientific) and incubated for 24 hours at 37 °C. Thereafter, MoMΦ were stimulated with 100 µL of various MAA/*S. aureus*/*E. coli*-Ad-CD dilutions and allowed to incubate another 24 hours at 37 °C. Subsequently, supernatants were removed and stored for eventual cytokine analysis. Wells were filled with cold PBS, and cells harvested by scraping with a pipette tip and transferring to a FACS V-bottom plate (Thermo Fischer Scientific). Cells were centrifuged at 350 RCF and 4 °C for 4 minutes and supernatant discarded. Pellets were resuspended in 50 µL Aqua solution (Thermo Fisher Scientific) and incubated on ice for 20 minutes. Thereafter, 150 µL 1.9% paraformaldehyde was added, and cells incubated on ice for 15 minutes. Cells were centrifuged at 350 RCF and 4 °C for 4 minutes and supernatant discarded. Pellets were resuspended in 200 µL PBS, centrifuged at 350 RCF and 4 °C for 4 minutes, and supernatant discarded. Pellets were then resuspended in 30 µL antibody mix and incubated for 30 minutes at 4 °C. After incubation, 170 µL PBS was added, cells were centrifuged at 350 RCF and 4 °C for 4 minutes, and supernatant was discarded. Pellets were resuspended in 50 µL FACS buffer (PBS + 0.5% BSA + 2 mM EDTA) and transferred to 1.4 mL FACS tubes. These samples were then run through a BD LSRFortessa ™ X-20 using BD FACSDiva ™ software.

Cytokine production in MoMΦ culture supernatants was assayed using kits from BD Biosciences; specifically, Human TNF ELISA Set (Cat. No. 555212) and Human IL-6 ELISA Set (Cat. No. 555220) kits were used according to the manufacturer's specifications and analyzed by a Thermo Fischer Scientific Multiskan FC plate reader.

Statistical analysis

Mean values were compared by Student's t-test performed using SPSS 25 software (IBM, Armonk, NY, USA).

Acknowledgments

The authors would like to acknowledge Sven van Leeuwen for helping generate the superlative graphics used in this paper.

Funding

The research leading to these results has received funding from a ZONMW VENI grant (016.156.076) financed by the Netherlands Organization for Scientific Research (NWO) and an LUMC PhD project grant (18-1919).

3

Cyclodextrin/adamantane-mediated targeting of inoculated bacteria in mice

Mick M. Welling, Nikolas Duszenko, Danny M. van Willigen, Wiep-Klaas Smits, Tessa Buckle, Meta Roestenberg and Fijs W. B. van Leeuwen

Adapted from:

Bioconjug Chem. 2021 Mar 17;32(3):607-614.
PMID: 33621052
DOI: doi: 10.1021/acs.bioconjchem.1c00061.

Abstract

Cyclodextrin (CD)-based host–guest interactions with adamantane (Ad) have demonstrated use for functionalizing living cells in vitro. The next step in this supramolecular functionalization approach is to explore the concept to deliver chemical cargo to living cells in vivo, e.g., inoculated bacteria, in order to study their dissemination. We validated this concept in two rodent Staphylococcus aureus models. Bacteria (1×10^8 viable S. aureus) were inoculated by (1) intramuscular injection or (2) intrasplenic injection followed by dissemination throughout the liver. The bacteria were prefunctionalized with ^{99m}Tc-UBI$_{29–41}$-Ad$_2$ (primary vector), which allowed us to both determine the bacterial load and create an in vivo target for the secondary host-vector (24 h post-inoculation). The secondary vector, i.e., chemical cargo delivery system, made use of a ^{111}In-Cy5$_{0.5}$CD$_9$PIBMA$_{39}$ polymer that was administered intravenously. Bacteria-specific cargo delivery as a result of vector complexation was evaluated by dual-isotope SPECT imaging and biodistribution studies (^{111}In), and by fluorescence (Cy5); these evaluations were performed 4 h post-injection of the secondary vector. Mice inoculated with nonfunctionalized S. aureus and mice without an infection served as controls. Dual-isotope SPECT imaging demonstrated that ^{111}In-Cy5$_{0.5}$CD$_9$PIBMA$_{39}$ colocalized with ^{99m}Tc-UBI$_{29–41}$-Ad$_2$-labeled bacteria in both muscle and liver. In inoculated muscle, a 2-fold higher uptake level (3.2 ± 1.0%ID/g) was noted compared to inoculation with nonfunctionalized bacteria (1.9 ± 0.4%ID/g), and a 16-fold higher uptake level compared to noninfected muscle (0.2 ± 0.1%ID/g). The hepatic accumulation of the host-vector was nearly 10-fold higher (27.1 ± 11.1%ID/g) compared to the noninfected control (2.7 ± 0.3%ID/g; $p < 0.05$). Fluorescence imaging of the secondary vector corroborated SPECT-imaging and biodistribution findings. We have demonstrated that supramolecular host–guest complexation can be harnessed to achieve an in vivo cargo delivery strategy, using two different bacterial models in soft tissue and liver. This proof-of-principle study paves a path toward developing innovative drug delivery concepts via cell functionalization techniques.

Introduction

Cyclodextrin (CD)-based host-guest supramolecular interactions with adamantane (Ad) have recently received considerable attention for the potential they hold for advancing precision medicine (Lai et al., 2017; Yu and Chen, 2019). In the past, CDs' ability to bind lipophilic drugs has led to CD mostly being used to improve solubility and biodistribution (Saokham et al., 2018). More recently, CD-based host-guest chemistry has been used to create a variety of nanoparticle and surface functionalizations (Challa et al., 2005; Paolino et al., 2013). Unique to such systems is the specificity of well-defined (multivalent) host-guest interaction, which allows a wide range of functionalities, like nanoparticles or polymers, to be introduced on various surfaces (Li et al., 2017; Rood et al., 2017; Wu et al., 2015). This chemical concept has even been used to bind bacteria to functionalized surfaces (Sankaran et al., 20155).

A further step has been taken by applying CD-based host-guest chemistry *in vitro* on surfaces of macro aggregated albumin microspheres (MAA; diameter 10-90 μm) (Spa et al., 2018; Welling et al., Accepted; Welling et al., 2019e). Hepatic transplantation of Ad-functionalized MAA microspheres helped drive local accumulation of a β-CD- and Cy5-functionalized poly(isobutylene-alt-maleic-anhydride, PIBMA) polymer; in essence, targeted chemical cargo delivery. The PIBMA backbone of the secondary vector first of all serves as a backbone that connects multiple CD-host molecules, a feature that helps improve the affinity for the Ad-guest functionalized surfaces by exploiting multivalent interactions (Rood et al., 2017). This same backbone can also serve as a carrier for various cargo molecules, e.g., fluorescent dyes and radioisotopes for imaging purposes. The same host-guest chemistry has also proven to be effectively introduced *in vitro* onto the surface of mammalian cancer cells (20-30 μm diameter), macrophages (21 μm diameter), and cardiac stem cells (4-6 μm in diameter) (Duszenko et al., 2020; Rood et al., 2017; Strebl et al., 2018). For all these cell types, host-guest chemistry created a chemical means of influencing the interaction between living cells and their environment – converting living cells into pseudo-chemical scaffolds suitable for supramolecular chemistry in a biological environment. Based on the above, the next step in further developing the technology would be validating whether these pseudo-chemical scaffolds could be applied to deliver chemical cargos *in vivo*. Such *in vivo* cargo delivery concepts create new opportunities for more efficient delivery of e.g. vaccines and immunomodulatory drugs, a concept we have already explored in earlier *in vitro* work in the area of host-guest functionalizations (Duszenko et al., 2020).

As an extension of our earlier *in vitro* work on host-guest functionalization, we hypothesized that we could translate the same concept into an *in vivo* cargo delivery system. To demonstrate the proof-of-principle, we made use of *S. aureus*

inoculation models where functionalized bacteria would serve as a target for the delivery of cargo. For this purpose, *S. aureus* bacteria functionalized with Ad (using the bacteria-specific UBI_{29-41} vector as previously described (Welling et al., 2019a)) were inoculated into thigh muscle or liver to establish infection (Scheme 1). Subsequently, this infection site, characterized by the presence of the Ad-functionalizations (the guest), then drove the local accumulation of an intravenously administered cargo, $^{111}In\text{-}Cy5_{0.5}CD_9PIBMA_{39}$ (the host).

Results

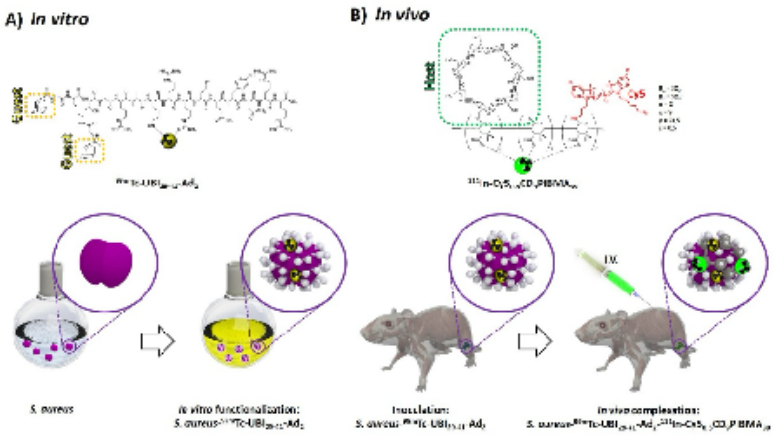

Scheme 1: Experimental setup. (A) *S. aureus* bacteria were Ad-functionalized using a $^{99m}Tc\text{-}UBI_{29-41}Ad_2$ vector (guest) *in vitro*. **(B)** Ad-functionalized bacteria were inoculated into either thigh muscle (shown) or liver (not shown), followed by intravenous injection of a $^{111m}In\text{-}Cy5_{0.5}CD_9PIBMA_{39}$ cargo (host). *In vivo* complexation of this host cargo with Ad-functionalized bacteria could then be assess by dual-isotope SPECT imaging.

In vitro host-guest interactions

In line with the wealth of literature that describes bacteria-specific labelling of bacterial with UBI_{29-41} (Welling et al., 2019c; Welling et al., 2019d), *in vitro* scintillation studies revealed that the guest-vector $^{99m}Tc\text{-}UBI_{29-41}\text{-}Ad_2$ gave a labelling efficiency with *S. aureus* of 86.6±7.0% after 1 h of incubation, and showed that the tracer remained stably associated for at least 24 h at 37 °C (Fig S4B). Confocal microscopy confirmed binding of host-vector (cargo) $Cy5_{0.5}CD_9PIBMA_{39}$ to $UBI_{29-41}\text{-}Ad_2$-labelled *S. aureus in vitro,* with the distribution of fluorescent signals throughout the bacteria (Fig 1B); additionally, the bacterial functionalization was here also shown to remain stable for at least 24 h (Fig 1A). Localization of the

host-vector $Cy5_{0.5}CD_9PIBMA_{39}$ was overwhelmingly on the bacterial surface, as evinced by the absence of overlap between Cy5 and Hoechst emissions (Fig 1A).

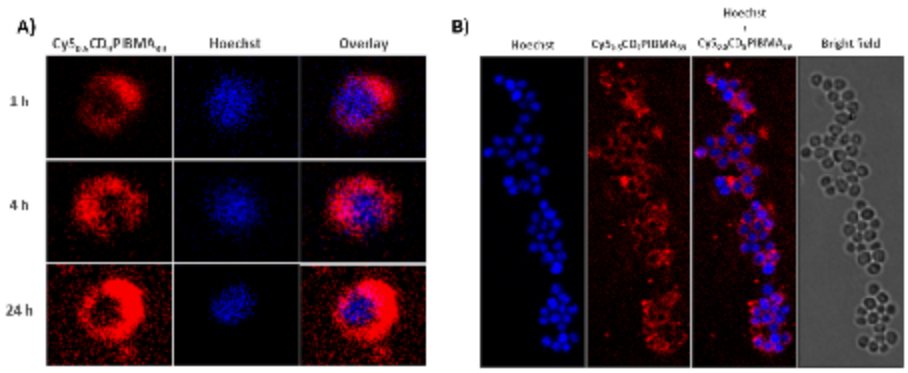

Fig 1: *In vitro* host-guest complexation in *S. aureus*. A) Time-dependent analysis of the presence of $Cy5_{0.5}CD_9PIBMA_{39}$ complexed onto UBI_{29-41}-Ad-functionalized *S. aureus* over 24 h of observation. **B)** Consistent complexation of host-vector $Cy5_{0.5}CD_9PIBMA_{39}$ onto UBI_{29-41}-Ad-functionalized bacteria after 1 h of labelling.

In vivo host-guest interactions

To establish whether host-guest interactions allow for chemical cargo delivery, we subjected animal models inoculated with ^{99m}Tc-UBI_{29-41}-Ad_2-functionalized *S. aureus* (the guest) to an i.v. injection of ^{111}In-$Cy5_{0.5}CD_9PIBMA_{39}$ (the host) (Scheme 1). In the muscle inoculation model, SPECT ^{99m}Tc imaging at 24 h post-injection confirmed focal radioactivity of ^{99m}Tc-UBI_{29-41}-Ad_2-functionalized *S. aureus* guest in the leg, though of relatively weak signal intensity after 4 physical half-lives of ^{99m}Tc (Fig 2A; left panel). At this same location, a distinct accumulation of the host ^{111}In-$Cy5_{0.5}CD_9PIBMA_{39}$ could be observed (Fig 2A). Calculations based on %ID/g data (Fig 2B, Table S1) showed that host accumulation in infected muscle was 16-fold ($p < 0.005$) higher compared to contralateral uninfected muscle (3.2 ± 1.0 %ID/g vs. 0.2 ± 0.2 %ID/g). Accumulation of ^{111}In-$Cy5_{0.5}CD_9PIBMA_{39}$ in thigh muscles of mice without an infection yielded similar uptake as the contralateral muscle, namely 0.4 ± 0.3 %ID/g. Accumulation of ^{111}In-$Cy5_{0.5}CD_9PIBMA_{39}$ in infections with UBI_{29-41}-Ad-functionalized *S. aureus* was 2-fold higher compared to infections with non-functionalized *S. aureus* (3.2 ± 1.0 %ID/g vs. 1.9 ± 0.4 %ID/g; $p < 0.05$; 2-fold), indicating that the contribution of the functionalization step is essential in host-guest complexation *in vivo*. Fluorescence imaging confirmed the abovementioned findings, with a strong Cy5 signal (host-vector) in UBI_{29-41}-Ad_2-functionalized *S. aureus*-infected muscle compared to non-infected contra-lateral thigh muscle (Fig 2C).

In the hepatic inoculation model, SPECT imaging (Fig 3A; left panel) of ^{99m}Tc-UBI$_{29-41}$-Ad$_2$-functionalized *S. aureus* (guest) identified radioactivity at various sites in the liver. This observation is in line with previous reports using ^{99m}Tc-Ad-MAA (Welling et al., 2019a; Welling et al., 2019e). Unfortunately, the short half-life of ^{99m}Tc meant that the signal intensity in the 140 KeV detection window after about 4 physical half-lives was weak (see Fig 3A). Imaging in the 240 KeV window of ^{111}In revealed accumulation in the spleen and the liver, which was not observed in the control mice (no functionalization; Fig 3A), suggesting bacterial dissemination. Biodistribution data indicated that these accumulations were significantly ($p < 0.001$) higher for mice with infected livers compared to control mice; (27.1 ± 11.1 %ID/g vs. 7.6 ± 2.3 %ID/g) and intestines (19.5 ± 8.7 %ID/g vs. 2.6 ± 0.5 %ID/g) (Fig 3B, Table S1). Liver-muscle ratios revealed a nearly 6-fold increase for infected mice (20.0 ± 7.8 %ID/g vs. 3.4 ± 0.8 %ID; $p < 0.001$). These data were further corroborated by fluorescence imaging of the liver, showing a higher Cy5 signal in infected (*i*) livers than in uninfected (*ii*) ones (Fig 3C).

To rule out dissociation of the guest-vector ^{99m}Tc-UBI$_{29-41}$-Ad$_2$ from the bacteria, the biodistribution of unbound ^{99m}Tc-UBI$_{29-41}$-Ad$_2$ was separately assessed. Gauged by the ^{99m}Tc signal (Table S3), ^{99m}Tc-UBI$_{29-41}$-Ad$_2$ was cleared via the renal pathway. Thus, as we did not observe ^{99m}Tc-activity in the bladder (Fig 2A, 3A), it appeared that throughout the experiment, ^{99m}Tc-UBI$_{29-41}$-Ad$_2$ remained attached to bacteria. This result was in good agreement with an earlier study of ours (Welling et al., 2019a).

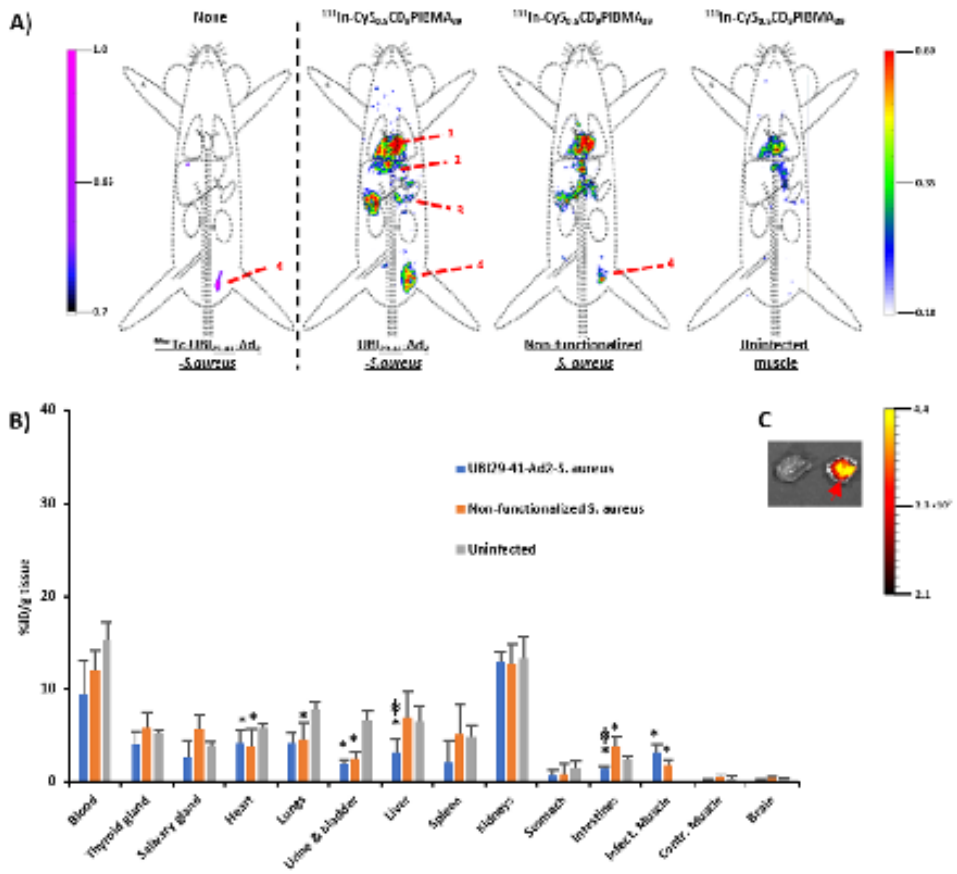

Fig 2: Cargo accumulation in bacteria-inoculated muscle. A) In vivo SPECT imaging of ^{99m}Tc-UBI$_{29-41}$-Ad$_2$-labelled S. aureus 44 h after inoculation in the thigh muscle (left panel; purple-to-pink colour coding) and imaging of host-vector ^{111}In-Cy5$_{0.5}$CD$_9$PIBMA$_{39}$ (rainbow colour coding). A clear co-localization of ^{99m}Tc and ^{111}In was seen for mice colonized with Ad-functionalized S. aureus, whereas co-localization of such signals was less or altogether absent in non-functionalized bacteria or uninfected muscle, respectively. Organs are marked as (1) heart/lungs, (2) liver, (3) intestines, and (4) inoculation site (thigh muscle). **B)** Biodistribution studies of ^{111}In-Cy5$_{0.5}$CD$_9$PIBMA$_{39}$ in mice inoculated with either ^{99m}Tc-UBI$_{29-41}$-Ad$_2$-functionalized S. aureus (blue bars), non-functionalized S. aureus (orange bars), or no infection (grey bars). The data (expressed as the mean ± S.D. ratios of the %ID/g) showed comparable activity in blood and major tissues for the 3 groups, whereas uptake between infected muscle and controls differed significantly (n=6 for each group). * = $p < 0.05$. **C)** Ex vivo fluorescence imaging of muscle tissue corroborated the abovementioned findings, with the infected muscle indicated with a red arrow. Scale bar indicates intensity as photons/sec/cm^2.

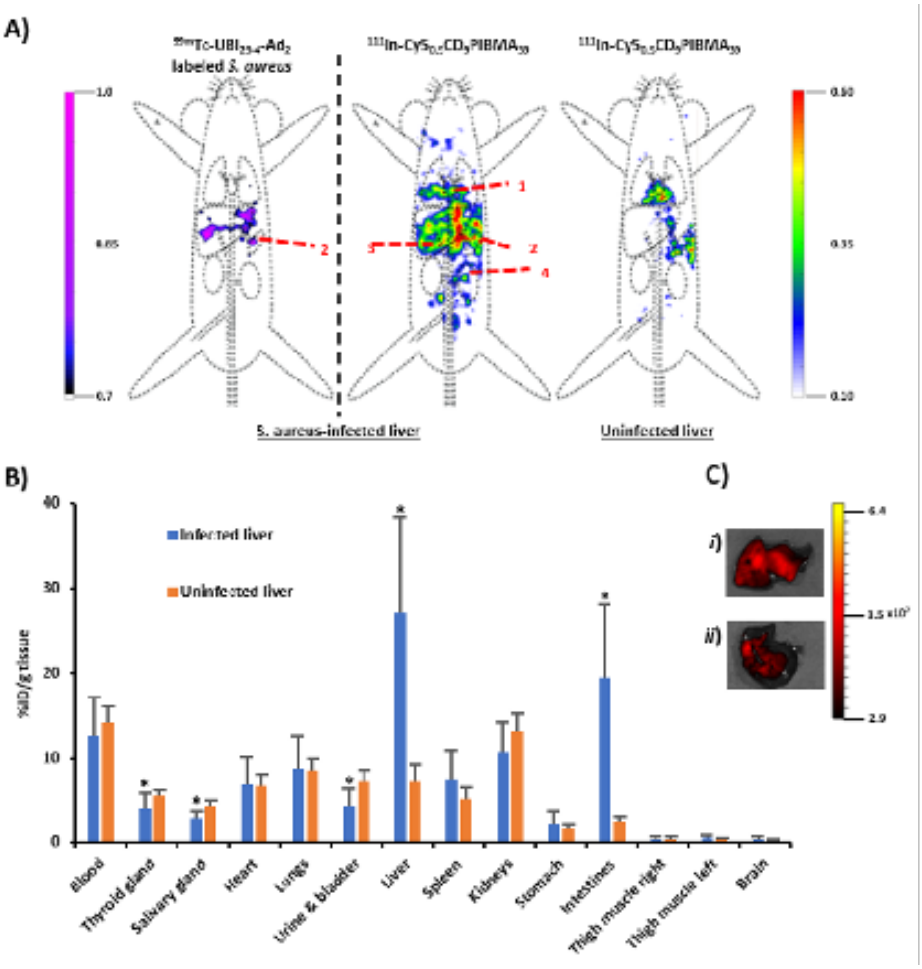

Fig 3: Cargo accumulation in the bacteria-inoculated liver. A) SPECT imaging of ^{99m}Tc-UBI$_{29-41}$-Ad$_2$-functionalized S. aureus showed activity in the liver and spleen (left panel; purple-to-pink colour coding). Imaging of ^{111}In-Cy5$_{0.5}$CD$_9$PIBMA$_{39}$ (rainbow colour coding) showed clear co-localization in the liver (middle panel), whereas mice without infection did not show any liver co-localization (right panel). Organs are marked as (1) heart/lungs, (2) inoculation site (spleen), (3) liver, (4) intestines. **B)** Biodistribution studies of ^{111}In-Cy5$_{0.5}$CD$_9$PIBMA$_{39}$ showed significantly higher uptake in the infected liver and intestines (blue bars) compared to mice with a non-infected liver (orange bars). Data are expressed as the mean ± S.D. ratios of the %ID/g in the liver and blood measured at 4 h p.i. of the host-vector (n=6 for each group). * = $p < 0.05$. **C)** Ex vivo fluorescence imaging of ^{111}In-Cy5$_{0.5}$CD$_9$PIBMA$_{39}$ in infected (top panel - i) and non-infected liver (bottom panel - ii). Scale bar indicates intensity as photons/sec/cm^2.

Discussion

In this study, we addressed the feasibility of harnessing cyclodextrin/adamantane (CD/Ad) host-guest chemistry to achieve targeted accumulation of a chemical cargo. To this end, we functionalized living *S. aureus* bacteria with Ad, inoculated the bacteria into either muscle or liver, and then intravenously administered a chemical cargo to target these Ad-functionalized bacteria. We found that for both muscle and liver models, the presence of Ad-functionalized bacteria (the guest) was able to drive accumulation of the injected chemical cargo (the host). Hence, this study demonstrates a crucial proof-of-principle of the utility offered by supramolecular host-guest chemistry in advancing precision medicine.

While our earlier efforts to translate CD-Ad-based supramolecular host-guest chemistry into *in vivo* applications made use of chemical microspheres designed for hepatic embolization (Spa et al., 2018; Welling et al., 2019e), the work presented here uses actual living cells. Furthermore, we here show that the approach has value outside the liver, in this case, being able to target a focal point in the muscle. While the presence of non-functionalized bacteria by themselves led to a slight accumulation of the chemical cargo, the accumulation was significantly improved upon by the presence of the Ad functionalization. These results are in line with previous work done in our group, which has shown that bacterial surfaces appear to possess structures capable of serving as a weaker "guest" (analogously to Ad) for binding host-vectors like the CD-polymers used in this study (Duszenko et al., 2020). Despite this property, bacteria nevertheless represented the most intriguing next step to take in developing this technology, because this technology could allow for long-term tracking of bacterial infections in animal models and provide opportunities for exploring targeted treatment modalities which may be grafted onto the CD polymer.

To expand upon this study's findings, future studies will need to further tweak the presented chemical cargo delivery system to increase its clinical value. For instance, while the Ad-functionalization of bacteria in this study took place *in vitro* prior to inoculation into mice to more reliably assess the concept's feasibility, clinical applications will likely depend on an initial *in vivo* Ad-functionalization. To this end, Ad-vectors must be designed to functionalize the target of interest specifically. For targeting bacteria, UBI_{29-41} potentially represents one such vector. In earlier studies we reported on a 10-fold higher binding to bacteria over host cells *in vitro*, which increased to 200-fold *in vivo* (Welling et al., 2000a). Since then, a number of other studies have demonstrated that this preferential binding to bacteria is maintained when a range of functionalizations are conjugated to UBI_{29-41} (Welling et al., 2019c). Other targeting vectors that instead target overexpressed receptors on tumor cells can represent another attractive option for specific *in vivo* Ad-functionalization, and would widen application of the cargo

delivery concept beyond infectious diseases (Rood et al., 2017). An additional consideration for future clinical applications will be investigating how compatible the presented chemical cargo delivery system is with various therapeutic agents. Such investigations have recently been initiated in our laboratory, and we hope that the findings presented here will also spur others to investigate supramolecular chemistry as a chemical instrument for advancing precision medicine.

Conclusion

In conclusion, we have here shown that host-guest chemistry is well-suited for *in vivo* cargo delivery to bacterial inoculations. Further development and refinement of the concept could pave the path towards therapeutic studies and innovative new treatment paradigms.

References

Challa, R., Ahuja, A., Ali, J., and Khar, R.K. (2005). Cyclodextrins in drug delivery: An updated review. AAPS PharmSciTech *6*, E329-E357.

Duszenko, N., van Willigen, D., M, Welling, M.M., de Korne, C.M., van Schuijlenburg, R., Winkel, B., M.F, van Leeuwen, F.W.B., and Roestenberg, M. (2020). A supramolecular platform technology for bacterial cell surface modification. ACS Inf Dis *6*, 1734-1744.

Lai, W.-F., Rogach, A.L., and Wong, W.-T. (2017). Chemistry and engineering of cyclodextrins for molecular imaging. Chem Soc Rev *46*, 6379-6419.

Li, Q., Wu, Y., Lu, H., Wu, X., Chen, S., Song, N., Yang, Y.-W., and Gao, H. (2017). Construction of supramolecular nanoassembly for responsive bacterial elimination and effective bacterial detection. ACS Appl Mat Interfaces *9*, 10180-10189.

Melendez-Alafort, L., Ramirez, F.D., Ferro-Flores, G., de Murphy, C.A., Pedraza-Lopez, M., and Hnatowich, D.J. (2003). Lys and Arg in UBI: A specific site for a stable Tc-99m complex? Nucl Med Biol *30*, 605-615.

Paolino, M., Ennen, F., Lamponi, S., Cernescu, M., Voit, B., Cappelli, A., Appelhans, D., and Komber, H. (2013). Cyclodextrin-adamantane host-guest interactions on the surface of biocompatible adamantyl-modified glycodendrimers. Macromolecules *46*, 3215-3227.

Rood, M.T.M., Spa, S.J., Welling, M.M., ten Hove, J.B., van Willigen, D.M., Buckle, T., Velders, A.H., and van Leeuwen, F.W.B. (2017). Obtaining control of cell surface functionalizations via pre-targeting and supramolecular host-guest interactions. Sci Rep *7*, 39908.

Sankaran, S., van Weerd, J., Voskuhl, J., Karperien, M., and Jonkheijm, P. (20155). Photoresponsive cucurbit[8]uril-mediated adhesion of bacteria on supported lipid bilayers. Small *11*, 6187-6196.

Saokham, P., Muankaew, C., Jansook, P., and Loftsson, T. (2018). Solubility of cyclodextrins and drug/cyclodextrin complexes. Molecules *23*, 1161.

Spa, S.J., Welling, M.M., van Oosterom, M.N., Rietbergen, D.D.D., Burgmans,

M.C., Verboom, W., Huskens, J., Buckle, T., and van Leeuwen, F.W.B. (2018). A Supramolecular Approach for Liver Radioembolization. Theranostics *8*, 2377-2386.

Strebl, M.G., Yang, J., Isaacs, L., and Hooker, J.M. (2018). Adamantane/Cucurbituril: A potential pretargeted imaging strategy in immuno-PET. Mol Imag *17*, 1-7.

Welling, M.M., Bunschoten, A., Kuil, J., Nelissen, R., Beekman, F.J., Buckle, T., and van Leeuwen, F.W.B. (2015). Development of a hybrid tracer for SPECT and optical imaging of bacterial infections. Bioconjugate Chem *26*, 839-849.

Welling, M.M., de Korne, C.M., Spa, S.J., van Willigen, D.M., Hensbergen, A.W., Bunschoten, A., Duszenko, N., Smits, W.K., Roestenberg, M., and van Leeuwen, F.W.B. (2019a). Multimodal tracking of controlled Staphylococcus aureus infections in mice. ACS Inf Dis *5*, 1160-1168.

Welling, M.M., de Korne, C.M., Spa, S.J., van Willigen, D.M., Hensbergen, A.W., Bunschoten, A., Duszenko, N., Smits, W.K., Roestenberg, M., and van Leeuwen, F.W.B. (2019b). Multimodal Tracking of Controlled Staphylococcus aureus Infections in Mice. ACS Infect Dis *5*, 1160-1168.

Welling, M.M., Duszenko, N., van Willigen, D.M., Hensbergen, A.W., Buckle, T., Rietbergen, D.D.D., Roestenberg, M., and van Leeuwen, F.W.B. (Accepted). Interventional Nuclear Medicine: "click" chemistry as an in vivo pre-targeting strategy for imaging microspheres and bacteria. Biomater Sci

Welling, M.M., Hensbergen, A.W., Bunschoten, A., Velders, A.H., Roestenberg, M., and van Leeuwen, F.W.B. (2019c). An update on radiotracer development for molecular imaging of bacterial infections. Clin Transl Imaging *7*, 105-124.

Welling, M.M., Hensbergen, A.W., Bunschoten, A., Velders, A.H., Scheper, H., Smits, W.K., Roestenberg, M., and van Leeuwen, F.W.B. (2019d). Fluorescent imaging of bacterial infections and recent advances made with multimodal radiopharmaceuticals. Clin Transl Imaging *7*, 125-138.

Welling, M.M., Paulusma-Annema, A., Balter, H.S., Pauwels, E.K., and Nibbering, P.H. (2000a). Technetium-99m labelled antimicrobial peptides discriminate between bacterial infections and sterile inflammations. Eur J Nucl Med *27*, 292-301.

Welling, M.M., Paulusma-Annema, A., Balter, H.S., Pauwels, E.K.J., and Nibbering, P.H. (2000b). Technetium-99m labelled antimicrobial peptides discriminate between bacterial infections and sterile inflammations. Eur J Nucl Med *27*, 292-301.

Welling, M.M., Spa, S.J., van Willigen, D.M., Rietbergen, D.D.D., Roestenberg, M., Buckle, T., and van Leeuwen, F.W.B. (2019e). In vivo stability of supramolecular host–guest complexes monitored by dual-isotope multiplexing in a pre-targeting model of experimental liver radioembolization. J Contr Rel *293*, 126-134.

Wu, Z., Song, N., Menz, R., Pingali, B., Yang, Y.W., and Zheng, Y. (2015). Nanoparticles functionalized with supramolecular host-guest systems for nanomedicine and healthcare. Nanomedicine (London, England) *10*, 1493-1514.

Yu, G., and Chen, X. (2019). Host-guest chemistry in supramolecular theranostics. Theranostics *9*, 3041-3047.

Methods

General

All chemicals were obtained from commercial sources and used without further purification. Solvents were obtained from Actu-All Chemicals (Oss, The Netherlands) in HPLC grade and used without further purification. The reactions were monitored by thin-layer chromatography (TLC) and mass spectrometry using a Bruker microflex™ LRF MALDI-TOF. HPLC was performed on a Waters (Etten-Leur, The Netherlands) HPLC system using a 1525EF pump and a 2489 UV/VIS detector. For preparative HPLC, a Dr Maisch GmbH (Ammerbuch, Germany) Reprosil-Pur 120 C18-AQ 10 μm (250 × 20 mm) column was used (12 mL/min). For analytical HPLC, a Dr Maisch GmbH Reprosil-Pur C18-AQ 5 μm (250 × 4.6 mm) column was used, applying a gradient of 0.1% TFA in H_2O/CH_3CN 95:5 to 0.1% TFA in H_2O/CH_3CN 5:95 in 40 min (1 mL/min).

Synthesis

UBI_{29-41}-Ad_2

Synthesis of adamantane-functionalized antimicrobial peptide ubiquicidin, UBI_{29-41}-Ad_2, was carried out as follows. The UBI_{29-41} peptide (H-TGRAKRRMQYN-RR-NH_2) was synthesized by Fmoc solid-phase peptide synthesis (SPPS). Four molar equivalents of Fmoc-Lys(Fmoc)-OH, PyBOP and 1-hydroxybenzotriazole, and 15 molar equivalents of DiPEA were dissolved in anhydrous DMF (3 mL), and this mixture was added to the UBI_{29-41} peptide on solid polymer support bearing a free amine on the N-terminal. After two h of shaking at room temperature, the solid was washed using DMF and after that DCM. A bromophenol blue test (BPB) was used to confirm the full conversion. After standard Fmoc deprotection using 20% piperidine in DMF and re-swelling of the polymer beads using DCM 4 molar equivalents of Fmoc-Gly-OH, PyBOP, 1-hydroxybenzotriazole, and 15 equivalents of DiPEA were dissolved in anhydrous DMF (3 mL) and added to the polymer beads. The suspension was shaken at room temperature for 18 h, whereafter washing, Fmoc deprotection and re-swelling was performed. Again, BPB was used to show full conversion. Hereafter, Fmoc protection and subsequent washing steps were performed, followed by coupling of 1-adamantane-carbonyl chloride (4 eq.) using DiPEA (15 eq.) and HOBt (4 eq.). Following confirmation by BPB and washing steps, the final product and protective groups were cleaved using TFA/TIPS/H_2O 38:1:1 and purified by preparative HPLC. After pooling the relevant fractions and lyophilization, a white solid was obtained; MALDI-TOF $[M+H]^+$ calculat-

ed: 2258,7; found 2285,2.

$Cy5_{0.5}CD_9PIBMA_{39}$

Synthesis and characterization of Cy5 functionalized β-cyclodextrin-poly(isobutylene-*alt*-maleic-anhydride) ($Cy5_{0.5}CD_9PIBMA_{39}$, ~18.7 kDa, diameter ≈ 11.7 nm) was carried out as previously described (Rood et al., 2017).

Radiolabelling and stability testing

Radiolabelling of guest vector UBI_{29-41}-Ad_2 with ^{99m}Tc

Radiolabelling of UBI_{29-41}-Ad_2 with ^{99m}Tc (^{99m}Tc-UBI_{29-41}-Ad_2) and the stability of the ^{99m}Tc-chelation was carried out as follows: to 5 µL of UBI_{29-41}-Cy5- Ad_2 (797 µM/mL H_2O), 4 µL of $SnCl_2.2H_2O$ (0.44 mg/mL saline, Technescan PYP, Mallinckrodt Medical B.V. Petten, The Netherlands), 4 µL of NaOH (0.1 M), and 100 µL of a freshly eluted ^{99m}Tc-Na-pertechnetate solution (1,000 MBq/mL, Mallinckrodt Medical B.V.) was added and the mixture was gently stirred in a shaking water bath for one h at 37 °C (Welling et al., 2019a; Welling et al., 2000b). The stability of the radiolabelling was determined at 37 °C at various intervals up to 24 h in 1 mL of PBS or fetal calf serum (20% vol/vol, FCS, Life Technologies Inc. CA). The release of radioactivity was assessed by instant thin-layer chromatography (ITLC) on 1x7 cm ITLC-SG paper strips (Agilent Technologies, USA) using PBS as the mobile phase.

Radiolabelling of $Cy5_{0.5}CD_9PIBMA_{39}$ with ^{111}In

Labelling of $Cy5_{0.5}CD_9PIBMA_{39}$ and stability testing of host-vector ^{111}In-$Cy5_{0.5}CD_9PIBMA_{39}$ was carried out as previously described (Spa et al., 2018; Welling et al., 2019e).

Labelling of S. aureus with ^{99m}Tc-UBI_{29-41}-Ad_2

To allow imaging of the administered bacteria in a whole mouse model, *S. aureus* (ATCC 25922) was labelled with the primary guest-vector ^{99m}Tc-UBI_{29-41}-Ad_2 as was previously used for labelling with the hybrid tracer ^{99m}Tc-UBI_{29-41}-Cy5 (Welling et al., 2019a). In short, 100 µL of ^{99m}Tc-UBI_{29-41}-Ad_2 (20-100 MBq) was added to 1 mL of *S. aureus* ($1x10^8$ CFU/mL in 25 mM Na-NH_4-acetate buffer pH5), and the mixture was gently stirred at room temperature. The efficiency of the rate of bacterial functionalization was measured at different intervals within a 24 h time frame. Before determining the tracer uptake at each interval, 0.1 mL of the bacteria in the labelling suspension was washed two times with phosphate-buffered saline (PBS) and centrifugation steps (4 min x 3,500 rpm).

The amount of radioactivity associated with bacteria was determined at various intervals. The efficiency of the bacterial functionalization was expressed as the % of the total added amount of radioactivity: (([MBq]added/[MBq]associated with bacteria)*100) (Welling et al., 2019a).

In vitro host-guest interactions

Mixtures of 0.1 mL containing 37 nmol UBI_{29-41}-Ad_2 labelled to $1x10^8$ colony forming units (CFU) of *S. aureus* were incubated with 0.1 mL ^{111}In-$Cy5_{0.5}CD_9PIBMA_{39}$ (10 μg/mL, 1 MBq) and 0.8 mL of PBS. The mixtures were incubated for one h in a shaking water bath at 37 °C. Cells were washed after spinning twice for 5 min at 1,500 × *g* and resuspending the pellet with PBS. The decay-corrected radioactivity associated with the pellet containing the bacteria and the supernatant was measured in a dose calibrator (VDC101, Veenstra Instruments, Joure, the Netherlands). Following correction for background activity, the host-guest interaction was expressed as the percentage of the total amount of radioactivity binding to the bacterial pellet. As a specificity control, non-specific binding of ^{111}In-$Cy5_{0.5}CD_9PIBMA_{39}$ to the same number of bacteria without UBI_{29-41}-Ad_2 labelling was evaluated.

Confocal microscopy

Confocal microscopy was used to confirm the *in vitro* accumulation of $Cy5_{0.5}CD_9PIBMA_{39}$ on UBI_{29-41}-Ad_2 labelled bacteria. 0.2 mL of 25 mM Na-NH_4-acetate buffer pH 5 solution containing $1x10^8$ CFUs *S. aureus*, 10 μM UBI_{29-41}-Ad_2, and 10 μM Hoechst 33342 was incubated for 30 min in a dark shaking water bath at 37 °C. Samples were washed twice in PBS as described above, after which they were incubated in 0.2 mL of a 1 μM solution of $Cy5_{0.5}CD_9PIBMA_{39}$ for 60 minutes in a dark shaking water bath at 37 °C. Samples were washed thrice in PBS as described above, and finally resuspended in 100 μL PBS. 10 μL of labelled bacteria were pipetted onto culture dishes with glass inserts (ø35mm glass-bottom dishes No. 15, poly-d-lysine coated, γ-irradiated, MatTek corporation). Images were acquired at intervals of 1 h, 4 h, and 24 h in a single field of view using a Leica SP8 WLL confocal microscope (λex 633 nm, λem 650-700 nm) under 100x magnification using Leica Application Suite Software Suite 4.8. Pictures were loaded in ImageJ software (ImageJ 1.44p, NIH, USA) to draw a profile line over a single representative stained bacterium in the Cy5 and the Hoechst spectrum to estimate the distribution of both dyes in the bacterial membrane and cytoplasm.

In vivo imaging experiments

Animals

In vivo studies were performed using 2−4-month-old Swiss mice (20-35 g, Crl:OF1 strain, Charles River Laboratories, USA). All animal studies were approved by the Institutional Animal Ethics Committee (DEC permit 12160) of the Leiden University Medical Center (LUMC). Mice were kept under specific pathogen-free conditions in the animal housing facility of the LUMC. Food and water were provided *ad libitum*. Two models were used: a thigh muscle and a hepatic embolization model.

For muscle inoculation, mice were injected in the right thigh muscle with 0.1 mL of ^{99m}Tc-UBI$_{29-41}$-Ad$_2$-labelled *S. aureus* (n=6). After 24 h, 0.1 mL secondary vector (host), ^{111}In-Cy5$_{0.5}$CD$_9$PIBMA$_{39}$ (10 μg/mL, approx. 15 MBq) was i.v. administered. As controls for the muscle model, 6 mice were either infected with non-functionalized *S. aureus* to demonstrate non-specific uptake of the secondary vector or with 6 mice which were not infected at all, to study the general biodistribution of ^{111}In-Cy5$_{0.5}$CD$_9$PIBMA$_{39}$.

For liver inoculation, a liver embolization set-up was performed according to previously described procedures (Spa et al., 2018; Welling et al., 2019e). In brief, animals were anaesthetized by intraperitoneal injection of a mixture containing Hypnorm (Vetapharma, Leeds, United Kingdom), dormicum (Roche, Basel, Switzerland), and water (1:1:2). After shaving and cleaning with ethanol (70%), the abdominal cavity was incised for 0.5 cm, and the spleen was exposed outside the peritoneum. After that, 1x10^8 CFU ^{99m}Tc-UBI$_{29-41}$-Ad$_2$-labelled *S. aureus* in a volume of 0.1 mL (5 MBq) was slowly injected into the spleen of mice (n=6) using a Myjector U-100 insulin syringe (29G x ½" 0.33 x12 mm, Terumo Europe, Leuven, Belgium). After 5 s the needle was removed, and the spleen was repositioned in the peritoneal cavity. 2-4 stitches sutured the incision, and the animals were placed under a heating lamp to maintain until recovery. After 24 h, 0.1 mL ^{111}In-Cy5$_{0.5}$CD$_9$PIBMA$_{39}$ (10 μg/mL, approx. 15 MBq) was administered intravenously (i.v.). Here, mice with non-infected livers were included as a control study (n=6) as we studied the non-specific uptake to bacteria *in vivo* and the general biodistribution of ^{111}In-Cy5$_{0.5}$CD$_9$PIBMA$_{39}$ already in the muscle inoculation model.

Imaging studies and biodistribution assays

SPECT imaging of mice either intramuscularly or hepatically inoculated by ^{99m}Tc-UBI$_{29-41}$-Ad$_2$-labelled *S. aureus* was performed (Welling et al., 2015; Welling et al., 2019a) using a U-SPECT-2 scanner and continuous 1-2% isoflurane anaesthesia, with imaging of ^{111}In-Cy5$_{0.5}$CD$_9$PIBMA$_{39}$ in mice with non-UBI$_{29-41}$ functionalized *S. aureus* and without bacterial infection as a control. Image acquisition took 20 min, and images were reconstructed according to the optimized settings

for ^{99m}Tc (140 KeV) and ^{111}In (170 & 240 KeV). Mice were imaged 4 h after the administration of ^{111}In-Cy5$_{0.5}$CD$_9$PIBMA$_{39}$ using SPECT. After imaging, mice were euthanized by an intraperitoneal injection of 0.25 mL Euthasol (ASTfarma, Oudewater, The Netherlands). Tissues were excised for use in quantitative biodistribution studies. Various organs and tissues were weighed and counted for their radioactive content using a gamma counter (2470 automatic gamma counter, Perkin–Elmer). Counts per minute were converted into decay corrected MBq at the time point of injection (t=0), and the percentage of the injected dose per gram of tissue (%ID/g) was calculated as follows: ((([MBq]tissue/[MBq]injected) x100)/g tissue). From biodistribution data, infection-to-background ratios and the % of excreted radioactivity were determined. To calculate the amount of excreted radioactivity, the entire mouse was weighed and counted for radioactivity in a dose-calibrator. At the time of dissection, and after the removal of various tissues, the radioactivity in the mouse was recalculated. Excreted radioactivity (in urine and faeces) was then calculated as = (radioactivity of injected dose) – (radioactivity of excised tissues + radioactivity carcass). To determine the biodistribution of free ^{99m}Tc-UBI$_{29-41}$-Ad$_2$ (not associated with *S. aureus*), three non-infected mice were injected and imaged as described above.

Ex vivo fluorescence imaging of excised infected and non-infected tissues of both models was carried out using the IVIS Spectrum imaging system (Caliper Life Science, Hopkinton, MA) (Welling et al., 2015). This helped verify the localization of the hybrid polymer via optical imaging.

Statistical analysis

All data are presented as mean value (±SD) of 3-6 independent measurements. Student's two-tailed independent samples T-test performed statistical analysis for differences between groups in the animal studies. Significance was assigned for p-values < 0.05. All analyses and calculations were performed using Microsoft® Office Excel 2010 and GraphPad Prism version 5.01 for Windows (GraphPad Software, San Diego, CA, USA).

Acknowledgements

We acknowledge Matthias N. van Oosterom and Sven I. van Leeuwen for generating the graphs.

Funding

The research leading to these results was funded with grants from the Neth-

erlands Organization for Scientific Research (Vici-fellowship - NWO 16141). Wiep-Klaas Smits was supported by an NWO-Vidi fellowship - 864.13.003.

Conflicts of interest

The authors have declared that no competing interest exists.

4

Chemically enhanced immunogenicity of bacteria by supramolecular functionalization with an adjuvant

Nikolas Duszenko, Danny M. van Willigen, Anton Bunschoten, Aldrik H. Velders, Meta Roestenberg and Fijs W.B. van Leeuwen

Adapted from:

Chembiochem. 2022 Sep 30;e202200434.
PMID: 36177993
DOI: 10.1002/cbic.202200434.

Abstract

Many pathogens blunt immune responses by lacking immunogenic structural features, which typically results in disease. Here, we show evidence suggesting that pathogen immunogenicity can be chemically enhanced. Using supramolecular host-guest chemistry, we complexed onto the surface of a poorly immunogenic bacterium (*Staphylococcus aureus*) a TLR7 agonist-based adjuvant. "Adjuvanted" bacteria were still readily recognized by macrophages and induced a more pro-inflammatory immunophenotype. Future applications of this concept could yield treatment modalities that bolster the immune system's response to pathogenic microbes.

Introduction

Immune responses to pathogens are critically dependent on recognition of pathogen-associated molecular patterns (PAMPs) (Medzhitov, 2007). Sentinel immune cells such as macrophages possess a suite of receptors facilitating recognition, such as Toll-like receptors (TLRs), activation of which triggers the development of an antimicrobial phenotype characterized by e.g. increased secretion of pro-inflammatory cytokines (Sica et al., 2015). Accordingly, many pathogens have evolved mechanisms for avoiding such activation (Ballou et al., 2016; Cambier et al., 2014; Gault et al., 2015). For example, the bacterium Staphylococcus aureus enzymatically cleaves some of its surface components and renders them inert to immune cells, endowing it with a low immunogenicity that yields suboptimal immune activation and can lead to chronic metastatic infection and disease (Chen and Alonzo, 2019).

The issue of low immunogenicity has long been known in vaccinology and led to the concept of adjuvanting: addition of exogenous immunogens called "adjuvants" to boost entities' immunogenicity (Di Pasquale et al., 2015). Clinically registered subunit vaccines such as Prevnar and RTS,S (Cadoz, 1998; Rutgers et al., 1988), as well as next-generation nanoparticle vaccines (Francica et al., 2016; Wilson et al., 2013), have shown that tightly tethering immunogens tends to yield better boosts in immunogenicity. We thus reasoned that the same concept might be translated to improve (pathogenic) microbes' immunogenicity.

Here, we show the conceptual feasibility of boosting the immunogenicity of S. aureus bacteria by chemically modifying the cell surface with the synthetic TLR7 agonist-based adjuvant CL307. This adjuvant was chosen due to a number of useful properties: 1) a reactive spermine moiety for conjugating to host polymers that would facilitate recognition of the agonist by TLR7; 2) a small size (597 Da) with minimal impact on the host polymers' chemical properties; and 3) an absorption at 298 nm that allowed for quantitation. The resulting "adjuvanted" bacteria were normally recognized by macrophages and yielded improved immune activation compared to unadulterated bacteria.

Results and Discussion

To introduce CL307 onto the surface of S. aureus bacteria, we adapted a supramolecular host-guest chemistry technique for functionalizing the cell surface of live bacterial and eukaryotic cells (Figure 1) (Duszenko et al., 2020a; Rood et al., 2017). An initial pre-functionalization of the surface with an adamantane (Ad) moiety was achieved via a bacteria-targeting Ad-UBI29-41 construct, as the UBI29-41 vector constitutes a cationic, antimicrobial peptide that inserts into the bacterial cell membrane (Welling et al., 2000). This Ad pre-functionalization was followed by the complexation of complementary β-cyclodextrin (CD)-bearing PIBMA polymers that can, in addition to CD, serve as carrier for other functionalities of interest. Here, these functionalities comprised 1) Cy5 dyes for tracking the polymers, and 2) the adjuvant CL307.

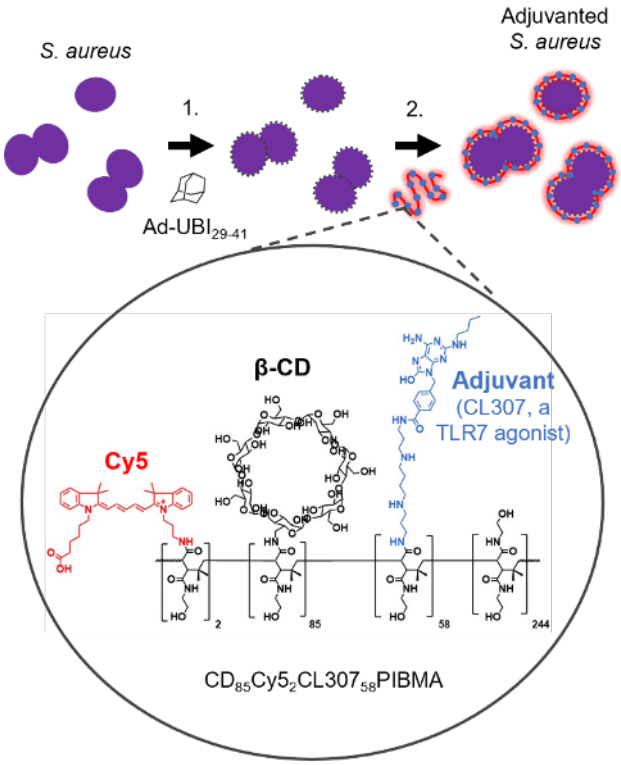

Figure 1: Schematic illustrating chemical strategy for introducing an adjuvant onto the surface of S. aureus bacteria. The bacterial surface was first pre-functionalized with Ad using the antibacterial peptide UBI29-41 as a vector, followed by supramolecular complexation of CD- and CL307-bearing polymers onto the cell surface. Ad = adamantane; UBI = ubiquicidin; CD = β-cyclodextrin.

Despite the presence of approximately 57 units of CL307 per host polymer (Supplemental Figure 2), the polymers could still complex well to the Ad-pre-functionalized S. aureus surface. Confocal imaging showed virtually all bacteria with strong Cy5 signals indicative of complexed polymer on the bacterial cell surface, signals adjacent to Hoechst counterstaining of the cytoplasm (Figure 2a). ImageJ analysis of an adjuvanted bacterium's cross section validated these findings, with distinct Cy5 signals flanking the Hoechst signal of the bacterium's cytoplasm (Figure 2b).

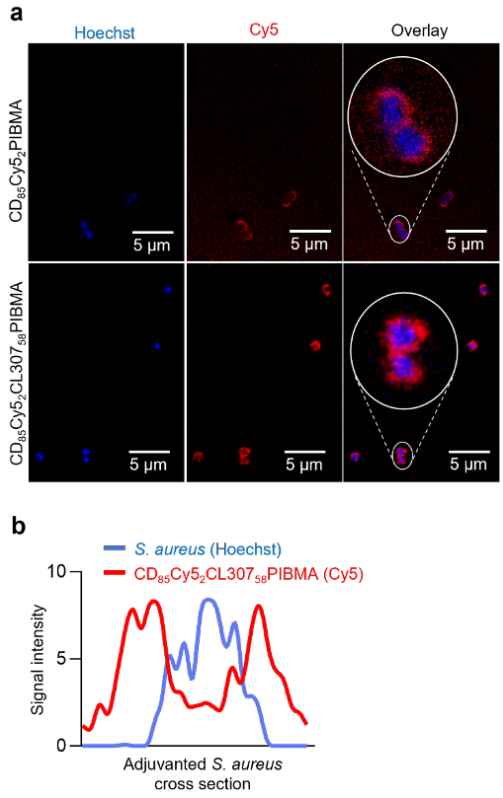

Figure 2: Complexation of CL307-bearing host polymers onto the bacterial cell surface to yield adjuvanted S. aureus. a) Confocal fluorescence microscopy images of bacteria with complexed host polymer (top row) and CL307-bearing host polymer (bottom row) showing Hoechst signal from the bacterial cytoplasm (left – blue), Cy5 signal from complexed (CL307-bearing) polymers on the bacterial cell surface (middle – red), and an overlay of the two signals (right). b) ImageJ analysis quantitating Hoechst and Cy5 signal intensities in a cross section of one adjuvanted bacterium.

Flow cytometric analysis was subsequently used to gauge the efficiency of generating adjuvanted S. aureus. The supramolecular system employed was found to be highly efficient, with virtually all bacteria showing varying quantities of CL307-bearing polymer complexed (Figure 3a; median Cy5 signal of 8,610±1,914 A.U. (i) vs. 0.9±0.7 A.U. (iv)). Notably, CL307-bearing polymers were much less effectively complexed to bacteria without Ad-pre-functionalization (Figure 3a, panel ii – 7-fold less). To estimate the average quantity of CL307 per bacterium, median Cy5 signal was converted into absolute equivalents Cy5 dye via commercial fluorescence quantification beads (Figure 3b). This conversion yielded an average of 105 polymers per bacterium, indicating the presence of about 107 units of CL307 per bacterium – a quantity on the same order of magnitude as seen in adjuvanted nanoparticle vaccines (Francica et al., 2016; Wilson et al., 2013).

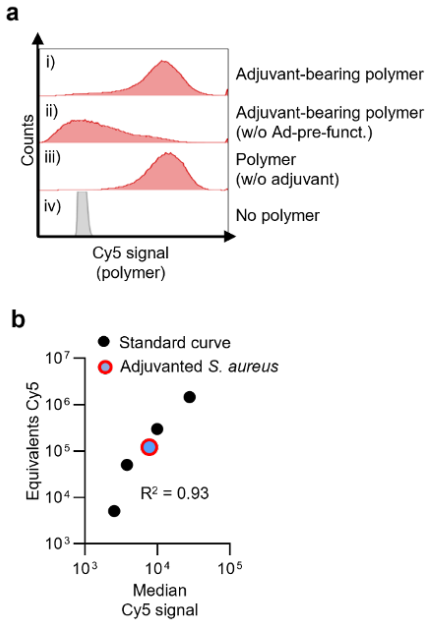

Figure 3: Quantitative flow cytometric analysis of adjuvanted S. aureus. a) Representative flow cytometry histogram of Cy5 signals (x-axis, log scale) in a sample of S. aureus complexed with CL307-bearing polymer (i), S. aureus complexed with little CL307-bearing polymer in the absence of Ad-pre-functionalization (ii), S. aureus complexed with polymer lacking CL307 (iii) and control S. aureus (iv). b) Plot of adjuvanted S. aureus' median Cy5 signal (red-blue) in relation to fluorescence quantification beads (black) of varying Cy5 intensities.

Flow cytometric analysis was further used to characterize the supramolecular chemical system when adapted for introducing adjuvants onto the S. aureus cell surface. The presence of about 57 CL307 units per polymer did not preclude complexation at levels comparable to parental polymer analog lacking CL307 (Figure 4a; 8,610±1,914 vs. 9,342±1,171 A.U., $p = 0.6020$). Remarkably, optimal complexation was however dependent on a slightly elevated salinity during complexation (Supplemental Figure 6), an effect that has previously been described for enhancing supramolecular host-guest interactions (Buvari and Barcza, 1979; Mochida et al., 1973). Supramolecular host-guest interactions were critical for maximizing polymer complexation: the absence of Ad-pre-functionalization decreased complexation 7-fold (Figure 4a; 1,130±122 vs. 8,610±1,914, $p < 0.01$), and competition experiments using an excess of 1 mM soluble Ad similarly decreased complexation (Figure 4b; 1,774±74 vs. 11,574±991 A.U., $p < 0.0001$). Once formed, adjuvanted S. aureus remained stably associated, with over 95% of CL307-bearing polymers remaining complexed after 24 hours incubation at physiological conditions (Figure 4c; 48,593±2,652 A.U. at t = 24h vs. 49,736±1,564 A.U. at t = 0). In line with previous work (Duszenko et al., 2020a; Rood et al., 2017), complexed CL307-bearing polymers did not adversely affect bacterial viability, with comparable culture growth relative to control bacteria (Figure 4d; 0.492±0.005 vs. 0.486±0.012 A.U., $p = 0.481$).

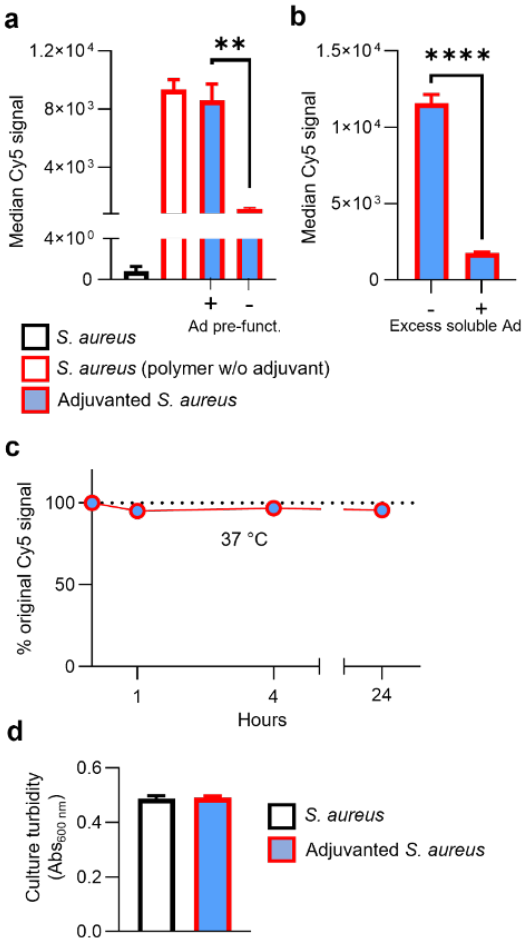

Figure 4: (Bio)chemical characteristics of supramolecular system underlying adjuvanted S. aureus. a) Median Cy5 signal (y-axis) of flow cytometric analysis of S. aureus controls (black), S. aureus with non-adjuvant polymer complexed (red), and adjuvanted S. aureus (red-blue) in the presence (+) and absence (-) of Ad-pre-functionalization (x-axis). b) Median Cy5 signal (y-axis) of flow cytometry-based competition experiment of adjuvanted S. aureus generated in the absence and presence (x-axis) of excess (1 mM) soluble Ad. c) Percent remaining median Cy5 signal (y-axis) of adjuvanted S. aureus after 24 hours incubation (x-axis) in PBS. d) Culture turbidity measurements by absorbance (y-axis) of adjuvanted S. aureus (red-blue) and control S. aureus (black) (x-axis) after 16 hours incubation at 37 °C in growth media. All data shown are from representative experiments of n = 3. Ad = adamantane; ** = $p < 0.01$, **** = $p < 0.0001$.

To investigate the immunological characteristics of adjuvanted S. aureus, a monocyte-derived macrophage assay was used as previously described (Duszenko et al., 2020a), as macrophages are reported to be key players in an effective immune responses to this pathogen (Flannagan et al., 2015; Pidwill et al., 2020). Confocal imaging showed that the presence of synthetic adjuvants on the S. aureus surface did not prevent macrophages from normally phagocytosing such bacteria (Figure 5) – all adjuvanted S. aureus were phagocytosed within 20 minutes.

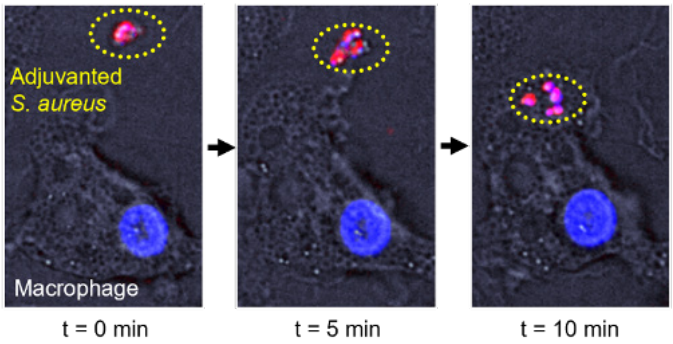

Figure 5: Phagocytosis of adjuvanted S. aureus by a monocyte-derived macrophage. Time-lapse confocal fluorescence microscopy images at t = 0 (left), t = 5 minutes (middle) and t = 10 minutes (right) of a macrophage (cell nucleus in blue) encountering and phagocytosing adjuvanted S. aureus (yellow dotted oval).

Finally, the immunogenicity of adjuvanted S. aureus relative to control S. aureus was assayed by measuring macrophage cytokine secretion during 24 hours of bacterial exposure. Adjuvanted S. aureus induced significantly increased secretion of pro-inflammatory IL-6 (Figure 6a), with 4-fold increases compared to both control S. aureus (1,686±238 vs. 480±193 pg/mL, $p < 0.01$) and S. aureus bearing polymer without CL307 (1,686±238 vs. 479±55 pg/mL, $p < 0.01$). CL307 conjugated to the S. aureus surface also induced a trend towards a higher IL-6 secretion compared to a mixture of S. aureus and soluble concentration-matched CL307 (1,686±238 vs. 940±322 pg/mL, $p = 0.1169$). Secretion of anti-inflammatory IL-10 was on the other hand less changed by adjuvanted S. aureus (Figure 6b). IL-10 secretion to adjuvanted S. aureus was comparable to both control S. aureus (117±37 vs. 67±13 pg/mL, $p = 0.6408$) and S. aureus bearing polymer without CL307 (117±37 vs. 60±6 pg/mL, $p = 0.5370$). Notably, IL-10 secretion in response to adjuvanted S. aureus was however significantly lower compared to S. aureus + CL307 mixture (117±37 vs. 261±45 pg/mL, $p < 0.05$).

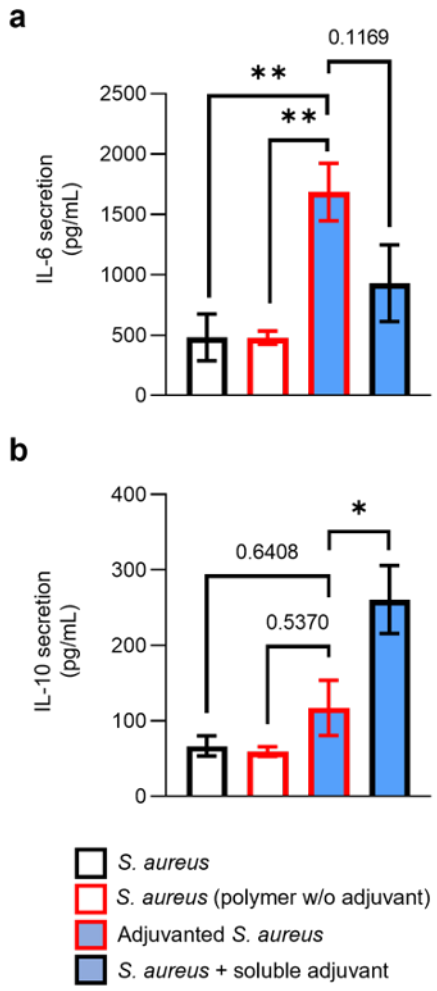

Figure 6: Cytokine secretion by monocyte-derived macrophages after 24 hours of exposure to adjuvanted S. aureus and controls. a) IL-6 secretion (y-axis, pg/mL) in response to S. aureus controls (black), S. aureus bearing polymer without CL307 (red), adjuvanted S. aureus (red-blue), and a mixture of S. aureus and soluble concentration-matched CL307 (black-blue) (x-axis). b) IL-10 secretion (y-axis, pg/mL) in response to S. aureus controls (black), S. aureus bearing polymer without CL307(red), adjuvanted S. aureus (red-blue), and a mixture of S. aureus and soluble concentration-matched CL307 (black-blue) (x-axis). Data shown are n = 5 from 2 independent experiments. IL-6 = interleukin-6; IL-10 = interleukin-10; * = $p < 0.05$, ** = $p < 0.01$.

Altogether, these results indicated that macrophages responded with a slightly more pro-inflammatory IL-6 response to S. aureus whose cell surface was chemically modified with CL307 – an effect that was positively impacted by physically connecting CL307 to the bacteria. Production of pro- and anti-inflammatory mediators such as IL-6 and IL-10, respectively, are constantly balanced to properly calibrate immune responses between too much and too little activation; usually, when one goes up, so does the other. The reversed trends in cytokine production patterns of IL-6 and IL-10 observed for the conjugated and soluble compound (Figure 6) exemplify a shift in that balance. Whereas soluble presentation of CL307 induced a mixed pro- and anti-inflammatory response in macrophages, conjugated CL307 induced a predominantly pro-inflammatory response. Future studies will need to determine if similar shifts towards a more pro-inflammatory response also apply to other immune cell models. Additionally, in vivo models will need to be used to gauge the potential (clinical) utility of the shifts here observed in vitro.

The findings here described suggest that chemical augmentation of microbial cell surfaces with adjuvants may indeed offer a strategy for improving such microbes' immunogenicity. In the future, UBI29-41 vectors' ability to "tag" offending bacteria in vivo (Chen et al., 2015; Ebenhan et al., 2014; Huang et al., 2017; Welling et al., 2019a; Zavadovskaya et al., 2021) could provide a basis to exploit supramolecular pre-targeting strategies (Spa et al., 2018; Welling et al., 2021; Welling et al., 2019b) that locally introduce immunogenic moieties. Introduction thereof could then help activate the immune system and promote clearance of the infectious agent. Another potential application of the presented concept is in the field of vaccinology. Despite the challenging regulatory complexity of bringing live attenuated vaccines to the clinic, there nevertheless exist several – most notably, against tuberculosis and malaria – that continue to be the subject of active investigation (Pai et al., 2016; Roestenberg et al., 2009; Seder et al., 2013). As these vaccines are still characterized by suboptimal performance attributed to a low immunogenicity (Behr and Small, 1997; Jongo et al., 2021), chemical modification could help provide a much needed boost in immunogenicity.

Conclusion

In conclusion, we have here shown that supramolecular introduction of a TLR7 agonist-based adjuvant (CL307) onto poorly immunogenic *S. aureus* bacteria yields increased production of the key pro-inflammatory cytokine IL-6. Future work will need to determine whether a similarly improved immune response is more broadly observed for other players of the immune system in the context of antimicrobial responses, such as neutrophils, and whether such improvements

ultimately help the immune system more effectively clear poorly immunogenic pathogens. A key area of research to this end will be investigating how the presented concept translates to an in vivo setting. Eventually, positive findings could open up the possibility of using chemical functionalization of (microbial) cells to fine-tune immunological properties, and in this way rationally guide effective immune responses.

References

Ballou, E.R., Avelar, G.M., Childers, D.S., Mackie, J., Bain, J.M., Wagener, J., Kastora, S.L., Panea, M.D., Hardison, S.E., Walker, L.A., *et al.* (2016). Lactate signalling regulates fungal beta-glucan masking and immune evasion. Nat Microbiol *2*, 16238.

Behr, M.A., and Small, P.M. (1997). Has BCG attenuated to impotence? Nature *389*, 133-134.

Buvari, A., and Barcza, L. (1979). Beta-Cyclodextrin Complexes of Different Type with Inorganic-Compounds. Inorg Chim Acta *33*, L179-L180.

Cadoz, M. (1998). Potential and limitations of polysaccharide vaccines in infancy. Vaccine *16*, 1391-1395.

Cambier, C.J., Takaki, K.K., Larson, R.P., Hernandez, R.E., Tobin, D.M., Urdahl, K.B., Cosma, C.L., and Ramakrishnan, L. (2014). Mycobacteria manipulate macrophage recruitment through coordinated use of membrane lipids. Nature *505*, 218-222.

Chen, H., Liu, C., Chen, D., Madrid, K., Peng, S., Dong, X., Zhang, M., and Gu, Y. (2015). Bacteria-Targeting Conjugates Based on Antimicrobial Peptide for Bacteria Diagnosis and Therapy. Mol Pharm *12*, 2505-2516.

Chen, X., and Alonzo, F., 3rd (2019). Bacterial lipolysis of immune-activating ligands promotes evasion of innate defenses. Proc Natl Acad Sci U S A *116*, 3764-3773.

Di Pasquale, A., Preiss, S., Da Silva, F.T., and Garcon, N. (2015). Vaccine Adjuvants: from 1920 to 2015 and Beyond. Vaccines *3*, 320-343.

Duszenko, N., van Willigen, D., M, Welling, M.M., de Korne, C.M., van Schuijlenburg, R., Winkel, B., M.F, van Leeuwen, F.W.B., and Roestenberg, M. (2020a). A supramolecular platform technology for bacterial cell surface modification. ACS Inf Dis *6*, 1734-1744.

Duszenko, N., van Willigen, D.M., Welling, M.M., de Korne, C.M., van Schuijlenburg, R., Winkel, B.M.F., van Leeuwen, F.W.B., and Roestenberg, M. (2020b). A Supramolecular Platform Technology for Bacterial Cell Surface

Modification. ACS Infect Dis *6*, 1734-1744.

Ebenhan, T., Zeevaart, J.R., Venter, J.D., Govender, T., Kruger, G.H., Jarvis, N.V., and Sathekge, M.M. (2014). Preclinical evaluation of 68Ga-labeled 1,4,7-triazacyclononane-1,4,7-triacetic acid-ubiquicidin as a radioligand for PET infection imaging. J Nucl Med *55*, 308-314.

Flannagan, R.S., Heit, B., and Heinrichs, D.E. (2015). Antimicrobial Mechanisms of Macrophages and the Immune Evasion Strategies of Staphylococcus aureus. Pathogens *4*, 826-868.

Francica, J.R., Lynn, G.M., Laga, R., Joyce, M.G., Ruckwardt, T.J., Morabito, K.M., Chen, M., Chaudhuri, R., Zhang, B., Sastry, M.*, et al.* (2016). Thermoresponsive Polymer Nanoparticles Co-deliver RSV F Trimers with a TLR-7/8 Adjuvant. Bioconjug Chem *27*, 2372-2385.

Gault, J., Ferber, M., Machata, S., Imhaus, A.F., Malosse, C., Charles-Orszag, A., Millien, C., Bouvier, G., Bardiaux, B., Pehau-Arnaudet, G.*, et al.* (2015). Neisseria meningitidis Type IV Pili Composed of Sequence Invariable Pilins Are Masked by Multisite Glycosylation. PLoS Pathog *11*, e1005162.

Hensbergen, A.W., Buckle, T., van Willigen, D.M., Schottelius, M., Welling, M.M., van der Wijk, F.A., Maurer, T., van der Poel, H.G., van der Pluijm, G., van Weerden, W.M.*, et al.* (2020). Hybrid Tracers Based on Cyanine Backbones Targeting Prostate-Specific Membrane Antigen: Tuning Pharmacokinetic Properties and Exploring Dye-Protein Interaction. J Nucl Med *61*, 234-241.

Huang, N., Chen, X., Zhu, X., Xu, M., and Liu, J. (2017). Ruthenium complexes/polypeptide self-assembled nanoparticles for identification of bacterial infection and targeted antibacterial research. Biomaterials *141*, 296-313.

Jongo, S.A., Urbano, V., Church, L.W.P., Olotu, A., Manock, S.R., Schindler, T., Mtoro, A., Kc, N., Hamad, A., Nyakarungu, E.*, et al.* (2021). Immunogenicity and Protective Efficacy of Radiation-Attenuated and Chemo-Attenuated Pf-SPZ Vaccines in Equatoguinean Adults. Am J Trop Med Hyg *104*, 283-293.

Medzhitov, R. (2007). Recognition of microorganisms and activation of the immune response. Nature *449*, 819-826.

Mochida, K., Kagita, A., Matsui, Y., and Date, Y. (1973). Effects of Inorganic

Salts on Dissociation of a Complex of Beta-Cyclodextrin with an Azo Dye in an Aqueous-Solution. B Chem Soc Jpn *46*, 3703-3707.

Pai, M., Behr, M.A., Dowdy, D., Dheda, K., Divangahi, M., Boehme, C.C., Ginsberg, A., Swaminathan, S., Spigelman, M., Getahun, H.*, et al.* (2016). Tuberculosis. Nat Rev Dis Primers *2*, 16076.

Pidwill, G.R., Gibson, J.F., Cole, J., Renshaw, S.A., and Foster, S.J. (2020). The Role of Macrophages in Staphylococcus aureus Infection. Front Immunol *11*, 620339.

Roestenberg, M., McCall, M., Hopman, J., Wiersma, J., Luty, A.J., van Gemert, G.J., van de Vegte-Bolmer, M., van Schaijk, B., Teelen, K., Arens, T.*, et al.* (2009). Protection against a malaria challenge by sporozoite inoculation. N Engl J Med *361*, 468-477.

Rood, M.T., Spa, S.J., Welling, M.M., Ten Hove, J.B., van Willigen, D.M., Buckle, T., Velders, A.H., and van Leeuwen, F.W. (2017). Obtaining control of cell surface functionalizations via Pre-targeting and Supramolecular host guest interactions. Sci Rep *7*, 39908.

Rutgers, T., Gordon, D., Gathoye, A.M., Hollingdale, M., Hockmeyer, W., Rosenberg, M., and Dewilde, M. (1988). Hepatitis-B Surface-Antigen as Carrier Matrix for the Repetitive Epitope of the Circumsporozoite Protein of Plasmodium-Falciparum. Bio-Technol *6*, 1065-1070.

Seder, R.A., Chang, L.J., Enama, M.E., Zephir, K.L., Sarwar, U.N., Gordon, I.J., Holman, L.A., James, E.R., Billingsley, P.F., Gunasekera, A.*, et al.* (2013). Protection against malaria by intravenous immunization with a nonreplicating sporozoite vaccine. Science *341*, 1359-1365.

Sica, A., Erreni, M., Allavena, P., and Porta, C. (2015). Macrophage polarization in pathology. Cell Mol Life Sci *72*, 4111-4126.

Spa, S.J., Welling, M.M., van Oosterom, M.N., Rietbergen, D.D.D., Burgmans, M.C., Verboom, W., Huskens, J., Buckle, T., and van Leeuwen, F.W.B. (2018). A Supramolecular Approach for Liver Radioembolization. Theranostics *8*, 2377-2386.

Welling, M.M., de Korne, C.M., Spa, S.J., van Willigen, D.M., Hensbergen,

A.W., Bunschoten, A., Duszenko, N., Smits, W.K., Roestenberg, M., and van Leeuwen, F.W.B. (2019a). Multimodal Tracking of Controlled Staphylococcus aureus Infections in Mice. ACS Infect Dis *5*, 1160-1168.

Welling, M.M., Duszenko, N., van Willigen, D.M., Smits, W.K., Buckle, T., Roestenberg, M., and van Leeuwen, F.W.B. (2021). Cyclodextrin/Adamantane-Mediated Targeting of Inoculated Bacteria in Mice. Bioconjug Chem *32*, 607-614.

Welling, M.M., Paulusma-Annema, A., Balter, H.S., Pauwels, E.K., and Nibbering, P.H. (2000). Technetium-99m labelled antimicrobial peptides discriminate between bacterial infections and sterile inflammations. Eur J Nucl Med *27*, 292-301.

Welling, M.M., Spa, S.J., van Willigen, D.M., Rietbergen, D.D.D., Roestenberg, M., Buckle, T., and van Leeuwen, F.W.B. (2019b). In vivo stability of supramolecular host-guest complexes monitored by dual-isotope multiplexing in a pre-targeting model of experimental liver radioembolization. J Control Release *293*, 126-134.

Wilson, J.T., Keller, S., Manganiello, M.J., Cheng, C., Lee, C.C., Opara, C., Convertine, A., and Stayton, P.S. (2013). pH-Responsive nanoparticle vaccines for dual-delivery of antigens and immunostimulatory oligonucleotides. ACS Nano *7*, 3912-3925.

Zavadovskaya, V.D., Larkina, M.S., Stasyuk, E.S., Zorkaltsev, M.A., Udodov, V.D., Ivanov, V.V., Shevtsova, N.M., Rogov, A.S., Lushchyk, A.Y., Yantsevich, A.V.*, et al.* (2021). Radiolabeled Complex of Antimicrobial Peptides UBI29-41 and UBI18-35 Labeled with (99m)Tc for Differential Diagnosis of Bone Infection of the Limbs. Bull Exp Biol Med *170*, 415-419.

Methods

Full procedures related to synthesis and analysis of the chemical compounds used can be found in the Supplemental Information.

Synthesis of supramolecular components

To create the Ad-UBI_{29-41} compound for pre-functionalizing the bacterial cell surface with supramolecular guest, a UBI29-41 peptide (H-TGRAKRRMQYN-RR-NH2) was synthesized in-house by automated Fmoc-based SPPS. Subsequently, Fmoc-Lys(Fmoc)-OH was coupled manually to the liberated N-terminus of the resin-bound peptide using PyBOP and DiPEA in DMF. After Fmoc deprotection of the lysine sidechain and N-terminus, Fmoc-Gly-OH was coupled using PyBOP and DiPEA by agitating in DMF. The glycine amines were liberated and, finally, 1-adamantanecarbonyl chloride was coupled using 1-hydroxybenzotriazole and DiPEA by agitating in DMF. The peptide was then cleaved by adding a mixture of v/v 38:1:1 TFA:TIPS:H2O and agitating for 3 hours, whereafter the mixture was added to ice-cold MTBE:Hexane 1:1. The crude peptide was collected by centrifugation, whereafter the pellet was resuspended in ice-cold MTBE:Hexane twice, followed by drying in vacuo. The off-white solid was then purified using preparative HPLC, followed by lyophilization to yield the white solid product.

To create the adjuvant-bearing host polymer $CD_{85}Cy5_2CL307_{58}$PIBMA for complexing onto Ad-pre-functionalized bacterial cell surface, poly(isobutylene-alt-maleic-anhydride was dissolved in dimethylsulfoxide, whereafter amino(6-monodeoxy-6-mono)-β-cyclodextrin hydrochloride and N,N-Diisopropylethylamine were added, followed by stirring at 80°C for 94 hours. The solution was purified by dialysis in water for 7 hours, followed by dialysis in phosphate buffer (0.2 M, pH 9) for 144 hours including refreshment of buffer twice, followed by dialysis in water for 7 hours. The dialysate was discarded and the residue was lyophilized, yielding an off-white solid. The product $PIBMA_{[389]}$-$CD_{[85]}$ was subsequently dissolved in water, whereafter N,N'-diisopropylcarbodiimide was added. The mixture was stirred at room temperature for 1 hour followed by addition of NH2-Cy5-COOH. The solution was stirred for 5 hours at room temperature whereafter it was dialysed in water for 24 hours with one refresh of water, followed by lyophilization of the product. The product $PIBMA_{[389]}$-$CD_{[85]}$-$Cy5_{[2]}$ was dissolved in water, followed by addition of DIC. After stirring for 1.3 hours at room temperature, CL307 was added. After shaking for 1.3 hours, ethanolamine was added and stirring was continued for another 16 hours at room temperature. Thereafter, the reaction mixture was dialyzed in water for 29 hours with one refreshment of water. The resulting adjuvant-bearing host polymer $CD_{85}Cy5_2CL307_{58}$PIBMA was used as is for experiments; PBS pH 7.4

was added where necessary.

Supramolecular complexation of CL307-bearing polymers onto S. aureus cell surface

S. aureus stocks (strain ATCC 29213) were thawed from -20 °C and washed twice in 25 mM ammonium acetate buffer pH 5 by centrifugation at 10k RCF for 5 minutes and subsequent removal of supernatant by pipet. From this washed stock, 108 bacteria were added to 1 mL of an 8 μM solution of Ad-UBI_{29-41} in 25 mM ammonium acetate buffer pH 5 and incubated for 30 minutes at 37 °C with shaking. Thereafter, bacteria were thrice washed with PBS containing 1% albumin by centrifugation at 10k RCF for 5 minutes and subsequent removal of supernatant by decanting. Washed, Ad-pre-functionalized bacteria were re-suspended in 1 mL PBS, wherefrom 100 μL aliquots were added to 100 μL of a 2 μM solution of the adjuvant-bearing host polymer ($CD_{85}Cy5_2CL307_{58}$PIB-MA) in PBS at a concentration of 1.9X (where 1X is equivalent to standard commercial PBS) and incubated overnight at 37 °C with shaking. Thereafter, bacteria were thrice washed with PBS containing 1% albumin by centrifugation at 10k RCF for 5 minutes and subsequent removal of supernatant by decanting. Washed, adjuvanted bacteria were then resuspended in PBS or RPMI for down-stream applications.

Analysis of adjuvanted S. aureus

To visually confirm the presence of CL307-bearing host polymers on the S. aureus surface via the polymers' Cy5 reporter, 10 μL aliquots (with the addition of 10 μg/mL Hoechst 33342) of adjuvanted bacteria were added to glass-bottom confocal dishes (MatTek Corporation, Ashland, MA, USA), overlaid with a coverslip and analyzed with a Leica (Wetzlar, Germany) SP8 confocal fluorescence microscope; Hoechst signal was acquired using a 405 nm laser at 20% maximal output and a HyD detector set to 425-475 nm, Cy5 signal was acquired using a 633 nm laser at 5% maximal output and a HyD detector set to 650-700 nm. Post-acquisition analyses of microscopic images was performed using Leica LasX and ImageJ software.

To quantitatively assay the presence of CL307-bearing host polymers on the S. aureus surface, adjuvanted bacteria were run through a BD (Franklin Lakes, NJ, USA) FACSCanto II instrument using signal acquisition in the instrument's "APC" channel to provide a quantitative measure of CL307-bearing host polymers present on the bacterial surface. Alongside adjuvanted bacteria, commercial fluorescence quantification beads (Bangs Laboratories, Inc., Fishers, IN, USA) were run on the instrument to generate a standard curve for converting the instrument's fluorescent signal intensities of arbitrary values to absolute values. Post-acquisition analyses was performed with FlowJo 10 software (Ashland, OR, USA).

For assessing stability of CL307-polymers complexed to the S. aureus surface, adjuvanted bacteria were incubated at 37 °C in PBS for up to 24 hours. For assessing their growth, bacteria were incubated at 37 °C in brain heart infusion growth media with shaking for 16 hours.

Immune response to adjuvanted S. aureus

Monocyte-derived macrophages were prepared as previously described.[16] To visually confirm that adjuvanted S. aureus could still be phagocytosed by macrophages, harvested macrophages were plated at a density of 100k macrophages in 200 μL RPMI containing 10% FBS onto glass-bottom confocal dishes and incubated overnight at 37 °C. The next day, 1.8 mL RPMI 10% FBS containing 10 μg/mL Hoechst 33342 was added to the confocal dishes and the dishes positioned on an Andor (Belfast, Northern Ireland) Dragonfly 500 spinning disk confocal fluorescence microscope. Immediately before image acquisition, a 10 μL aliquot containing 106 adjuvanted bacteria was carefully added just above the macrophage layer. Subsequently, z-stack images of approximately 40 μm in depth at 1 μm intervals were acquired every 2.5 minutes for a total duration of 30 minutes. Post-acquisition analyses of images were performed using Imaris software (Zurich, Switzerland).

To assay the immunogenicity of adjuvanted S. aureus, macrophages post-harvesting were plated at a density of 100k macrophages in 100 μL RPMI 10% FBS in 96-well flat-bottom plates (Nunc, Thermo Fisher Scientific, Waltham, MA, USA) and incubated overnight at 37 °C. The next day, 400k adjuvanted bacteria in 100 μL RPMI 10% FBS were added to the wells, and the macrophages incubated for another 24 hours. Following this, supernatants were removed from wells and stored at -20 °C for eventual cytokine analysis using BD Biosciences human IL-6 (Cat. No. 555220) and IL-10 (Cat. No. 555157) ELISA kits according to the manufacturer's specifications.

Statistical analyses

Significance of differences between groups was analyzed by ANOVA with t-test for multiple comparison's or Student's t-test for two groups, using Graphpad Prism 9.3.1.

Supplementary Information

Chemical Procedures

1. General

1.1 Chemicals

Chemicals were obtained commercially from Merck (Darmstadt, Germany), TCI (Tokyo, Japan) or Cyclodextrin-Shop (Tilburg, The Netherlands) and used without further purification; these were deemed free of any significant endotoxin contamination by respective manufacturers. Amino acids were obtained from either Bachem (Bubendorf, Switzerland) or Iris Biotech (Marktredwitz, Germany). Solvents were obtained from Actu-All (Oss, The Netherlands), Biosolve (Valkenswaard, The Netherlands) or Merck (Darmstadt, Germany). Acetonitrile, N,N-Dimethylformamide and Dimethylsulfoxide were dried using 4Å molecular sieves Merck (Darmstadt, Germany) unless stated otherwise. Reactions were carried out under normal atmosphere unless stated otherwise. Column chromatography was performed with 40–63 μm silica from Screening Devices (Amersfoort, The Netherlands). SPPS was carried out either by a Biotage Syro II (Uppsala, Sweden) or by hand using fritted tubes (6, 10 or 25 mL) from Screening Devices (Amersfoort, The Netherlands) and in-house N_2 flow/vacuum.

1.2 HPLC

High-performance liquid chromatography was performed on a Waters HPLC system using either a 1525EF or 2545 pump and a 2489 UV/VIS detector. For preparative HPLC either a Dr. Maisch GmbH Reprosil-Pur 120 C18-AQ 10 *μm* (250 × 20 mm) column using a flow of 12 mL/min or an XBridge Prep C8 10 *μm* OBD (250 × 30 mm column) with a flow of 25 mL/min was used. For semi-preparative HPLC a Dr. Maisch GmbH Reprosil-Pur C18-AQ 10 *μm* (250 × 10 mm) column was used with a flow of 5 mL/min. For analytical HPLC a Dr. Maisch GmbH Reprosil-Pur C18-AQ 5 *μm* (250 × 4.6 mm) column with a flow of 1 mL/min and a gradient of 5→95% CH_3CN in H_2O) (0.1% TFA) in 40 min (1 mL/min) was used.

1.3 Mass spectrometry

Mass spectrometry was performed using a Bruker Microflex Matrix-assisted laser desorption ionization time-of-flight (MALDI-TOF) mass spectrometer (Billerica, MA, United States).

1.4 NMR

^{1}H NMR, COSY and ^{13}C NMR of the dyes were recorded on a Bruker AV-300 spectrometer (300 MHz) (Billerica, MA, United States) in methanol-d_4. Quantification of the number of β-CD units per polymer with ^{1}H NMR and DOSY was done in D_2O using a Bruker Avance III spectrometer (500 MHz), equipped with a 5 mm TXI probe.

1.5 Dialysis

Dialysis was performed using Pur-A-Lyzer (either Mega/Maxi 3500 MWCO or Mini 12000 MWCO) dialysis kits from (Sigma-Aldrich, St. Louis, MO, USA).

1.6 Photometry

Absorbance spectra were recorded using an Ultrospec 2100 pro (Amersham Biosciences, Little Chalfont, United Kingdom).

2. Chemical analyses

2.1 Quantification of β-CD

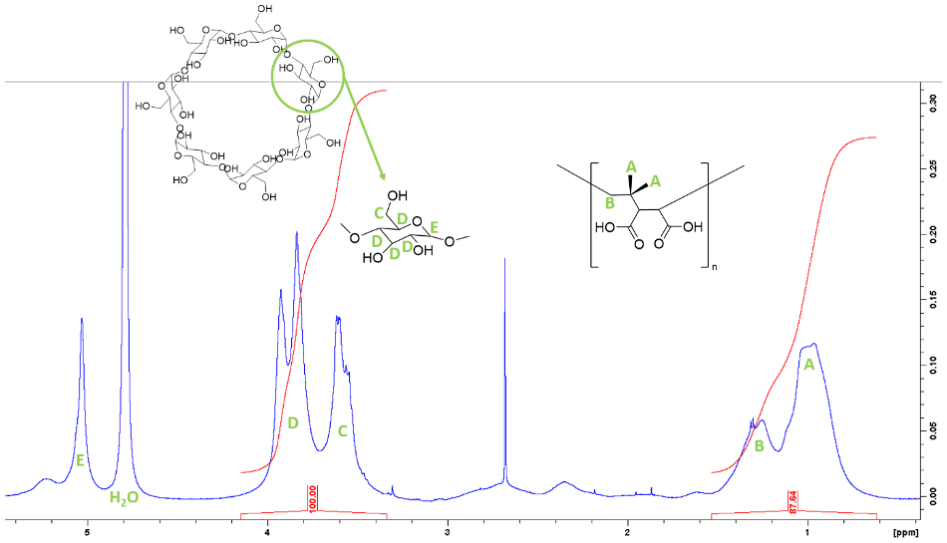

Figure S1: ^{1}H NMR spectrum with integrated peaks and annotation of *PIB-MA$_{[389]}$-CD$_{[85]}$ (6)* confirming presence of β-CD, which was used for calculation of the average amount of β-CD per polymer unit.

The amount of β-CD per polymer was determined as previously described (Duszenko et al., 2020b; Rood et al., 2017) using ^{1}H NMR; briefly: the polymer peaks at 0.8 - 1.4 ppm (CH_3 and CH_2) were integrated (87.6), as well as the β-CD peaks at 4.0 - 3.5 ppm originating from the β-CD protons. These integrals were used for calculation of the amount of β-CD per polymer using the following rationale:

Monomer protons=βCD protons=87.6 : 100=8 : 9.13

βCD per monomer=(Integrated βCD protons)/(Total protons in βCD)= 9.13/42=0.217 βCD=1 βCD per 4.6 monomers

βCD units per polymer unit=(Monomer units per polymer)/(Monomer units per βCD)= 389/4.6=84.6

This was rounded to 85 for clarity of illustration and calculation.

2.2 Quantification of Cy5

The molar extinction coefficient of NH_2-Cy5-COOH was determined as previously described;(Hensbergen et al., 2020) briefly: a weighed amount of Cy5 was dissolved in water to create a 5 mM stock solution. From this stock a dilution range from 7.5 μm to 0.25 μm was made in triplicate, of which the absorption was measured at Abs_{max} = 640 nm. Using linear regression, the molar extinction coefficient was then determined to be 62900 $L^{-1} \cdot mol^{-1} \cdot cm^{-1}$ in water. This was used with the Lambert-Beer equation to determine the dye molarity in a 3.1 μM solution of **$PIBMA_{[389]}$-$CD_{[85]}$-$Cy5_{[x]}$ (7)**. Dividing the dye molarity by 3.1 μM thus provided an average number of 1.53 Cy5 molecules per polymer; for clarity of illustration and calculation this was rounded to 2 Cy5 dyes per polymer.

2.3 Quantification of CL307 (the adjuvant) on polymer

The molar extinction coefficient of CL307 was estimated as previously described (Hensbergen et al., 2020); briefly: a weighed quantity of CL307 was dissolved in water to yield a 1 mM stock solution. From this stock a dilution range from 7.5 μm to 0.25 μm was made in triplicate, of which the absorption was measured at Abs_{max} = 298 nm. Using linear regression, the molar extinction coefficient was determined to be 5200 $L^{-1} \cdot mol^{-1} \cdot cm^{-1}$ in water. This was used with the Lambert-Beer equation to determine the CL307 molarity in a 0.5 μM solution of **$PIBMA_{[389]}$-$CD_{[85]}$-$Cy5_{[2]}$-$CL307_{[x]}$ (9)**. Dividing the CL307 molarity by 0.5 μM thus gave an average number of 58 CL307 molecules per polymer.

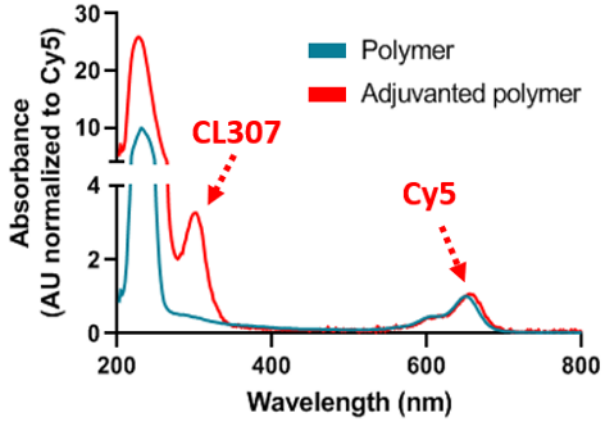

Figure S2: Confirmation of CL307 presence on the polymer was obtained using UV-Vis spectroscopy by measuring a solution of $PIBMA_{[389]}$-$CD_{[85]}$-$Cy5_{[2]}$-$CL307_{[58]}$-$NEtOH_{[633]}$ (9) in water (red line). This shows amide-bond absorption around 214 nm, absorption of CL307 around 300 nm and Cy5 absorption around 650 nm. As a control, $PIBMA_{[389]}$-$CD_{[85]}$-$Cy5_{[2]}$ (7) was also measured (turquoise line) showing only amide-bond and Cy5 absorption around 214 nm and 650 nm, respectively.

2.4 HPLC

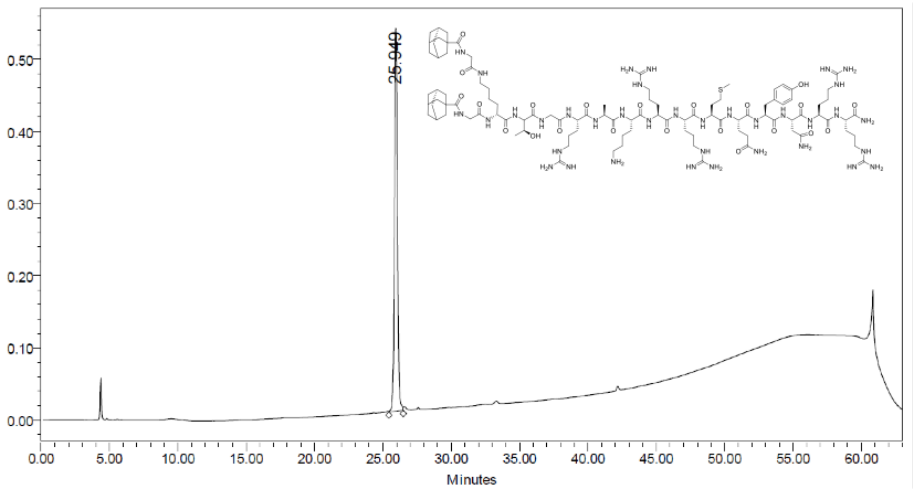

Figure S3: HPLC (220 nm) of *UBI-Lys(Gly-Ad)$_2$ (1.)*

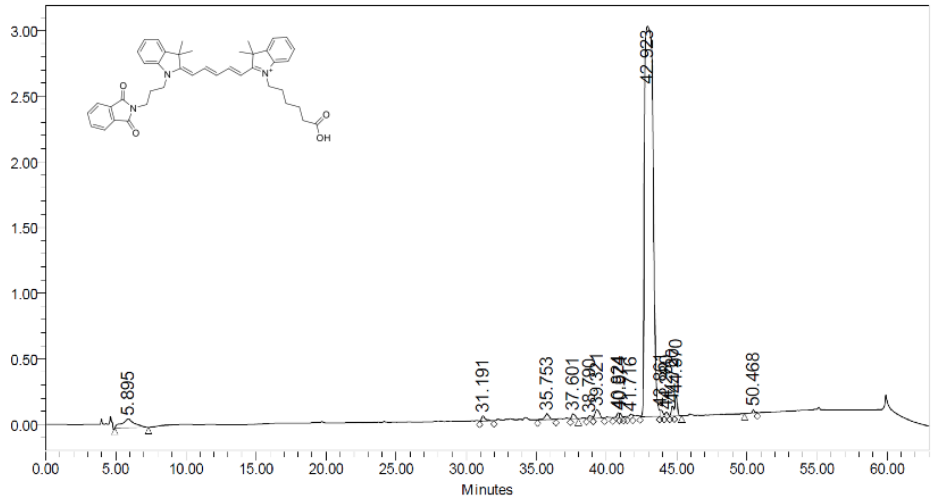

Figure S4: HPLC (220 nm) of Phth-Cy5-COOH (4).

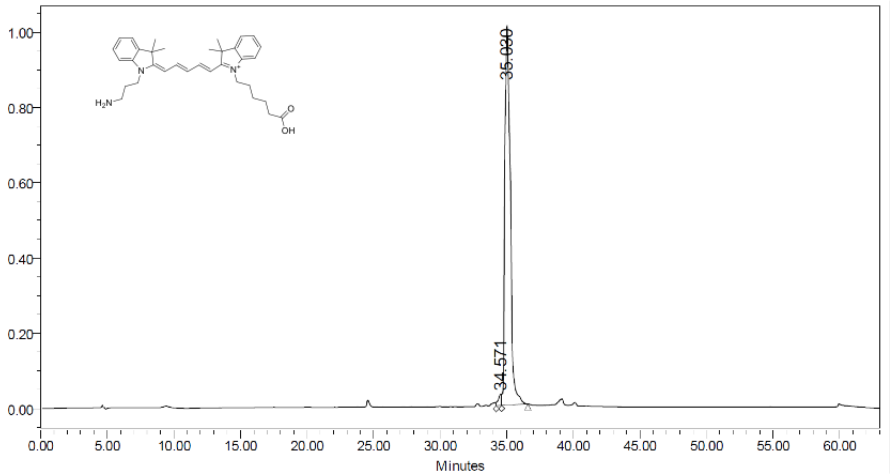

Figure S5: HPLC (220 nm) of NH_2-Cy5-COOH (5).

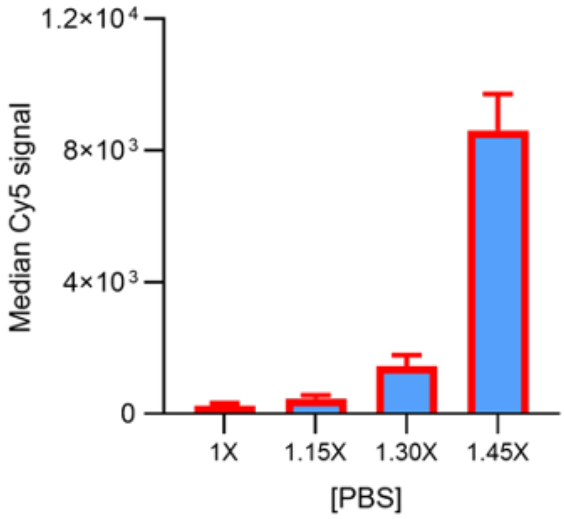

Figure S6: Complexation of adjuvant-bearing polymers onto *S. aureus* at varying PBS concentrations. Median Cy5 signal (y-axis) of complexed adjuvant-bearing polymer at differing concentrations of PBS (x-axis) during complexation.

Supplementary References

[1] D. Oushiki, H. Kojima, T. Terai, M. Arita, K. Hanaoka, Y. Urano, T. Nagano, *J Am Chem Soc* **2010**, *132*, 2795-2801.

[2] A. W. Hensbergen, T. Buckle, D. M. van Willigen, M. Schottelius, M. M. Welling, F. A. van der Wijk, T. Maurer, H. G. van der Poel, G. van der Pluijm, W. M. van Weerden, H. J. Wester, F. W. B. van Leeuwen, *J Nucl Med* **2020**, *61*, 234-241.

[3] M. T. Rood, S. J. Spa, M. M. Welling, J. B. Ten Hove, D. M. van Willigen, T. Buckle, A. H. Velders, F. W. van Leeuwen, *Sci Rep* **2017**, *7*, 39908.

[4] N. Fattahi, M. Ayubi, A. Ramazani, *Tetrahedron* **2018**, *74*, 4351-4356.

[5] N. Duszenko, D. M. van Willigen, M. M. Welling, C. M. de Korne, R. van Schuijlenburg, B. M. F. Winkel, F. W. B. van Leeuwen, M. Roestenberg, *ACS Infect Dis* **2020**, *6*, 1734-1744.

5

Chemically augmented malaria sporozoites display an improved immunogenic profile

Nikolas Duszenko, Roos van Schuijlenburg, Severine Chevalley-Maurel, Danny M. van Willigen, Laura de Bes-Roeleveld, Stefanie van der Wees, Chanel Naar, Els Baalbergen, Graham Heieis, Anton Bunschoten, Aldrik H. Velders, Blandine Franke-Fayard, Fijs W.B. van Leeuwen and Meta Roestenberg

Adapted from:

Front Immunol. 2023 Aug 31;14:1204606.
PMID: 37720224
DOI: 10.3389/fimmu.2023.1204606.

Abstract

Despite promising results in malaria-naïve individuals, whole sporozoite (SPZ) vaccine efficacy in malaria-endemic settings has been suboptimal. Vaccine hypo-responsiveness due to previous malaria exposure has been posited as responsible, indicating the need for SPZ vaccines of increased immunogenicity. To this end, we here demonstrate a proof-of-concept for altering SPZ immunogenicity, where supramolecular chemistry enables chemical augmentation of the parasite surface with a TLR7 agonist-based adjuvant (SPZ-SAS(CL307)). *In vitro*, SPZ-SAS(CL307) remained well recognized by immune cells and induced a 35-fold increase in production of pro-inflammatory IL-6 ($p < 0.001$). More promisingly, immunization of mice with SPZ-SAS(CL307) yielded improved SPZ-specific IFN-γ production in liver-derived NK cells (percentage IFN-γ^+ cells 11.1±1.8 vs. 9.4±1.5%, $p < 0.05$), $CD4^+$ T cells (4.7±4.3 vs. 1.8±0.7%, $p < 0.05$) and $CD8^+$ T cells (3.6±1.4 vs. 2.5±0.9%, $p < 0.05$). These findings demonstrate the potential of using chemical augmentation strategies to enhance the immunogenicity of SPZ-based malaria vaccines.

Introduction

The World Health Organization's recent endorsement of the world's first malaria vaccine, RTS,S, marks an important step in the fight against malaria. RTS,S – a subunit-based vaccine that targets the circumsporozoite protein (CSP) abundantly expressed on malaria sporozoites (SPZ) – has yielded a protective efficacy of ±30% (Rts, 2015). To improve on these numbers, whole-cell vaccines based on SPZ offer a promising alternative, as they display a broader range of antigens and can induce high levels of protection in malaria-naïve populations (Mordmuller et al., 2017; Roestenberg et al., 2009; Seder et al., 2013). Problematically, however, this high efficacy in malaria-naïve populations has thus far not been replicated in malaria-endemic settings using similar vaccination regimens (Oneko et al., 2021; Sissoko et al., 2017). It thus appears that in individuals pre-exposed to malaria, the intrinsic tolerogenicity of SPZ blunts the induction of robust immune responses to SPZ vaccines (Illingworth et al., 2013; Jongo et al., 2019; Winkel et al., 2020).

A well-established approach to overcoming suboptimal vaccine immunogenicity is supplementing vaccine with adjuvants, immunogenic compounds that induce (pro-inflammatory) activation (Di Pasquale et al., 2015). Though such strategies are nowadays routinely applied for subunit vaccines, their use for whole microbe-based vaccines is a novel concept. Adjuvanted subunits vaccines, as well as next-generation nanoparticle vaccines, have been shown to be most potent when vaccine and adjuvant are somehow physically linked to ensure co-delivery to immune cells (Cadoz, 1998; Francica et al., 2016; Lynn et al., 2020; Wilson et al., 2013). Devising an analogous vaccine formulation that co-delivers microbe and adjuvant is conceptually challenging but potentially important for improving SPZ-based vaccines' immunogenicity, especially given the preferred intravenous administration thereof; here, accurate co-localization of vaccine and adjuvant is necessary to promote targeted (antigen-specific) immune activation whilst minimizing harmful systemic effects.

Chemically mediated cell surface functionalization offers a potential route to realizing SPZ/adjuvant co-localization. Numerous strategies have been reported showing the feasibility of harnessing diverse chemical methodologies to functionalize cell surfaces (Roy et al., 2020). In our group we have developed one such strategy, wherein supramolecular host-guest chemistry is leveraged to functionalize microparticles (Spa et al., 2018), eukaryotic cells (Rood et al., 2017) and bacteria (Duszenko et al., 2020). More recently, we have shown that supramolecular functionalization of bacteria with an adjuvant yields an improved immunogenicity (Duszenko et al., 2022). Based on this work, we reasoned that it should similarly be possible to chemically augment the malaria SPZ cell surface with adjuvants, and in so doing alter the parasite's immunogenicity.

Here, we demonstrate the conceptual feasibility of chemically augmenting *Plasmodium berghei* SPZ (PbSPZ) with a so-called "**S**upramolecular **A**djuvanting **S**ystem" (SAS) that introduces a TLR7 agonist, CL307, onto the SPZ surface. These chemically augmented PbSPZ, referred to as PbSPZ-SAS(CL307), had their immunogenicity assayed *in vitro* via a macrophage model and *in vivo* using a mouse immunization model.

Results

Chemical augmentation of PbSPZ yields adjuvanted PbSPZ-SAS(CL307)

To generate chemically augmented PbSPZ-SAS(CL307), PbSPZ in salivary gland extract (SGE) were harvested from infected mosquitoes and pre-functionalized with adamantane (the supramolecular guest), followed by host-guest complexation with poly(isobutylene-alt-maleic anhydride) ($PIBMA_{389}$) polymers bearing: 1) β-cyclodextrin (CD - the supramolecular host) (85 units/polymer); 2) Cy5 fluorophores for tracking the polymers (2 units/polymer); and 3) the TLR7 agonist-based adjuvant CL307 (57 units/polymer) (Figure 1a) – thus yielding the envisioned PbSPZ-SAS(CL307). Strong Cy5 signals could be observed along the surface of PbSPZ-SAS(CL307) indicative of effective chemical augmentation (Figure 1b). Flow cytometric analysis validated these findings and indicated about 90% of PbSPZ with SAS(CL307) present (Figure 1c; median fluorescent intensity of 27,965 for PbSPZ-SAS(CL307) versus 6 for control SPZ, $p < 0.001$).

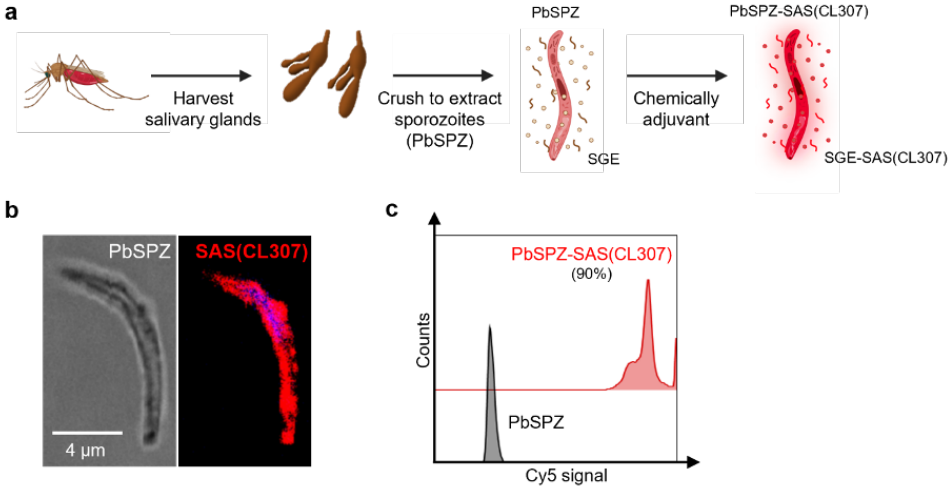

Figure 1: Chemical augmentation of PbSPZ yields adjuvanted PbSPZ-SAS(CL307). a) Schematic illustrating generation of chemically augmented PbSPZ-SAS(CL307). Malaria-infected mosquitoes were dissected to harvest PbSPZ-containing salivary glands. Pooled salivary glands were crushed to obtain PbSPZ in salivary gland extract (SGE), which were then chemically augmented with adjuvant by complexing onto their surface CL307-bearing supramolecular polymers (SAS(CL307)) to yield PbSPZ-SAS(CL307). **b)** Confocal fluorescence microscopy image of a PbSPZ-SAS(CL307) (left: brightfield) with SAS(CL307) (right: Cy5 signal) complexed to the surface. **c)** Flow cytometry histograms of Cy5 signal of PbSPZ-SAS(CL307) (top: red) and wild-type SPZ (bottom: grey). PbSPZ = *P. berghei* sporozoite; SAS = supramolecular adjuvanting system; CL307 = a Toll-like receptor 7 agonist; SGE = salivary gland extract.

PbSPZ-SAS(CL307) induce a more pro-inflammatory response *in vitro* in macrophages

The immunological characteristics of PbSPZ-SAS(CL307) were first characterized *in vitro* using bone marrow-derived macrophages. Confocal imaging confirmed that PbSPZ-SAS(CL307) were normally phagocytosed by macrophages (Figure 2a). By fluorescently tagging PbSPZ with a FITC-based mitotracker we further assessed phagocytic uptake via flow cytometry (Figure 2b), and in so doing determined that the degree of phagocytosis of PbSPZ-SAS(CL307) was comparable to that of wild-type PbSPZ (Figure 2c; 21.3±2.9% vs. 18.8±2.9% at a ratio of 1 PbSPZ to 4 macrophages, $p = 0.34$).

Subsequently, we characterized the phenotype of macrophages after 24-hour co-culture with PbSPZ-SAS(CL307). Overall, macrophage surface marker expression showed increased median expression of CD80 (Figure S-1a; 3.1±0.5 vs. 1.3±0.3 fold-change over medium, $p < 0.001$) and PD-L1 (Figure S-1b, 3.6±0.3 vs. 1.8±0.3 fold-change over medium, $p < 0.001$) for PbSPZ-SAS(CL307) compared to wild-type SPZ. Changes in surface marker expression were paralleled by large increases in cytokine production: IL-6 levels in response to PbSPZ-SAS(CL307) were increased 35-fold compared to wild-type PbSPZ (Figure 2d; 5,742±1,391 vs. 166±205 pg/mL, $p < 0.0001$), and increased 27-fold compared to both control PbSPZ-SAS (without adjuvant) (Figure 2d; 5,742±1,391 vs. 211±113 pg/mL, $p < 0.0001$) and to a cocktail of PbSPZ + concentration-matched soluble CL307 (Figure 2d; 5,742±1,391 vs. 209±206 pg/mL; $p < 0.0001$). Production of regulatory IL-10 was less dramatically increased, with 10-fold increases after incubation with PbSPZ-SAS(CL307) compared to both wild-type PbSPZ (Figure 2e; 2,543±495 vs. 234±89 pg/mL, $p < 0.0001$) and PbSPZ-SAS controls lacking adjuvant (Figure 2e; 2,543±495 vs. 248±89 pg/mL, $p < 0.0001$). However, compared to a PbSPZ + CL307 cocktail, IL-10 secretion by PbSPZ-SAS(CL307) was less than 2-fold increased (Figure 2e; 2,543±495 vs. 1,431±871 pg/mL, $p < 0.01$). Altogether, these data suggested that PbSPZ-SAS(CL307) induced immune responses *in vitro* that skewed distinctly more pro-inflammatory than those induced by wild-type PbSPZ.

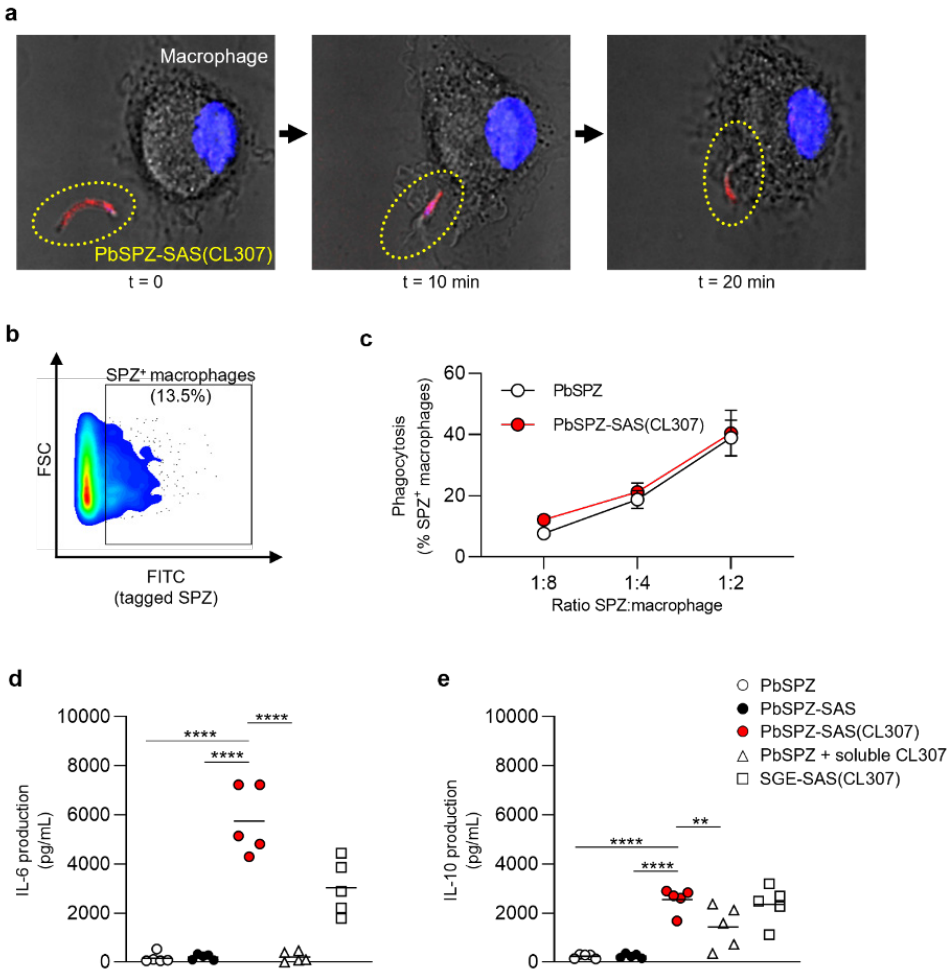

Figure 2: PbSPZ-SAS(CL307) induce a more pro-inflammatory response *in vitro* in macrophages. a) Time-lapse confocal fluorescence microscopy images showing phagocytosis of a PbSPZ-SAS(CL307) (yellow dotted oval) by a bone marrow-derived macrophage (cell nucleus in blue). **b)** Representative flow cytometry dot plot of macrophage cell size (y-axis) and FITC signal (x-axis) to isolate the proportion macrophages (13.5%) positive for FITC-tagged PbSPZ. **c)** Proportion macrophages positive for FITC-tagged PbSPZ (y-axis) at differing ratios of SPZ:macrophages (x-axis) for PbSPZ-SAS(CL307) (red) versus control PbSPZ (white). Data of n = 3 from a representative experiment. **d)** Production (pg/mL) of IL-6 cytokine (y-axis) by macrophages stimulated for 24h with PbSPZ-SAS(CL307) and controls. Data of n = 5 from three independent experiments. **e)** Production (pg/mL) of IL-10 cytokine (y-axis) by macrophages stimulated for 24h with PbSPZ-SAS(CL307) and controls. Data of n = 5 biological replicates from three independent experiments. Statistical significance between groups was assessed by one-way ANOVA with multiple comparisons.

PbSPZ = P. berghei sporozoite; SAS = supramolecular adjuvanting system; CL307 = a Toll-like receptor 7 agonist; SGE = salivary gland extract; CD = cluster of differentiation, PD-L = programmed death ligand, IL = interleukin; ** = $p < 0.01$, **** = $p < 0.0001$; figure legend: PbSPZ = wild-type PbSPZ (white circle), PbSPZ-SAS = PbSPZ with supramolecular polymer but lacking adjuvant (black circle), PbSPZ-SAS(CL307) = chemically adjuvanted PbSPZ (red circle), PbSPZ + soluble CL307 = wild-type PbSPZ + soluble adjuvant (white triangle), SGE-SAS(CL307) = chemically adjuvanted salivary gland extract (white square).

Liver and spleen immune cells of mice immunized with PbSPZ-SAS(-CL307) display a more proinflammatory phenotype after stimulation with PMA/ionomycin

To assess the *in vivo* immunogenicity of PbSPZ-SAS(CL307), female C57BL/6 mice were intravenously immunized twice at one-week intervals, followed by bulk immunophenotyping of liver and spleen at one week after second immunization (Figure 3a). There was a 50% increase in number of liver leukocytes in mice immunized with PbSPZ irrespective of adjuvant status relative to PBS-immunized control mice (Figure 3b; $6.4\pm1.3*10^6$ vs. $6.5\pm0.9*10^6$ vs. $4.4\pm1.1*10^6$ cells for PbSPZ-SAS(CL307) vs. PbSPZ vs. PBS, respectively, $p < 0.05$). In contrast to liver, splenocyte counts were mostly unaffected by PbSPZ-SAS(CL307) immunization, with comparable numbers found relative to controls immunized with PBS (Figure 3c; $1.03\pm0.31*10^8$ vs. $9.7\pm1.5*10^7$ cells, $p = 0.54$).

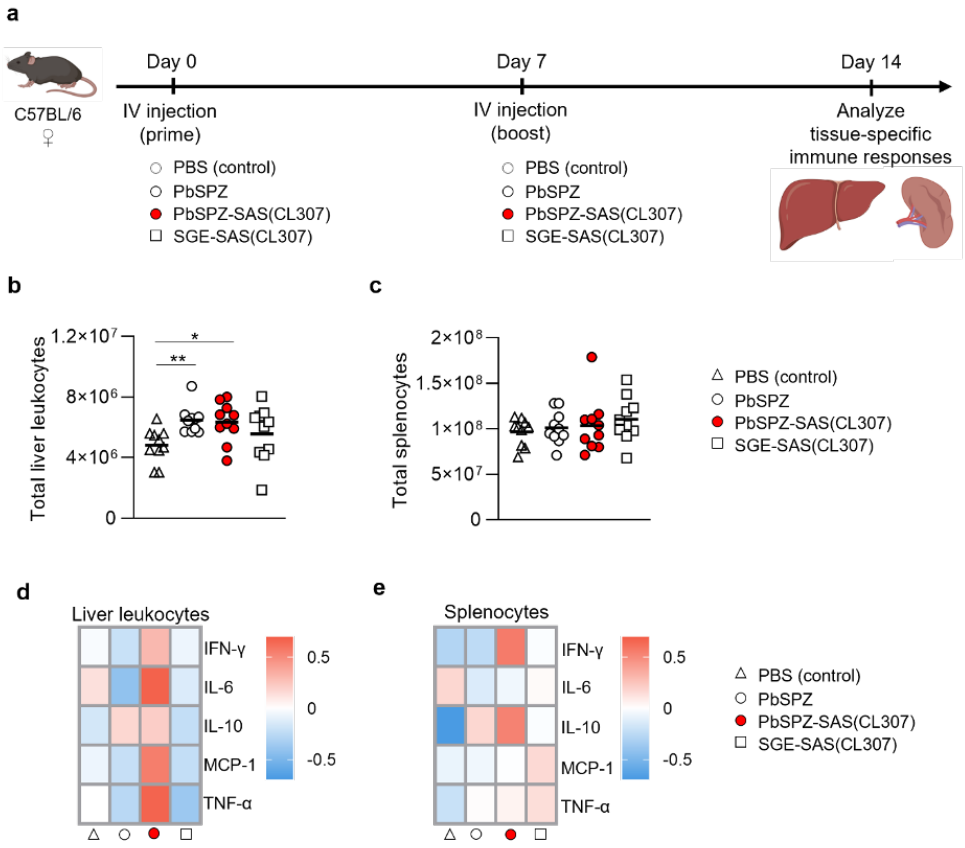

Figure 3: Liver and spleen immune cells of mice immunized with PbSPZ-SAS(CL307) display a more proinflammatory phenotype after stimulation with PMA/ionomycin. a) Schematic of experimental setup: mice were twice immunized at one-week intervals with either PBS (white triangle), 25,000 PbSPZ (white circle), 25,000 PbSPZ-SAS(CL307) (red circle) or concentration-matched SGE-SAS(CL307) controls (white square). One week after the second immunization, livers and spleens were harvested and processed for immunophenotyping. **b)** Total liver leukocyte counts (y-axis) of mice immunized with PbSPZ-SAS(CL307) or controls (x-axis). **c)** Total splenocyte counts (y-axis) of mice immunized with PbSPZ-SAS(CL307) or controls (x-axis). **d)** Heatmap of mean normalized values of secreted cytokines IFN-γ, IL-6, IL-10, MCP-1 and TNF-α (rows) by liver leukocytes from mice immunized with PbSPZ-SAS(-CL307) or controls (columns) after 36 hours stimulation with PMA/ionomycin. **e)** Heatmap of mean normalized values of secreted cytokines IFN-γ, IL-6, IL-10, MCP-1 and TNF-α (rows) by splenocytes from mice immunized with PbSPZ-SAS(CL307) or controls (columns) after 36 hours stimulation with PMA/ionomycin. All data shown are n = 10 biological replicates from two independent experiments. Statistical significance between groups was assessed by one-way ANOVA with multiple comparisons.

PbSPZ = *P. berghei* sporozoites; SAS = supramolecular adjuvanting system; CL307 = a Toll-like receptor 7 agonist; SGE = salivary gland extract; IFN = interferon, IL = interleukin, MCP = monocyte chemoattractant protein, TNF = tumor necrosis factor; PMA = phorbol 12-myristate 13-acetate; * = $p < 0.05$.

We next assessed immune responsiveness of liver leukocytes and splenocytes towards a generic PMA/ionomycin stimulus in PbSPZ-SAS(CL307)-immunized animals as compared to controls. Liver leukocytes from PbSPZ-SAS(CL307)-immunized animals showed increased production of several pro-inflammatory cytokines (Figure 3d), most notably IL-6 (Figure S-2a; mean fold-change of 0.67 vs. -0.42, $p < 0.05$) and TNF-α (Figure S-2a; mean fold-change of 0.66 vs. -0.27, $p < 0.05$) compared to wild-type PbSPZ, though not in production of regulatory IL-10 (Figure S-2a; mean fold-change of 0.21 vs. 0.17, $p = 0.89$). This effect appeared attributable to PbSPZ-SAS(CL307) themselves, as immunization with SGE-SAS(CL307) controls did not yield such increases (Figure 3d, Figure S-2a). Splenocytes from mice immunized with PbSPZ-SAS(CL307) showed less evident increases in pro-inflammatory cytokine production (Figure 3e), limited to an increased production of IFN-γ compared to wild-type PbSPZ (Figure S-2b; mean fold-change of 0.56 vs. -0.25, $p < 0.05$). These data suggested that immunization with PbSPZ-SAS(CL307) induced a more pro-inflammatory responsiveness of particularly liver leukocytes.

Liver leukocytes of PbSPZ-SAS(CL307)-immunized mice show enhanced SPZ-specific recall responses

Given the overall increased pro-inflammatory responsiveness of liver leukocytes after PbSPZ-SAS(CL307) immunization, we next evaluated SPZ-specific activation of liver leukocytes by co-culturing them with SPZ for 4 hours, followed by flow cytometric immunophenotyping (Figure 4a). Here, we found increased frequencies of activated cells in several different compartments for PbSPZ-SAS(CL307)-immunized animals. In the myeloid compartment (defined as $CD45^+CD3^-B220^-$ cells; see Fig S-4a), we observed an increased frequency of activated $CD86^+$ cells in PbSPZ-SAS(CL307)-immunized mice compared to wild-type PbSPZ (Figure S-4b, 25.4±4.3 vs. 21.3±2.5%, $p < 0.05$), as well as increased frequencies in $CD11b^+$ (Figure S-4b, 23.3±4.3 vs. 18.8±3.9%, $p < 0.05$) and $CD11c^+$ (Figure S-4b, 26.7±4.6 vs. 20.6±3.0%, $p < 0.01$) subsets. Liver NK cells of mice immunized with PbSPZ-SAS(CL307) also showed increased expression of several activation markers compared to those immunized with wild-type PbSPZ (Figure 4b), including significant increases in IFN-γ^+ (Figure 4c; 11.1±1.8 vs. 9.4±1.5% IFN-γ^+ NK cells, $p < 0.05$) and TNF-α^+ (Figure 4c; 9.4±7.2 vs. 3.8±2.1% TNF-α^+ NK cells, $p < 0.05$) NK cells. Similarly increased

activation in PbSPZ-SAS(CL307)-immunized mice was furthermore seen for $CD4^+$ T cells (Figure 4d) and $CD8^+$ T cells (Figure 4f). In particular, $CD4^+$ T cells showed significantly increased frequencies of IFN-γ^+ (Figure 4e; 4.7±4.3 vs. 1.8±0.7% IFN-γ^+ CD4 T cells, $p < 0.05$), $CD44^+$ (Figure 4e; 42.1±5.8 vs. 37.1±4.3% $CD44^+$ CD4 T cells, $p < 0.05$), and TNF-α^+ (Figure 4e; 7.2±3.7 vs. 4.2±1.3% TNF-α^+ CD4 T cells, $p < 0.05$) cells; $CD8^+$ T cells showed significant increases in frequency of IFN-γ^+ (Figure 4g; 3.6±1.4 vs. 2.5±0.9% IFN-γ^+ CD8 T cells, $p < 0.05$) and increased frequency in $CD44^+$ (Figure 4g; 24.5±4.6 vs. 20.9±3.4% $CD44^+$ CD8 T cells, $p = 0.0621$) cells. Notably, there was considerable within-group heterogeneity of SPZ-specific activation, with some mice showing exceptionally high cytokine profiles and others more comparable to controls. Altogether, these results indicated an enhanced SPZ-specific pro-inflammatory response of important subsets of both innate and adaptive immune cells in the livers of mice immunized with PbSPZ-SAS(CL307).

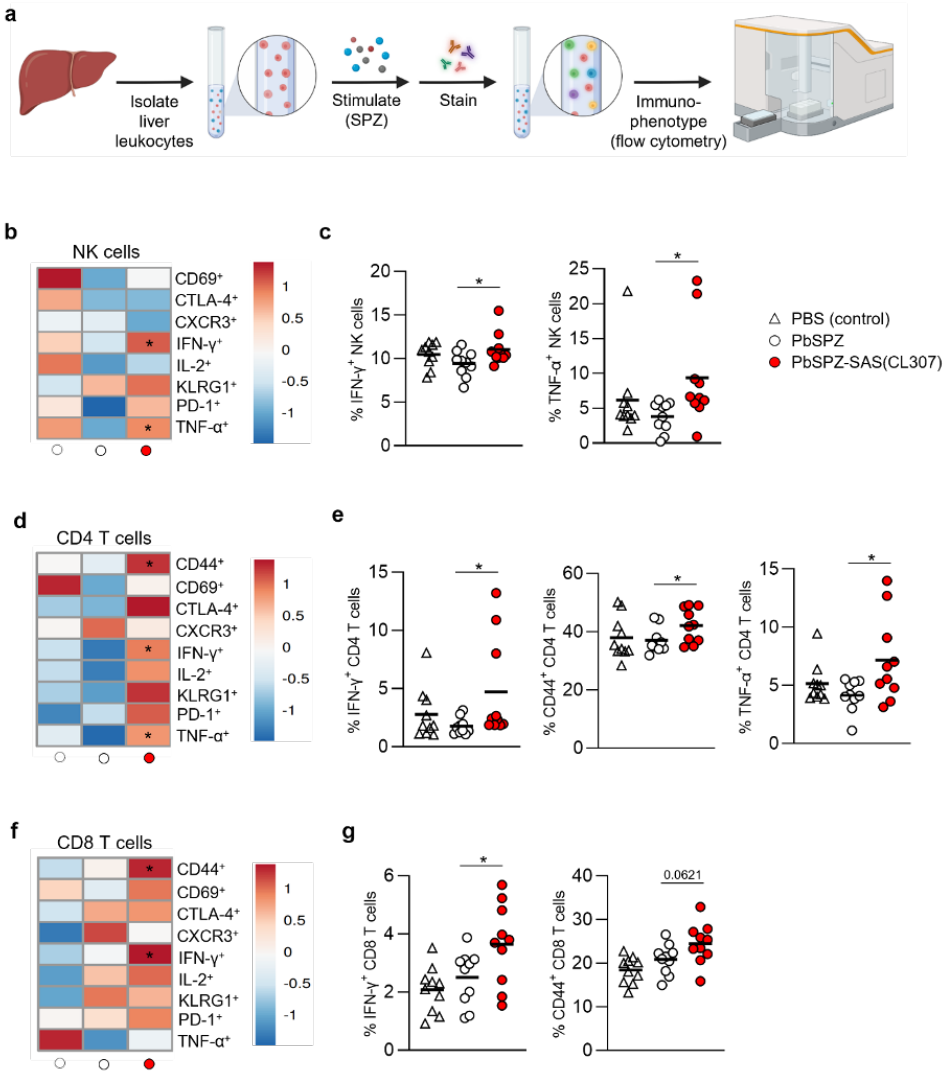

Figure 4: Liver leukocytes of PbSPZ-SAS(CL307)-immunized mice show enhanced SPZ-specific recall responses. a) Schematic illustrating experimental setup. Harvested livers from immunized mice were processed to yield liver leukocytes that were stimulated with SPZ in the presence of BrefA, stained with a fluorescent antibody panel and immunophenotyped by flow cytometry. **b)** Heatmap of mean normalized values of activation markers CD69, CTLA-4, CXCR3, IFN-γ, IL-2, KLRG1, PD-1 and TNF-α in NK cells (rows) after SPZ stimulation of liver leukocytes of mice immunized with PbSPZ-SAS(CL307) or controls (columns). **c)** Frequency of IFN-γ$^+$ and TNF-α$^+$ NK cells (y-axis) after SPZ stimulation of liver leukocytes of mice immunized PbSPZ-SAS(CL307) or controls (x-axis). **d)** Heatmap of mean normalized values of activation markers CD44, CD69, CTLA-4, CXCR3, IFN-γ, IL-2, KLRG1, PD-1 and

TNF-α in $CD4^+$ T cells (rows) after SPZ stimulation of liver leukocytes of mice immunized with PbSPZ-SAS(CL307) hybrids or controls (columns). **e)** Frequency of IFN-γ^+, $CD44^+$ and TNF-α^+ $CD4^+$ T cells (y-axis) after SPZ stimulation of liver leukocytes of mice immunized with PbSPZ-SAS(CL307) or controls (x-axis). **f)** Heatmap of mean normalized values of activation markers CD44, CD69, CTLA-4, CXCR3, IFN-γ, IL-2, KLRG1, PD-1 and TNF-α in $CD8^+$ T cells (rows) after SPZ/BrefA stimulation of liver leukocytes of mice immunized with PbSPZ-SAS(CL307) or controls (columns). **g)** Frequency of IFN-γ^+, $CD44^+$ and TNF-α^+ $CD8^+$ T cells (y-axis) after SPZ stimulation of liver leukocytes of mice immunized PbSPZ-SAS(CL307) or controls (x-axis). All data shown are n = 10 biological replicates from two independent experiments. Statistical significance between groups was assessed by one-way ANOVA with multiple comparisons.

PbSPZ = *P. berghei* sporozoite; SAS = supramolecular adjuvanting system; CL307 = a Toll-like receptor 7 agonist; CD = cluster of differentiation, CTLA = cytotoxic T-lymphocyte-associated protein, CXCR = chemokine receptor, IFN = interferon, IL = interleukin, KLRG = killer cell lectin-like receptor, PD = programmed death, TNF = tumor necrosis factor; BrefA = brefeldin A; * = $p < 0.05$, ** = $p < 0.01$; figure legend: PBS = vehicle (negative control – white triangle), PbSPZ = wild-type SPZ (white circle), PbSPZ-SAS(CL307) = chemically adjuvanted

Discussion

Here, we have shown the conceptual feasibility of chemically augmenting SPZ with adjuvants to alter their immunogenicity both *in vitro* and *in vivo*. Macrophages stimulated *in vitro* with chemically augmented PbSPZ-SAS(CL307) displayed a more pro-inflammatory phenotype, especially with regard to increased production of IL-6. *In vivo*, intravenous immunization of mice with PbSPZ-SAS(CL307) skewed in particular liver leukocytes towards more pro-inflammatory responses in response to a generic PMA/ionomycin stimulus, and furthermore induced an enhanced pro-inflammatory, SPZ-specific activation of both innate (e.g. $CD86^+$ myeloid; IFN-γ^+ NK cells) and adaptive (e.g. IFN-γ^+ $CD4^+$ and $CD8^+$ T cells) liver cell compartments.

There exists a clear need for innovative strategies that increase the potency, i.e. immunogenicity, of SPZ-based vaccines. Our findings extend on work that previously established the feasibility of improving SPZ immunogenicity via the traditional adjuvanting method of administering a mixture of SPZ and adjuvant (Ghilas et al., 2021; Gonzalez-Aseguinolaza et al., 2002; Li et al., 2015; Othman et al., 2018). Specifically, we find that chemically augmented SPZ-SAS(CL307) can be stably formed and show considerably boosted immunogenicity *in vitro*, with 35-fold increases in IL-6 production by macrophages compared to unadulterated SPZ. This large increase in immunogenicity seemed in particular attributable to the physical co-localization ensured by supramolecularly complexed adjuvant, as SPZ-SAS(CL307) induced 27-fold increases in IL-6 production compared to a mixture of SPZ and CL307. We thus conclude that chemical augmentation may indeed provide a platform for realizing vaccine/adjuvant

co-localization with whole SPZ-based vaccines. Possibly, such platforms could address the challenge of achieving targeted immune activation with intravenous administration of such vaccines.

In this proof-of-concept study for chemically augmenting SPZ immunogenicity, we chose a TLR7 agonist as the adjuvanting moiety, given their excellent track record of inducing cytotoxic T-cell responses (Ahonen et al., 1999; Vascotto et al., 2019; Wille-Reece et al., 2005). Such responses, in particular manifested in the form of IFN-γ^+ immune cells, are thought to be important mediators of malarial protection (Ewer et al., 2013; Schofield et al., 1987; Wolf et al., 2017), making a TLR7 agonist a logical first choice. We found that chemical augmentation of SPZ with a TLR7 agonist did indeed induce more cytotoxic responses in immunized mice's livers, with significantly increased frequencies of IFN-γ^+ NK cells, $CD4^+$ T cells and $CD8^+$ T cells upon SPZ restimulation. These findings suggest that 1) physically co-localized adjuvants retain their immunogenic properties for eliciting specific types of immune responses, and 2) that these immune responses are coupled to the antigenic stimulus – in this case, SPZ. Future modifications of this proof-of-concept would thus be well-suited for producing refinements of PbSPZ-SAS(CL307) that e.g. harness the synergistic effects reported between different TLR agonists (Napolitani et al., 2005; Warger et al., 2006).

The proof-of-concept here shown does not take into account the potential role of SPZ motility in vaccine efficacy. In adapting our SAS technology to SPZ, we found that motile SPZ mostly shed surface-localized adjuvant – an effect similarly described in antibody studies (Aliprandini et al., 2018). Robust chemical augmentation thus necessitated immobilization of SPZ. The use of immobilized SPZ for vaccination does present certain advantages, especially in obviating the need for costly liquid nitrogen storage and transportation logistics, but comes at the cost of decreasing protective efficacy (Doolan and Martinez-Alier, 2006). Hence, subsequent refinements of the concept would do well to explore the feasibility of anchoring adjuvant intracellularly as a means to preserving SPZ motility.

In conclusion, we have here provided a proof-of-concept indicating the potential for chemically altering the immunogenic profile of malaria SPZ. Further refinements of the concept could pave the way towards generating more efficacious SPZ-based vaccines for use in malaria-endemic areas.

References

Ahonen, C.L., Gibson, S.J., Smith, R.M., Pederson, L.K., Lindh, J.M., Tomai, M.A., and Vasilakos, J.P. (1999). Dendritic cell maturation and subsequent enhanced T-cell stimulation induced with the novel synthetic immune response modifier R-848. Cell Immunol *197*, 62-72.

Aliprandini, E., Tavares, J., Panatieri, R.H., Thiberge, S., Yamamoto, M.M., Silvie, O., Ishino, T., Yuda, M., Dartevelle, S., Traincard, F*., et al.* (2018). Cytotoxic anti-circumsporozoite antibodies target malaria sporozoites in the host skin. Nat Microbiol *3*, 1224-1233.

Cadoz, M. (1998). Potential and limitations of polysaccharide vaccines in infancy. Vaccine *16*, 1391-1395.

Di Pasquale, A., Preiss, S., Da Silva, F.T., and Garcon, N. (2015). Vaccine Adjuvants: from 1920 to 2015 and Beyond. Vaccines-Basel *3*, 320-343.

Doolan, D.L., and Martinez-Alier, N. (2006). Immune response to pre-erythrocytic stages of malaria parasites. Curr Mol Med *6*, 169-185.

Duszenko, N., van Willigen, D.M., Bunschoten, A., Velders, A.H., Roestenberg, M., and van Leeuwen, F.W.B. (2022). Chemically enhanced immunogenicity of bacteria by supramolecular functionalization with an adjuvant. Chembiochem.

Duszenko, N., van Willigen, D.M., Welling, M.M., de Korne, C.M., van Schuijlenburg, R., Winkel, B.M.F., van Leeuwen, F.W.B., and Roestenberg, M. (2020). A Supramolecular Platform Technology for Bacterial Cell Surface Modification. ACS Infect Dis *6*, 1734-1744.

Ewer, K.J., O'Hara, G.A., Duncan, C.J., Collins, K.A., Sheehy, S.H., Reyes-Sandoval, A., Goodman, A.L., Edwards, N.J., Elias, S.C., Halstead, F.D*., et al.* (2013). Protective CD8+ T-cell immunity to human malaria induced by chimpanzee adenovirus-MVA immunisation. Nat Commun *4*, 2836.

Fattahi, N., Ayubi, M., and Ramazani, A. (2018). Amidation and esterification of carboxylic acids with amines and phenols by N,N'-diisopropylcarbodiimide: A new approach for amide and ester bond formation in water. Tetrahedron *74*, 4351-4356.

Francica, J.R., Lynn, G.M., Laga, R., Joyce, M.G., Ruckwardt, T.J., Morabito, K.M., Chen, M., Chaudhuri, R., Zhang, B., Sastry, M.*, et al.* (2016). Thermoresponsive Polymer Nanoparticles Co-deliver RSV F Trimers with a TLR-7/8 Adjuvant. Bioconjug Chem *27*, 2372-2385.

Ghilas, S., Enders, M.H., May, R., Holz, L.E., Fernandez-Ruiz, D., Cozijnsen, A., Mollard, V., Cockburn, I.A., McFadden, G.I., Heath, W.R.*, et al.* (2021). Development of Plasmodium-specific liver-resident memory CD8(+) T cells after heat-killed sporozoite immunization in mice. Eur J Immunol *51*, 1153-1165.

Gonzalez-Aseguinolaza, G., Van Kaer, L., Bergmann, C.C., Wilson, J.M., Schmieg, J., Kronenberg, M., Nakayama, T., Taniguchi, M., Koezuka, Y., and Tsuji, M. (2002). Natural killer T cell ligand alpha-galactosylceramide enhances protective immunity induced by malaria vaccines. J Exp Med *195*, 617-624.

Illingworth, J., Butler, N.S., Roetynck, S., Mwacharo, J., Pierce, S.K., Bejon, P., Crompton, P.D., Marsh, K., and Ndungu, F.M. (2013). Chronic exposure to Plasmodium falciparum is associated with phenotypic evidence of B and T cell exhaustion. J Immunol *190*, 1038-1047.

Jongo, S.A., Church, L.W.P., Mtoro, A.T., Chakravarty, S., Ruben, A.J., Swanson, P.A., Kassim, K.R., Mpina, M., Tumbo, A.M., Milando, F.A.*, et al.* (2019). Safety and Differential Antibody and T-Cell Responses to the Plasmodium falciparum Sporozoite Malaria Vaccine, PfSPZ Vaccine, by Age in Tanzanian Adults, Adolescents, Children, and Infants. Am J Trop Med Hyg *100*, 1433-1444.

Li, X., Kawamura, A., Andrews, C.D., Miller, J.L., Wu, D., Tsao, T., Zhang, M., Oren, D., Padte, N.N., Porcelli, S.A.*, et al.* (2015). Colocalization of a CD1d-Binding Glycolipid with a Radiation-Attenuated Sporozoite Vaccine in Lymph Node-Resident Dendritic Cells for a Robust Adjuvant Effect. J Immunol *195*, 2710-2721.

Lynn, G.M., Sedlik, C., Baharom, F., Zhu, Y., Ramirez-Valdez, R.A., Coble, V.L., Tobin, K., Nichols, S.R., Itzkowitz, Y., Zaidi, N.*, et al.* (2020). Peptide-TLR-7/8a conjugate vaccines chemically programmed for nanoparticle self-assembly enhance CD8 T-cell immunity to tumor antigens. Nat Biotechnol *38*, 320-332.

Mordmuller, B., Surat, G., Lagler, H., Chakravarty, S., Ishizuka, A.S., Lalremruata, A., Gmeiner, M., Campo, J.J., Esen, M., Ruben, A.J.*, et al.* (2017). Sterile

protection against human malaria by chemoattenuated PfSPZ vaccine. Nature *542*, 445-449.

Napolitani, G., Rinaldi, A., Bertoni, F., Sallusto, F., and Lanzavecchia, A. (2005). Selected Toll-like receptor agonist combinations synergistically trigger a T helper type 1-polarizing program in dendritic cells. Nat Immunol *6*, 769-776.

Oneko, M., Steinhardt, L.C., Yego, R., Wiegand, R.E., Swanson, P.A., Kc, N., Akach, D., Sang, T., Gutman, J.R., Nzuu, E.L.*, et al.* (2021). Safety, immunogenicity and efficacy of PfSPZ Vaccine against malaria in infants in western Kenya: a double-blind, randomized, placebo-controlled phase 2 trial. Nat Med *27*, 1636-1645.

Othman, A.S., Franke-Fayard, B.M., Imai, T., van der Gracht, E.T.I., Redeker, A., Salman, A.M., Marin-Mogollon, C., Ramesar, J., Chevalley-Maurel, S., Janse, C.J.*, et al.* (2018). OX40 Stimulation Enhances Protective Immune Responses Induced After Vaccination With Attenuated Malaria Parasites. Front Cell Infect Microbiol *8*, 247.

Roestenberg, M., McCall, M., Hopman, J., Wiersma, J., Luty, A.J., van Gemert, G.J., van de Vegte-Bolmer, M., van Schaijk, B., Teelen, K., Arens, T.*, et al.* (2009). Protection against a malaria challenge by sporozoite inoculation. N Engl J Med *361*, 468-477.

Rood, M.T., Spa, S.J., Welling, M.M., Ten Hove, J.B., van Willigen, D.M., Buckle, T., Velders, A.H., and van Leeuwen, F.W. (2017). Obtaining control of cell surface functionalizations via Pre-targeting and Supramolecular host guest interactions. Sci Rep *7*, 39908.

Roy, S., Cha, J.N., and Goodwin, A.P. (2020). Nongenetic Bioconjugation Strategies for Modifying Cell Membranes and Membrane Proteins: A Review. Bioconjug Chem *31*, 2465-2475.

Rts, S.C.T.P. (2015). Efficacy and safety of RTS,S/AS01 malaria vaccine with or without a booster dose in infants and children in Africa: final results of a phase 3, individually randomised, controlled trial. Lancet *386*, 31-45.

Schofield, L., Villaquiran, J., Ferreira, A., Schellekens, H., Nussenzweig, R., and Nussenzweig, V. (1987). Gamma interferon, CD8+ T cells and antibodies required for immunity to malaria sporozoites. Nature *330*, 664-666.

Seder, R.A., Chang, L.J., Enama, M.E., Zephir, K.L., Sarwar, U.N., Gordon, I.J., Holman, L.A., James, E.R., Billingsley, P.F., Gunasekera, A.*, et al.* (2013). Protection against malaria by intravenous immunization with a nonreplicating sporozoite vaccine. Science *341*, 1359-1365.

Sissoko, M.S., Healy, S.A., Katile, A., Omaswa, F., Zaidi, I., Gabriel, E.E., Kamate, B., Samake, Y., Guindo, M.A., Dolo, A.*, et al.* (2017). Safety and efficacy of PfSPZ Vaccine against Plasmodium falciparum via direct venous inoculation in healthy malaria-exposed adults in Mali: a randomised, double-blind phase 1 trial. Lancet Infect Dis *17*, 498-509.

Spa, S.J., Welling, M.M., van Oosterom, M.N., Rietbergen, D.D.D., Burgmans, M.C., Verboom, W., Huskens, J., Buckle, T., and van Leeuwen, F.W.B. (2018). A Supramolecular Approach for Liver Radioembolization. Theranostics *8*, 2377-2386.

Vascotto, F., Petschenka, J., Walzer, K.C., Vormehr, M., Brkic, M., Strobl, S., Rosemann, R., Diken, M., Kreiter, S., Tureci, O.*, et al.* (2019). Intravenous delivery of the toll-like receptor 7 agonist SC1 confers tumor control by inducing a CD8+ T cell response. Oncoimmunology *8*, 1601480.

Warger, T., Osterloh, P., Rechtsteiner, G., Fassbender, M., Heib, V., Schmid, B., Schmitt, E., Schild, H., and Radsak, M.P. (2006). Synergistic activation of dendritic cells by combined Toll-like receptor ligation induces superior CTL responses in vivo. Blood *108*, 544-550.

Wille-Reece, U., Flynn, B.J., Lore, K., Koup, R.A., Kedl, R.M., Mattapallil, J.J., Weiss, W.R., Roederer, M., and Seder, R.A. (2005). HIV Gag protein conjugated to a Toll-like receptor 7/8 agonist improves the magnitude and quality of Th1 and CD8+ T cell responses in nonhuman primates. Proc Natl Acad Sci U S A *102*, 15190-15194.

Wilson, J.T., Keller, S., Manganiello, M.J., Cheng, C., Lee, C.C., Opara, C., Convertine, A., and Stayton, P.S. (2013). pH-Responsive nanoparticle vaccines for dual-delivery of antigens and immunostimulatory oligonucleotides. ACS Nano *7*, 3912-3925.

Winkel, B.M.F., Pelgrom, L.R., van Schuijlenburg, R., Baalbergen, E., Ganesh, M.S., Gerritsma, H., de Korne, C.M., Duszenko, N., Langenberg, M.C.C., Chevalley-Maurel, S.C.*, et al.* (2020). Plasmodium sporozoites induce regulatory

macrophages. PLoS Pathog *16*, e1008799.

Wolf, A.S., Sherratt, S., and Riley, E.M. (2017). NK Cells: Uncertain Allies against Malaria. Front Immunol *8*, 212.

Methods

Production of PbSPZ

Plasmodium berghei SPZ (PbSPZ) were produced in *Anopheles* mosquitoes that fed on male OF1 mice 4-5 days prior infected with *P. berghei* and having reached a blood gametocytemia of 0.2-0.8%.

Production of bone marrow-derived macrophages

Femur and tibia bones from female C57BL/6 mice were washed for 1 minute in ethanol and then rinsed with RPMI. Bones' ends were cut, and the marrow within flushed out via syringe into RPMI. Cells were centrifuged at 300 RCF for 10 minutes at 4 °C, supernatant discarded by decant, and cells resuspended in 3 mL red blood cell lysis buffer (specs) for 3 minutes on ice. Cells had added to them 7 mL RPMI, centrifuged again at 300 RCF for 10 minutes at 4 °C, supernatant discarded, and resuspended in 5 mL TCM (RPMI + 5% FBS + 0.1% β-mercaptoethanol). Cells were counted by Buerker counting chamber and subsequently plated in plastic Petri dishes (Thermo Fisher) at a density of $2*10^7$ cells in 10 mL TCM supplemented with 20 ng/mL murine M-CSF (derived in-house via M-CSF-producing L929 cells) to promote differentiation of monocytes into macrophages. Medium was refreshed once at day 2. On day 6, medium was removed from cells, cells rinsed once with PBS, and then incubated with 2 mL Accutase (STEMCELL Technologies, Vancouver, Canada) for 15 minutes at 37 °C to promote macrophage detachment. Eight mL of TCM was added and macrophages resuspended by serological pipet. Macrophages were centrifuged at 300 RCF for 10 minutes at 4 °C and supernatant discarded, followed by resuspension of cell pellets in 5 mL TCM by serological pipet. Macrophages were counted by Buerker counting chamber and then ready for downstream applications.

Mouse model for immunization studies

Female C57BL/6J mice (Charles River Laboratories, France) were obtained at 4-6 weeks of age and acclimatized for 1 week prior to use. Mice were group-housed (random allocation to groups of same-sex littermates) in ventilated cages with autoclaved aspen woodchip, fun tunnel, wood chew block and nestlets (12:12 hour (h) light-dark cycle; 21 ± 2°C; relative humidity of 55 ± 10%), and fed with a commercially-prepared, autoclaved dry rodent diet pellets and provided with water, both available *ad libitum*. Animal experiments were granted with a license AVD1160020173304 by the Competent Authority after advice on ethical

evaluation by the Animal Experiments Committee Leiden, and were performed in accordance with the Experiments on Animals Act (Wod, 2014), the applicable legislation in the Netherlands in accordance with the European guidelines (EU directive no. 2010/63/EU). Experiments were executed in a licensed establishment for experimental animals.

Chemical synthesis/analysis miscellany

Chemicals were obtained commercially from Merck (Darmstadt, Germany), TCI (Tokyo, Japan) or Cyclodextrin-Shop (Tilburg, The Netherlands) and used without further purification. Amino acids were obtained from either Bachem (Bubendorf, Switzerland) or Iris Biotech (Marktredwitz, Germany). Solvents were obtained from Actu-All (Oss, The Netherlands), Biosolve (Valkenswaard, The Netherlands) or Merck (Darmstadt, Germany). Acetonitrile, N,N-dimethylformamide and dimethylsulfoxide were dried using 4Å molecular sieves Merck (Darmstadt, Germany) unless stated otherwise. Reactions were carried out under normal atmosphere unless stated otherwise. Column chromatography was performed with 40–63 μm silica from Screening Devices (Amersfoort, The Netherlands). SPPS was carried out either by a Biotage Syro II (Uppsala, Sweden) or by hand using fritted tubes (6, 10 or 25 mL) from Screening Devices (Amersfoort, The Netherlands) and in-house N_2 flow/vacuum.

High-performance liquid chromatography was performed on a Waters HPLC system using either a 1525EF or 2545 pump and a 2489 UV/VIS detector. For preparative HPLC either a Dr. Maisch GmbH Reprosil-Pur 120 C18-AQ 10 *μm* (250 × 20 mm) column using a flow of 12 mL/min or an XBridge Prep C8 10 *μm* OBD (250 × 30 mm column) with a flow of 25 mL/min was used. For semi-preparative HPLC, a Dr. Maisch GmbH Reprosil-Pur C18-AQ 10 *μm* (250 × 10 mm) column was used with a flow of 5 mL/min. For analytical HPLC a Dr. Maisch GmbH Reprosil-Pur C18-AQ 5 *μm* (250 × 4.6 mm) column with a flow of 1 mL/min and a gradient of 5→95% CH_3CN in H_2O) (0.1% TFA) in 40 min (1 mL/min) was used. Mass spectrometry was performed using a Bruker Microflex Matrix-assisted laser desorption ionization time-of-flight (MALDI-TOF) mass spectrometer (Billerica, MA, United States). ^{1}H NMR, COSY and ^{13}C NMR of the dyes were recorded on a Bruker AV-300 spectrometer (300 MHz) (Billerica, MA, United States) in methanol-d_4. Quantification of the number of β-CD units per polymer with ^{1}H NMR and DOSY was done in D_2O using a Bruker Avance III spectrometer (500 MHz), equipped with a 5 mm TXI probe. Dialysis was performed using Pur-A-Lyzer (either Mega/Maxi 3500 MWCO or Mini 12000 MWCO) dialysis kits from (Sigma-Aldrich, St. Louis, MO, USA). Absorbance spectra were recorded using an Ultrospec 2100 pro (Amersham Biosciences, Little Chalfont, United Kingdom). Analyses can be found in the

Supporting Information.

Synthesis of chemical compounds

Ad-Osu esters were prepared as follows: amineC3Ad-(SO3)Cy3(SO3)COOH was dissolved in 330μL of dried DMSO. DiPEA (1uL, 5.83μmol) and 20uL of a 10mg/mL HsPyU were added and the reaction mixture was left to stir at room temperature for 90 minutes. Subsequently, MilliQ and CH_3CN were added to the solution and the crude product was purified using preparative HPLC (15 - 95% CH_3CN in Milli Q over 46 minutes) to yield the title product as a blue solid. This solid was resuspended in DMSO to yield a 1.2 mM stock for downstream applications.

The CL307-bearing host polymers were synthesized based on a previously published procedure (Rood et al., 2017). To initial graft β-cyclodextrins onto the polymers, poly(isobutylene-alt-maleic-anhydride (200.0 mg, 3.3 μmol) was dissolved in dimethylsulfoxide (3.0 mL), whereafter amino(6-monodeoxy-6-mono)-β-cyclodextrin hydrochloride (620.3 mg, 530.0 μmol) and N,N-diisopropylethylamine (29.0 μL, 166.7 μmol) were added, and stirring at 80°C was carried out for 94 hours. The solution was purified by dialysis in water (1000.0 mL) for 7 hours, followed by dialysis in phosphate buffer (0.2 M, pH 9, 1000.0 mL) for 144 hours including refreshment of buffer twice, followed by dialysis in water (1000.0 mL) for 7 hours. The dialysate was discarded and the residue was lyophilized, yielding an off-white solid (453.6 mg, 85.1% isolated yield).

Next, Cy5 dyes were coupled using a method published by Fattahi et al (Fattahi et al., 2018). $PIBMA_{[389]}$-$CD_{[85]}$ (420.0 mg, 2.6 μmol) was dissolved in water, whereafter N,N'-diisopropylcarbodiimide (122.8 μL, 798.0 μmol) was added. The mixture was stirred at room temperature for 1 hour followed by addition of 2.4 mL of a 1.1 mg/mL solution of NH_2-Cy5-COOH (5) in 1:8 ethanol/water (2.8 mg, 5.3 μmol). The solution was stirred for 5 hours at room temperature whereafter it was dialysed in water (5000.0 mL) for 24 hours while refreshing the water once, followed by lyophilization of the residue.

Thereafter, CL307 (Invitrogen, Waltham, MA, USA) was coupled to polymers by dissolving $PIBMA_{[389]}$-$CD_{[85]}$-$Cy5_{[2]}$ (8.05 mg, 50.3 nmol) in water (805 μL), followed by addition of DIC (7.7 μL, 50.3 μmol). After stirring for 1.3 hours at room temperature, CL307 (1.5 mg, 2.5 μmol) in water (1.5 mL) was added. After shaking for 1.3 hours ethanolamine (9.1 μL, 150.9 μmol) was added (to react with leftover free carboxylates and thereby sequester the polymers' negative charges), and stirring was continued for another 16 hours at room temperature. Thereafter, the reaction mixture was dialyzed in water (5 L) for 29 hours with

one refreshment of water. The residue was used as is for experiments; PBS pH 7.4 was added where necessary.

Supramolecular complexation of CL307-bearing host polymers (SAS(-CL307)) onto PbSPZ to generate PbSPZ-SAS(CL307)

Salivary glands from infected mosquitoes containing PbSPZ, and from uninfected mosquitoes for salivary gland extra (SGE) controls, were manually dissected at days 21-28 post-infection. Immediately prior to use, glands were homogenized to isolate PbSPZ. Isolated PbSPZ were pre-functionalized by incubating in 100 uL RPMI (Gibco, Thermo Fisher, Waltham, MA, USA) containing 1 μM Ad-OSu ester, a construct reactive toward the cell surface lysine residues present on the circumsporozoite protein sheath enveloping the parasite, and 10 μg/mL Hoechst 33342 for 15 minutes at 37 °C. Thereafter, PbSPZ were twice washed in 1.3 mL PBS supplemented with 1% fetal bovine serum (FBS) by centrifugation at 13k RCF for 5 minutes and decanting of supernatant. PbSPZ were resuspended in remaining supernatant by pipetting and bringing total volume to 100 μL PBS, followed by addition of 100 μL of 2 μM CL307-bearing host polymer ($CD_{85}Cy5_2CL307_{57}PIBMA_{389}$) in 1.9X PBS (where 1X is standard PBS concentration) and incubation for 4 hours at 37 °C that included mixing by pipet every 30 minutes. Then, PbSPZ were thrice washed in 1.3 mL PBS supplemented with 1% FBS by centrifugation at 13k RCF for 5 minutes and decanting of supernatant. PbSPZ were resuspended by pipetting and counted via Buerker chamber, and then ready for downstream applications.

Confocal imaging of PbSPZ-SAS(CL307)

PbSPZ-SAS(CL307) were added to glass-bottom confocal dishes (MatTek, Ashland, MA, USA) at a density of 25k in 10 μL and overlaid with a coverslip. Confocal dishes were sealed with parafilm and left for 30 minutes in a humidified chamber to allow parasites to settle to the bottom. Imaging of PbSPZ-SAS(-CL307) was performed on a Leica (Wetzlar, Germany) SP8 confocal fluorescence microscope.

Flow cytometric analysis of PbSPZ-SAS(CL307)

PbSPZ-SAS(CL307) at a density of 100k/mL were run through a BD (Franklin Lakes, NJ, USA) FACSCantoII instrument. Gating on the Hoechst signal discriminated PbSPZ-SAS(CL307) from contaminating salivary gland debris. Cy5 signal originating from the complexed CL307-bearing host polymers was measured in the instrument's "APC" channel. Post-acquisition analysis was per-

formed using FlowJo 10 (Ashland, OR, USA).

Confocal imaging of macrophage phagocytosis of PbSPZ-SAS(CL307)

Harvested macrophages were plated at a density of 200k in 200 μL TCM onto glass-bottom confocal dishes (MatTek) and placed overnight into a 37 °C incubator to allow macrophages to adhere. The next day, 1.8 mL TCM containing 10 μg/mL Hoechst 33342 was added per dish prior to imaging. Confocal dishes were positioned on an Andor (Belfast, UK) Dragonfly 500 spinning disk fluorescence microscope and prepared for image acquisition. Immediately prior to acquisition, 50k PbSPZ-SAS(CL307) in 10 μL were carefully added just above the macrophage layer. Images were acquired as z-stacks of approximately 40 μm in depth at an interval of 1 μm every 2.5 minutes for a total of 30 minutes. Post-acquisition analysis was performed using Imaris software (Zurich, Switzerland).

Flow cytometry quantitation of macrophage phagocytosis of PbSPZ-SAS(CL307)

Harvested macrophages were plated at a density of 100k in 100 μL TCM into flat-bottom 96-well plates (vendor) and placed overnight into a 37 °C incubator to allow macrophages to adhere. The next day, 100 μL aliquots of 50k, 25k or 12.5k PbSPZ-SAS(CL307) or wild-type SPZ tagged with a FITC-based mitotracker (Thermo Fisher) were added per well, and the plate centrifuged at 300 RCF for 10 minutes at room temperature. Plates were incubated for 45 minutes at 37 °C. Then, supernatant was removed by pipet, and 200 μL cold FACS buffer (PBS supplemented with 0.5% bovine serum albumin and 20 mM EDTA) added per well. Plates were incubated on ice for 15 minutes to promote macrophage detachment. Complete detachment was achieved by manual scraping with pipet tips and resuspending by pipet, after which macrophages were transferred to FACS tubes. Macrophages were finally run through a BD FACSCanto II instrument to assess the presence of FITC-tagged SPZ within. Post-acquisition analysis was performed using FlowJo 10 software.

In vitro immune response of macrophages to PbSPZ-SAS(CL307)

Harvested macrophages were plated at a density of 100k in 100 μL TCM into flat-bottom 96-well plates (Thermo Fisher) and placed overnight into a 37 °C incubator to allow macrophages to adhere. The next day, 100 μL aliquots of 50k PbSPZ-SAS(CL307) or relevant controls were added per well, and plates incubated at 37 °C for 24 hours. Thereafter, cell culture supernatants were removed and stored at -80 °C for eventual cytokine analysis. 200 μL cold PBS was added

per well, and plates incubated for 15 minutes on ice to promote macrophage detachment. Complete detachment of macrophages was achieved by manual scraping with pipet tips and resuspending by pipet, after which macrophages were transferred to V-bottom 96-well plates (Thermo Fisher) on ice. Macrophages were centrifuged at 200 RCF for 4 minutes at 4 °C and supernatant discarded by decant. Cell pellets were resuspended in 50 μL 400-fold diluted (in PBS) Aqua live/dead stain (Thermo Fisher) and incubated for 20 minutes on ice in the dark. Then, 150 μL 1.9% para-formaldehyde (Thermo Fisher) in PBS was added per well to fix cells, followed by another 15 minutes of incubation on ice in the dark. Macrophages were then centrifuged at 200 RCF for 4 minutes at 4 °C and supernatant discarded by decant. Cell pellets were resuspended in 200 μL FACS buffer by pipet and centrifuged at 200 RCF for 4 minutes at 4 °C, followed by supernatant decant. Cell pellets were finally resuspended in 200 μL FACS buffer and macrophages stored at 4 °C for up to a week prior to FACS analysis. On the day of FACS analysis, macrophages were centrifuged at 200 RCF for 4 minutes at 4 °C, followed by supernatant decant. Cell pellets were resuspended in 30 μL of antibody mix and incubated for 30 minutes at 4 °C in the dark. Thereafter, 170 μL of FACS buffer was added, macrophages centrifuged at 200 RCF for 4 minutes at 4 °C, and supernatant discarded by decant. Cell pellets were resuspended in 80 μL FACS buffer and transferred to FACS tubes. Macrophages were finally run through a BD Fortessa flow cytometer to measure surface marker expression levels. Post-acquisition analysis was performed using FlowJo 10 software.

In vivo immunization of mice with PbSPZ-SAS(CL307)

Mice were immunized with 25k PbSPZ-SAS(CL307) or wild-type SPZ in 200 μL PBS by injection into the tail vein, with negative controls receiving the PBS vehicle only. The initial prime immunization took place on day 0, with a second boost following on day 7.

Processing of tissues (liver, spleen, blood) from immunized mice

Fourteen days after the initial prime immunization, mice were anaesthetized by 10% ketamine (Dechra Pharmaceuticals, Northwich, UK)/20 mg/mL xylazine (Alfasan, Woerden, The Netherlands) cocktail. Following this, animals were perfused with 10 mL PBS, followed by excision of liver and spleen. These organs were immediately processed as follows.

To process livers, livers were minced by scalpel and added to 20 mL RPMI containing 1 mg/mL Collagenase IV (Sigma-Aldrich, St. Louis, MO, USA) and 2000 U/mL DNase I (Sigma-Aldrich) in 50 mL conical tubes. Livers were digested

for 45 minutes at 37 °C, with one mix of tubes' contents by inversion halfway through. Thereafter, digested livers were run through 100 μm filters (BD), and filters washed twice with 10 mL aliquots of Wash Buffer (WB – PBS supplemented with 1% FBS and 2.5 mM EDTA). Tubes were spun at 50 RCF for 3 minutes at 4 °C to pellet hepatocytes. Supernatants were carefully removed by serological pipet, leaving behind the hepatocyte cell pellets, and transferred to fresh 50 mL tubes. Hepatocyte-bereft cells were washed once by centrifugation at 300 RCF for 10 minutes at 4 °C and careful decant of supernatant, resuspension in 20 mL WB, and identical centrifugation/decant. Cell pellets were resuspended in 3 mL red blood cell lysis buffer and incubated on ice for 2 minutes, followed by addition of 7 mL WB. Cell were centrifuged at 300 RCF for 10 minutes at 4 °C and supernatant carefully discarded by decant, resuspension in 10 mL MACS buffer (PBS with 0.5% bovine serum albumin and 20 mM EDTA), followed by identical centrifugation/decant. Cell pellets were resuspended in 1 mL MACS buffer and had added to them 35 μL CD45 MicroBeads (Miltenyi Biotec, Bergisch Gladbach, Germany). After 15 minutes incubation at 4 °C, cells had added to them 10 mL MACS buffer and were centrifuged at 300 RCF for 10 minutes at 4 °C, followed by careful decant of supernatant. Cell pellets were resuspended in 5 mL MACS buffer and run through pre-wetted LS columns (Miltenyi Biotec) attached to a magnetic stand. These columns were thrice washed with 3 mL MACS buffer afterwards. Columns were removed from magnetic stands and $CD45^+$ cells therein displaced by flushing the column vigorously with 5 mL RPMI, which was thereafter supplemented with 1% FBS. $CD45^+$ cells, i.e. liver leukocytes, were centrifuged at 300 RCF for 10 minutes at 4 °C, had supernatant decanted, and were finally resuspended in 2 mL TCM. (Viable) cells were counted using a Buerker counting chamber and trypan blue, and then ready for downstream applications.

To process spleens, spleens in 1 mL HBSS (Gico) in 24-well flat-bottom plates (Thermo Fisher) were first mashed with a syringe plunger and then digested with 1 mg/mL Collagenase D (Roche, Basel, Switzerland) and 2000 U/mL DNase I (Sigma-Aldrich) for 20 minutes at 37 °C. Digestate was then passed through 100 μm filters that were thrice rinsed with 3 mL MACS buffer. Filtered cells were centrifuged at 300 RCF for 10 minutes at 4 °C and supernatant discarded. Cell pellets were resuspended in 3 mL red blood cell lysis buffer and incubated for 2 minutes on ice, followed by addition of 7 mL MACS buffer. Cells were centrifuged at 300 RCF for 10 minutes at 4 °C and supernatant discarded by decant. Cell pellets were resuspended in 10 mL TCM. (Viable) cells were counted using a Buerker counting chamber and trypan blue, and then ready for downstream applications.

Analysis of liver and spleen bulk immunophenotypes

Liver leukocytes and splenocytes were plated at a density of 200k and 500k per well, respectively, into U-bottom 96-well plates (Thermo Fisher) in 100 µL TCM. Each well then received an additional 100 µL of TCM containing phorbol 12-myristate 13-acetate (PMA) at a concentration of 0.2 µg/mL and ionomycin at a concentration of 2 µg/mL. Cells were then incubated for 36 hours at 37 °C. Thereafter, cell culture supernatants were removed and stored at -20 °C for eventual cytokine analysis by cytometric bead assay (BD) according to the manufacturer's specifications.

Analysis of liver cellular immune responses

Liver leukocytes were plated at a density of 200k per well into U-bottom 96-well plates (Thermo Fisher) in 100 µL TCM. Each well then received an additional 100 µL of TCM containing 100k SPZ and 20 µg/mL brefeldin A. Cells were then incubated for 4 hours at 37 °C. Thereafter, liver leukocytes were transferred to V-bottom 96-well plates (Thermo Fisher) on ice. Liver leukocytes were centrifuged at 200 RCF for 4 minutes at 4 °C and supernatant discarded by decant. Cell pellets were resuspended in 50 µL 400-fold diluted (in PBS) Aqua live/dead stain (Thermo Fisher) and incubated for 20 minutes on ice in the dark. Then, 150 µL 1.9% para-formaldehyde in PBS was added per well to fix cells, followed by another 15 minutes of incubation on ice in the dark. Cells were then centrifuged at 200 RCF for 4 minutes at 4 °C and supernatant discarded by decant. Cell pellets were resuspended in 200 µL FACS buffer by pipet and centrifuged at 200 RCF for 4 minutes at 4 °C, followed by supernatant decant. Cell pellets were finally resuspended in 200 µL FACS buffer and liver leukocytes stored at 4 °C for up to 2 days prior to FACS analysis. On the day of FACS analysis, liver leukocytes were centrifuged at 200 RCF for 4 minutes at 4 °C, followed by supernatant decant. Cell pellets were resuspended in 30 µL of antibody mix and incubated for 45 minutes at 4 °C in the dark. Thereafter, 170 µL of FACS buffer was added, liver leukocytes centrifuged at 200 RCF for 4 minutes at 4 °C, and supernatant discarded by decant. Cell pellets were resuspended in 80 µL FACS buffer and transferred to FACS tubes. Liver leukocytes were finally run through a BD Fortessa flow cytometer to measure surface marker expression levels. Post-acquisition analysis was performed using FlowJo 10 software.

Statistical analysis

Statistical analyses were performed using IBM SPSS Statistics 25 and Graphpad Prism 9.3.1 software. Details thereof can be found in the manuscripts figure legends. Significance was defined as a p-value of less than 0.05. Sample size estimations where appropriate were performed with a power analysis using an alpha of 0.05 and power of 90%. Data subjected to parametric statistical

analyses had its normality confirmed beforehand.

Acknowledgements

The work here presented was funded by a ZONMW VENI grant (016.156.076) financed by the Netherlands Organization for Scientific Research (NWO) and an LUMC PhD project grant (18-1919). Confocal microscopy and flow cytometry analyses were enabled by the LUMC's Light Microscopy Facility and Flow Core Facility, respectively. The authors wish to thank members of the LUMC's CHIC and IMI Laboratory for valuable critiques, and extend a special thanks to T.A. Patente, L.P. Almeida and J.M. Lambooij for time well spent in the lab and elsewhere.

Supplemental Information

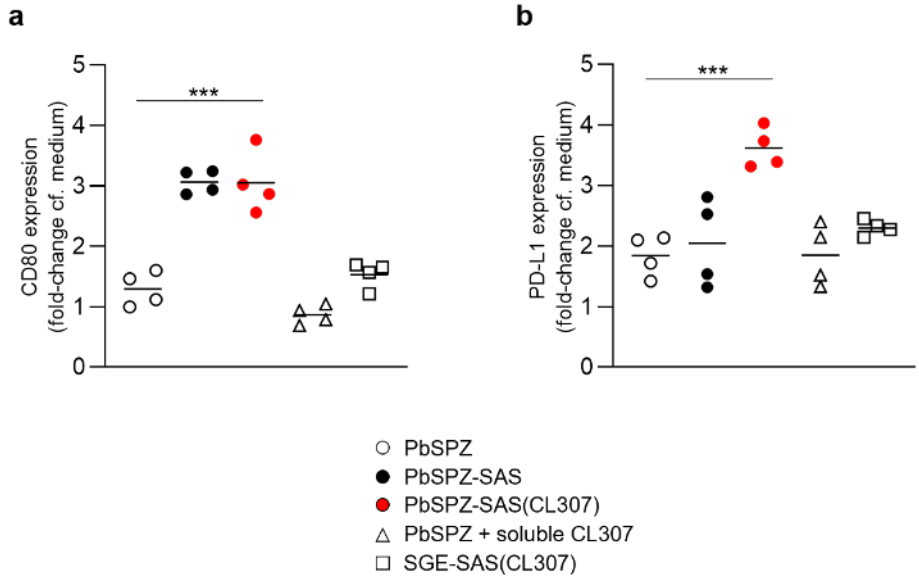

Figure S1: PbSPZ-SAS(CL307) induce a more pro-inflammatory response *in vitro* in macrophages. a) Fold-change (relative to medium) of surface marker CD80 (y-axis) in macrophages stimulated for 24h with PbSPZ-SAS(CL307) and controls. **b)** Fold-change (relative to medium) of surface marker PD-L1 (y-axis) in macrophages stimulated for 24h with PbSPZ-SAS(CL307) and controls. Data shown are n = 4 biological replicates from three independent experiments. SPZ (red circle).

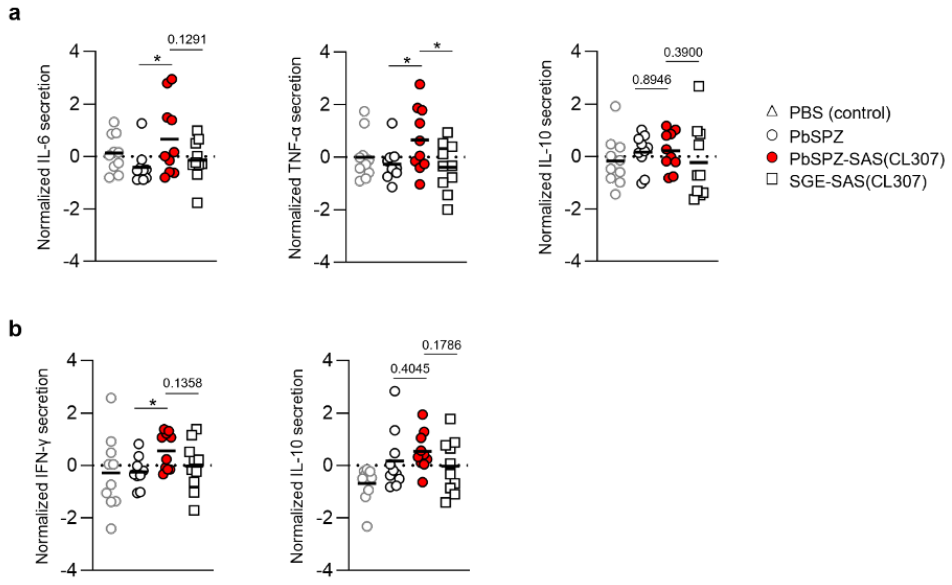

Figure S2: Liver and spleen immune cells of mice immunized with PbSPZ-SAS(CL307) display a more proinflammatory phenotype after stimulation with PMA/ionomycin. a) Normalized values of secreted cytokines IL-6, TNF-α and IL-10 (y-axis) by liver leukocytes from mice immunized with PbSPZ-SAS(CL307) or controls (columns) after 36 hours stimulation with PMA/ionomycin. **b)** Normalized values of secreted cytokines IFN-γ and IL-10 (y-axis) by splenocytes from mice immunized with PbSPZ-SAS(CL307) or controls (columns) after 36 hours stimulation with PMA/ionomycin. Data shown are n = 10 biological replicates from two independent experiments.

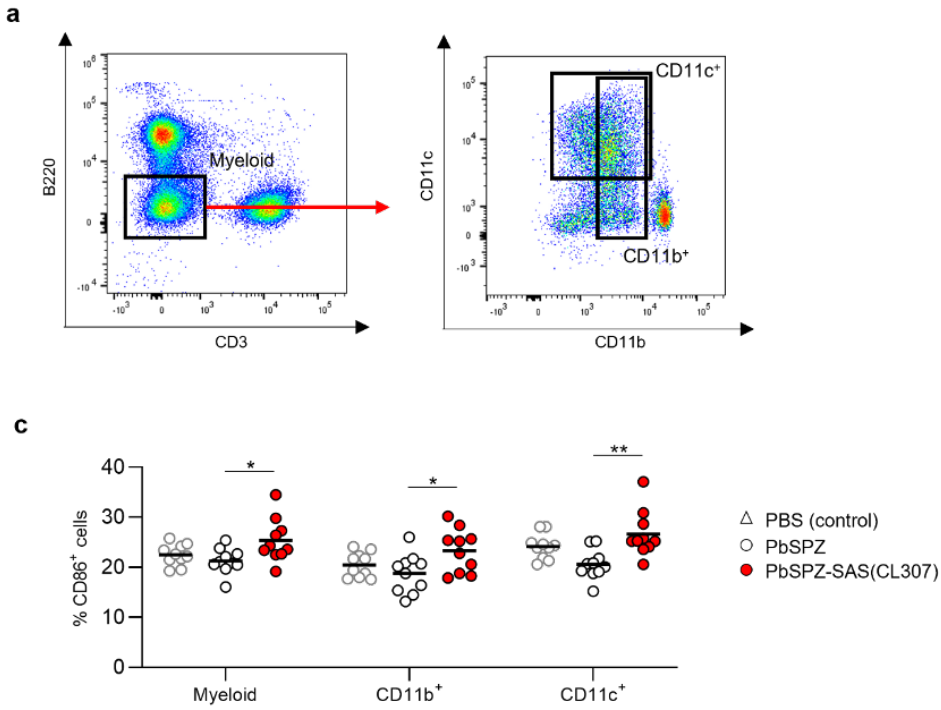

Figure S3: Myeloid liver leukocytes of PbSPZ-SAS(CL307)-immunized mice show enhanced SPZ-specific recall responses. a) Gating strategy for isolating myeloid liver cells (defined as $CD45^+$ $B220^-$ $CD3^-$ cells), as well as $CD11b^+$ and $CD11c^+$ subpopulations therein. **b)** Frequency activated $CD86^+$ cells (y-axis) in myeloid, $CD11b^+$ and $CD11c^+$ cell compartments (x-axis) in livers of mice immunized with PBS (white triangle), control PbSPZ (white circle) and chemically augmented PbSPZ-SAS(CL307) (red circle). Data shown are n = 10 biological replicates from two independent experiments.

6

Summarizing Discussion

In this dissertation, the development of a strategy for chemically tuning SPZ immunogenicity has been presented. This strategy envisioned the use of supramolecularly complexed polymers to introduce adjuvants onto the SPZ cell surface. **Chapter 2** described adaptation of the strategy – previously used to functionalize eukaryotic cells (Rood et al., 2017) and microparticles (Spa et al., 2018) – to bacterial cells, and assessed its compatibility with immune functioning. In **Chapter 3**, the functionalization strategy's *in vivo* compatibility was gauged using a bacterial pre-targeting paradigm. **Chapter 4** added an adjuvant to the chemical system and investigated whether doing so could augment the immunogenicity of poorly immunogenic bacteria. **Chapter 5** outlined translation of this chemical augmentation strategy to malaria SPZ, and assessed their immunogenicity *in vitro* and *in vivo*. Altogether, the results demonstrate the conceptual feasibility of chemically tuning the immune response to SPZ, thus indicating a path forward to generating SPZ-based malaria vaccines of high efficacy for use in malaria-endemic areas.

A key step in developing a (supramolecular) strategy for chemically augmenting SPZ lay in adapting a recently developed supramolecular host-guest functionalization strategy. In this strategy, initial pre-functionalization of a cell surface with a supramolecular guest, adamantane (Ad), is followed by complexation of polymers bearing the cyclodextrin (CD) host – polymers that can theoretically serve as a vehicle for introducing other moieties of interest. Adaptation of the chemical strategy, to bacteria, was first described in **Chapter 2**. Here, pre-functionalization of bacterial cell membranes with the supramolecular guest Ad was achieved by conjugating it to a cationic antibacterial peptide (UBI_{29-41}) previously shown to have an affinity for bacterial cell surfaces (Welling et al., 2000). The UBI_{29-41}-Ad construct yielded excellent pre-functionalization of bacterial surfaces, with >98% of Gram-positive and -negative bacteria showing complexed polymer *in situ*. **Chapter 3** built on these findings by demonstrating the concept's compatibility *in vivo*: tissue-resident bacteria pre-functionalized with UBI_{29-41}-Ad led to a 16-fold higher accumulation of intravenously administered polymer in infected tissue. Ultimate adaptation of the chemical strategy to SPZ in **Chapter 5** involved another, different method of Ad pre-functionalization. Here, the target was the abundant circumsporozoite protein (CSP) sheathing malaria SPZ (Yoshida et al., 1980). Pre-functionalizing CSP with Ad was accomplished by chemically conjugating Ad to lysine residues of CSP, which yielded excellent functionalization of parasites *if* permanently immobilized by metabolic inactivation. In general, these findings suggest that supramolecular functionalization techniques can be flexibly adapted to different cell types given effective Ad pre-functionalization.

An important first test of the chemical strategy was its compatibility with (normal) immune functioning. To this end, **Chapter 2** investigated the response

of macrophages, immune cells important for initiating immune responses, to chemically functionalized bacteria. The classic response of macrophages to microbes is to engulf them. This process was unimpaired by functionalization: time-lapse confocal microscopy showed that macrophages effectively phagocytosed functionalized bacteria within 10 minutes of encounter. Furthermore, two key macrophage effector mechanisms – surface marker modulation and cytokine production – remained responsive to functionalized bacteria. Addition of adjuvant to the chemical system, for bacteria in **Chapter 4** and SPZ in **Chapter 5**, similarly yielded normal responses by macrophages. These findings validated supramolecularly complexed polymers as good vehicles for introducing immunomodulatory moieties onto microbial cell surfaces, at least in the context of attempting to modulate the immune responses of promiscuous players such as macrophages – further investigation in relation to more discerning immune cells, such as dendritic cells, is needed to fully assess the presented chemical system's general applicability.

Does introduction of immunomodulatory agents onto microbial cell surfaces in fact boost immunogenicity? This key question was the primary focus of **Chapter 4**, where the poorly immunogenic bacterium *Staphylococcus aureus* served as a model system. Here, addition of a TLR7 agonist-based adjuvant (CL307) to the chemical system introduced about 10^7 units of adjuvant per bacterium. These chemically augmented bacteria did indeed possess an improved immunogenicity, inducing four-fold increases in production of pro-inflammatory IL-6 by *in vitro* macrophages compared to wild-type bacteria. **Chapter 5** showed the same effect for SPZ, but to an even greater degree: SPZ chemically augmented with adjuvant induced large, 35-fold increases in IL-6 production by *in vitro* macrophages compared to control SPZ. These data confirmed the feasibility of boosting microbial immunogenicity by augmentation with immunomodulatory agents. Notably, for both bacteria and SPZ pro-inflammatory responses by macrophages were superior when adjuvant was complexed to the cell surface as compared to delivered in soluble form. This observation is in good keeping with previous adjuvanting studies for subunit and nanoparticle-based vaccines showing the benefit of physically co-localizing adjuvant (Cadoz, 1998; Francica et al., 2016; Lynn et al., 2020; Rutgers et al., 1988; Wilson et al., 2013), and is to our knowledge the first direct demonstration thereof for cells.

In vivo mouse models provided a more comprehensive assessment of chemically augmented SPZ's immunogenicity. As mentioned above, **Chapter 3** had shown the *in vivo* compatibility of the chemical system in a bacterial pre-targeting model, with good stability for up to 24 hours post administration. These findings supported the use of a well-established *in vivo* paradigm in **Chapter 5**, where a prime-boost immunization regimen with (chemically augmented) SPZ was followed by analysis of tissue-specific immune responses. This analysis, particularly

for the liver (where malaria infection begins), showed several indicators of an improved immune response. One was the reactivity of liver leukocytes towards a generic pro-inflammatory stimulus, with significantly increased production of several pro-inflammatory cytokines. More strikingly, SPZ re-stimulation of liver leukocytes from animals immunized with chemically augmented SPZ produced higher frequencies of IFN-γ^+ NK cells, $CD4^+$ T cells and $CD8^+$ T cells – cells shown to play an important role in malarial immunity (Ewer et al., 2013; Schofield et al., 1987; Wolf et al., 2017). These data indicated an improved liver immune response, especially towards SPZ, and confirmed the conceptual feasibility of chemically augmenting SPZ as a means to improving immunogenicity. Moreover, the specific increases in IFN-γ^+ cells induced by a chemically coupled TLR7 agonist, a response similar in nature to previous studies also using TLR7 agonists (Ahonen et al., 1999; Vascotto et al., 2019; Wille-Reece et al., 2005), suggest that chemical augmentation with specific adjuvants can boost specific immune responses. That being said, the functional benefit of these boosts – *i.e.*, improved protection from malaria challenge post immunization – remain to be elucidated in future studies of the concept, in order to more fully gauge the utility of chemical augmentation of SPZ-based malaria vaccines with adjuvants.

Future perspectives:

This dissertation has shown that chemically augmented SPZ engender improved immune responses. The next step in moving the concept forward will be assessing whether these improved immune responses translate into improved protection in an immunization-challenge model. Here, it will be particularly interesting to see how the variable of SPZ immobilization, which yielded robust chemical augmentation, factors into protection. Immobilized SPZ are recognized to be logistically preferable to motile parasites, given that no liquid nitrogen is required for storage and transport. However, their inability to initiate a liver infection appears to lower their protective efficacy (Doolan and Martinez-Alier, 2006). It will thus be interesting to see whether chemical augmentation could shore up this shortcoming, and actually exceed the efficacy of motile, unadulterated SPZ. Should this not be the case, a refinement of the chemical strategy here presented would involve adapting the method to motile, infectious SPZ.

To this end, heparin oligosaccharides appear potentially good candidate scaffolds for chemically augmenting motile SPZ. Mechanistic studies have demonstrated that SPZ's rapid invasion of the liver after entering the bloodstream is mediated by a strong affinity between the parasite's circumsporozoite protein (CSP) sheath and the highly sulfated glycans decorating hepatocytes (Cerami et al., 1992; Pancake et al., 1992). Logically, then, a highly sulfated glycan, such as heparin, should be able to bind SPZ – possibly, without adversely affecting

motility. Preliminary data supports this concept's feasibility. Heparins fluorescently labeled with Cy5 dyes (Figure 1a) appear to indeed have excellent affinity for SPZ, with confocal analysis showing strong Cy5 signals co-localized with SPZ (Figure 1b). Quantitation by flow cytometry similarly showed SPZ reliably bound with large quantities of heparin (Figure 1c). Crucially, SPZ with heparin bound showed unimpaired movement during time-lapse microscopy analysis (Figure 1d). These promising results indicate a path forward to chemically functionalizing SPZ whilst preserving motility, and offer another tool for continuing to optimize the immunogenic properties of SPZ in pursuit of more efficacious malaria vaccines for use in endemic areas.

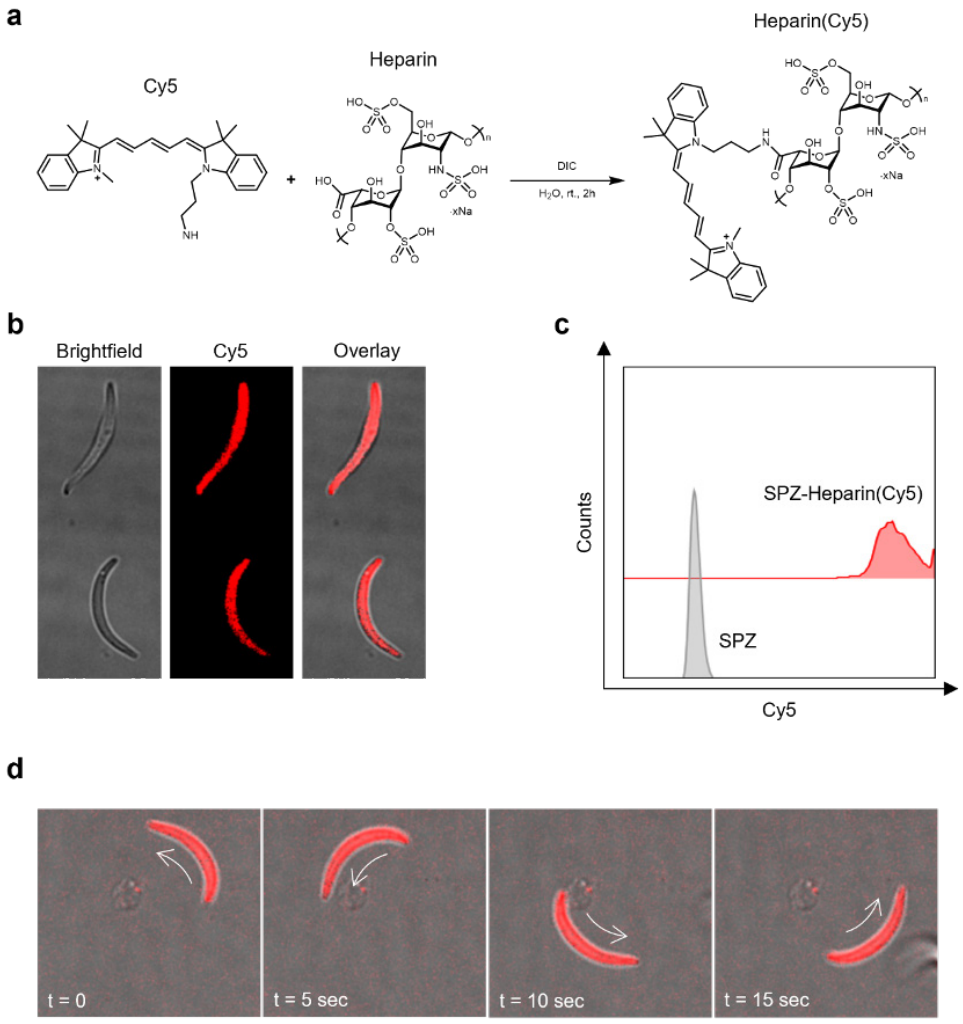

Figure 1: Heparin oligosaccharides can functionalize SPZ without perturbing motility. a) Reaction scheme showing synthetic route for generation of Cy5-labeled heparin construct. **b)** Confocal images showing co-localization of heparin(Cy5) construct with SPZ. **c)** Flow cytometry histogram showing Cy5 signal of heparin-bound SPZ (top: red) versus control SPZ (bottom: gray). **d)** Time-lapse confocal images showing a heparin-bound SPZ moving over the course of 15 seconds.

Beyond malaria, chemically augmenting cellular immunogenicity may also offer value for other (cell-based) vaccines lacking in efficacy. An obvious candidate here is the tuberculosis (TB) vaccine Bacillus Calmette-Guerin (BCG), derived

from an attenuated strain of bovine TB. BCG, the only licensed TB vaccine in the world, is reasonably effective in providing infants with protection, but its efficacy for adults is much lower (Mangtani et al., 2014). It stands to reason that (chemically) boosting BCG immunogenicity could offer a strategy for increasing that efficacy. On the oncological side, there is growing interest in developing vaccines that can trigger potent anti-tumor immune responses (Vermaelen, 2019). Many studies have examined the utility of antigen-based vaccines for overcoming this obstacle (Neek et al., 2019), and more recently cell-based vaccines have been explored also (Alson et al., 2020; Remic et al., 2022). For the latter, a chemical augmentation strategy like the one presented in this dissertation could provide a tool for increasing their immunogenicity, and with it anti-tumor efficacy.

Appendix

Summary (English)

Malaria continues to wreak havoc in tropical regions, due largely to the lack of an effective vaccine. Vaccine candidates based on whole parasites have shown promising results in malaria-naïve individuals, but their potency in malaria-exposed individuals is considerably lower. This dissertation described the development of a chemical strategy for boosting such parasites' potency in pursuit of more efficacious malaria vaccines for use in endemic areas.

Chapter 2 outlined the adaptation of a method for chemically modifying microbial cell surfaces.

Chapter 3 showed the chemistry underlying this modification system to be stably compatible with *in vivo* usage.

Chapter 4 demonstrated that when the chemical modification system was used to introduce immune-potentiating agents onto bacteria, better immune responses ensued.

Chapter 5 tied it all together by using the chemical modification system to potentiate malaria parasites, and showed that doing so markedly improved immune responses in an *in vivo* immunization model.

Chapter 6 summarized these findings in the context of malaria vaccine development and posited next steps forward.

Samenvatting (Nederlands)

Malaria blijft grote schade aanrichten in tropische gebieden, grotendeels als gevolg van het ontbreken van een effectief vaccin. Kandidaat-vaccins op basis van hele parasieten hebben veelbelovende resultaten laten zien bij malaria-naïeve proefpersonen, maar hun potentie bij aan malaria blootgestelde personen is aanzienlijk lager. Dit proefschrift beschreef de ontwikkeling van een chemische strategie om de potentie van dergelijke parasieten te versterken en zo bij te dragen aan het streven naar effectievere malariavaccins voor gebruik in endemische gebieden.

Hoofdstuk 2 schetste de aanpassing van een methode voor het chemisch modificeren van microbiële celoppervlakken.

Hoofdstuk 3 toonde aan dat de chemie die ten grondslag ligt aan dit modificatiesysteem stabiel compatibel is met *in vivo* gebruik.

Hoofdstuk 4 toonde aan dat wanneer het chemische modificatiesysteem werd gebruikt om immuunversterkende middelen in bacteriën te introduceren, er betere immuunresponsen volgden.

Hoofdstuk 5 bracht alles samen door het chemische modificatiesysteem te gebruiken om malariaparasieten te potentiëren, en liet zien dat dit de immuunresponsen aanzienlijk verbeterde in een *in vivo* immunisatiemodel.

Hoofdstuk 6 vat deze bevindingen samen in de context van de ontwikkeling van malariavaccins en poneert volgende stappen voorwaarts.

Acknowledgements

Clichés notwithstanding: science, and the research that drives it, is a fundamentally collaborative endeavor. The work presented in this dissertation seeks to provide its own humble contribution to that endeavor, and was in itself an endeavor made possible by contributions of many. I am deeply grateful to all of you, for contributions big and small, that made this dissertation possible.

I would like to first acknowledge the supervisors that shepherded this work to fruition. Meta: an initial two-week project in your group during my masters studies has, without exaggeration, literally steered my life's trajectory since. You have an infectious enthusiasm for what you do and a keen sense of how to best do it. Fijs: your passion and drive in research have helped immeasurably in honing my critical thinking skills, in all arenas of life. Thank you both for what you have taught me.

Many thanks to all my colleagues past and present in the Department of Parasitology, my first real home in a research setting. Here, I found community. My time here will be one I think back on fondly. Thanks also to the Interventional Molecular Imaging Lab for taking me in and showing me another side of community.

Finally, I'd like to thank my friends and family, on both sides of the Atlantic, for their steadying presence throughout this endeavor – without it, I would not be here.

Curriculum vitae

Nikolas Duszenko was born in Hamburg, Germany on 1 September, 1991. After shuttling back and forth across the Atlantic throughout childhood he attended Central High School in Aberdeen, South Dakota, USA, where graduated in 2010. He then headed for neighboring Nebraska to pursue an undergraduate degree in biochemistry at the University of Nebraska-Lincoln, graduating magna cum laude in 2014. Following two years of work at a clinical laboratory, he moved to the Netherlands to pursue a master's degree in biomedical science at the Leiden University Medical Center (LUMC), and obtained his degree in 2018. Here, he developed an interest in malaria vaccine research during his master's internship in the groups of Prof. Meta Roestenberg and Prof. Fijs van Leeuwen, which led him to continue the work with a PhD jointly performed at the Departments of Parasitology and Radiology of the LUMC – the results of which have been presented in this here dissertation. He plans to use the interdisciplinary competences gained during his PhD training to continue driving forward innovative scientific endeavors in the commercial sector.

List of Publications

Duszenko, N., van Schuijlenburg, R., Chevalley-Maurel, S., van Willigen, D.M., de Bes-Roeleveld, L., van der Wees, S., Naar, C., Baalbergen, E., Heieis, G., Bunschoten, A., Velders, A.H., Franke-Fayard, B., van Leeuwen, F.W.B., & Roestenberg, M. (2022). Chemically augmented malaria sporozoites display an improved immunogenic profile. *Front Immunol. 2023 Aug 31;14:1204606. doi: 10.3389/fimmu.2023.1204606. eCollection 2023.*

Duszenko, N., van Willigen, D. M., Bunschoten, A., Velders, A. H., Roestenberg, M., & van Leeuwen, F. W. B. (2022). Chemically Enhanced Immunogenicity of Bacteria by Supramolecular Functionalization with an Adjuvant. *Chembiochem: a European journal of chemical biology*, e202200434. Advance online publication. https://doi.org/10.1002/cbic.202200434

Welling, M. M., **Duszenko, N.**, van Willigen, D. M., Smits, W. K., Buckle, T., Roestenberg, M., & van Leeuwen, F. W. B. (2021). Cyclodextrin/Adamantane-Mediated Targeting of Inoculated Bacteria in Mice. *Bioconjugate chemistry*, *32*(3), 607–614. https://doi.org/10.1021/acs.bioconjchem.1c00061

Welling, M. M., **Duszenko, N.**, van Willigen, D. M., Hensbergen, A. W., Buckle, T., Rietbergen, D. D. D., Roestenberg, M., & van Leeuwen, F. W. B. (2021). Interventional nuclear medicine: "click" chemistry as an *in vivo* targeting strategy for imaging microspheres and bacteria. *Biomaterials science*, *9*(5), 1683–1690. https://doi.org/10.1039/d0bm01823f

Winkel, B. M. F., Pelgrom, L. R., van Schuijlenburg, R., Baalbergen, E., Ganesh, M. S., Gerritsma, H., de Korne, C. M., **Duszenko, N.**, Langenberg, M. C. C., Chevalley-Maurel, S. C., Smits, H. H., de Jong, E. C., Everts, B., Franke-Fayard, B., & Roestenberg, M. (2020). Plasmodium sporozoites induce regulatory macrophages. *PLoS pathogens*, *16*(9), e1008799. https://doi.org/10.1371/journal.ppat.1008799

Duszenko, N., van Willigen, D. M., Welling, M. M., de Korne, C. M., van Schuijlenburg, R., Winkel, B. M. F., van Leeuwen, F. W. B., & Roestenberg, M. (2020). A Supramolecular Platform Technology for Bacterial Cell Surface Modification. *ACS infectious diseases*, *6*(7), 1734–1744. https://doi.org/10.1021/acsinfecdis.9b00523

Welling, M. M., de Korne, C. M., Spa, S. J., van Willigen, D. M., Hensbergen, A. W., Bunschoten, A., **Duszenko, N.**, Smits, W. K., Roestenberg, M., & van Leeuwen, F. W. B. (2019). Multimodal Tracking of Controlled *Staphylococcus aureus* Infections in Mice. *ACS infectious diseases*, *5*(7), 1160–1168. https://doi.org/10.1021/acsinfecdis.9b00015

Crobach, M. J. T., Baktash, A., **Duszenko, N.**, & Kuijper, E. J. (2018). Diagnostic Guidance for C. difficile Infections. *Advances in experimental medicine and biology*, *1050*, 27–44. https://doi.org/10.1007/978-3-319-72799-8_3

Crobach, M. J. T.[#], **Duszenko, N.[#]**, Terveer, E. M., Verduin, C. M., & Kuijper, E. J. (2018). Nucleic Acid Amplification Test Quantitation as Predictor of Toxin Presence in Clostridium difficile Infection. *Journal of clinical microbiology*, *56*(3), e01316-17. https://doi.org/10.1128/JCM.01316-17

Duszenko, N., & Buan, N. R. (2017). Physiological Evidence for Isopotential Tunneling in the Electron Transport Chain of Methane-Producing Archaea. *Applied and environmental microbiology*, *83*(18), e00950-17. https://doi.org/10.1128/AEM.00950-17

Walter, M. E., Ortiz, A., Sondgeroth, C., Sindt, N. M., **Duszenko, N.**, Catlett, J. L., Zhou, Y., Valloppilly, S., Anderson, C., Fernando, S., & Buan, N. R. (2016). High-throughput mutation, selection, and phenotype screening of mutant methanogenic archaea. *Journal of microbiological methods*, *131*, 113–121. https://doi.org/10.1016/j.mimet.2016.10.010

Shea, M. T., Walter, M. E., **Duszenko, N.**, Ducluzeau, A. L., Aldridge, J., King, S. K., & Buan, N. R. (2016). pNEB193-derived suicide plasmids for gene deletion and protein expression in the methane-producing archaeon, Methanosarcina acetivorans. *Plasmid*, *84-85*, 27–35. https://doi.org/10.1016/j.plasmid.2016.02.003